Quantifying Steganographic Embedding Capacity in DCT-Based Embedding Schemes

by

Anna Zawilska

BScEng (Electronic) *Summa Cum Laude*

Submitted in fulfilment of the requirements for the Degree of Master of Science in Electronic Engineering in the School of Electrical, Electronic and Computer Engineering at the University of KwaZulu-Natal, Durban

January 2012

Supervisor: Professor Roger Peplow

Preface

The research discussed in this dissertation was done at the University of KwaZulu-Natal, Durban from February 2011 until January 2012 by Anna Zawilska under the supervision of Professor Roger Peplow.

As the candidate's supervisor, I, Roger Peplow, approve this dissertation for submission.

Signed:

Date:

I, Anna Zawilska, declare that

i. The research reported in this dissertation/thesis, except where otherwise indicated, is my original work.
ii. This dissertation/thesis has not been submitted for any degree or examination at any other university.
iii. This dissertation/thesis does not contain other persons' data, pictures, graphs or other information, unless specifically acknowledged as being sourced from other persons.
iv. This dissertation/thesis does not contain other persons' writing, unless specifically acknowledged as being sourced from other researchers. Where other written sources have been quoted, then:
    (a) their words have been re-written but the general information attributed to them has been referenced;
    (b) where their exact words have been used, their writing has been placed inside quotation marks, and referenced.
v. Where I have reproduced a publication of which I am an author, co-author or editor, I have indicated in detail which part of the publication was actually written by myself alone and have fully referenced such publications.
vi. This dissertation/thesis does not contain text, graphics or tables copied and pasted from the Internet, unless specifically acknowledged, and the source being detailed in the dissertation/thesis and in the References sections.

Signed:

Date:

Acknowledgements

I would like to thank my supervisor, Professor Roger Peplow, for his time and energy in providing insightful advice and encouraging me even when I doubted myself.

I wish to thank my family who have provided me with constant support and encouragement. Their courage and wise words have been essential to my personal and academic development and no number of thanks would ever be enough.

I would also like to thank all of the other staff and postgraduates at the department for their guidance, fellowship and for the laughs.

Abstract

Digital image steganography has been made relevant by the rapid increase in media sharing over the Internet and has thus experienced a renaissance. This dissertation starts with a discussion of the role of modern digital image steganography and cell-based digital image stego-systems which are the focus of this work. Of particular interest is the fact that cell-based stego-systems have good security properties but relatively poor embedding capacity. The main research problem is stated as the development of an approach to improve embedding capacity in cell-based systems.

The dissertation then tracks the development of digital image stego-systems from spatial and naïve to transform-based and complex, providing the context within which cell-based systems have emerged and re-states the research problem more specifically as the development of an approach to determine more efficient data embedding and error coding schemes in cell-based stego-systems to improve embedding capacity while maintaining security.

The dissertation goes on to describe the traditional application of data handling procedures particularly relating to the likely eventuality of JPEG compression of the image containing the hidden information (i.e. stego-image) and proposes a new approach. The approach involves defining a different channel model, empirically determining channel characteristics and using them in conjunction with error coding systems and security selection criteria to find data handling parameters that optimise embedding capacity in each channel. Using these techniques and some reasoning regarding likely cover image size and content, image-global error coding is also determined in order to keep the image error rate below 1% while maximising embedding capacity.

The performance of these new data handling schemes is tested within cell-based systems. Security of these systems is shown to be maintained with an up to 7 times improvement in embedding capacity. Additionally, up to 10% of embedding capacity can be achieved versus simple LSB embedding. The 1% image error rate is also confirmed to be upheld.

The dissertation ends with a summary of the major points in each chapter and some suggestions of future work stemming from this research.

Table of Contents

Acronyms

Joint Photographic Experts Group	JPEG
Mean Square Error	MSE
Peak Signal to Noise Ratio	PSNR
Red, Green and Blue	RGB
Least Significant Bit	LSB
Pseudo-random Number Generator	PRNG
Least Significant Bit Matching	LSBM
Least Significant Bit Matching Revisited	LSBMR
Bit Plane Complexity Steganography	BPCS
Discrete Cosine Transform	DCT
Inverse Discrete Cosine Transform	IDCT
Discrete Wavelet Transform	DWT
Yet Another Steganographic System	YASS
Repeat-Accumulate	RA
Quantisation Index Modulation	QIM
Forward Error Correcting	FEC
Bose, Chaudhuri and Hocquenghem	BCH
Cycle Redundancy Check	CRC

List of Figures

List of Tables

Chapter 1. Introduction

If all of the users of Facebook formed a country, it would be the third most highly populated country in the world at over 800 million inhabitants (Facebook, 2011), trailing not very far behind India (1.2 billion population) and China (1.4 billion population) (Rosenberg, 2011). Each month, users share more than 30 billion pieces of content such as status posts, photo albums, web links etc. (Facebook, 2011). Consider then that Facebook is just one of thousands of websites created especially to allow users to share content and ideas, add the effect of blogs, email and instant messaging - and a picture of the scale of the booming media-sharing culture begins to form. This culture is changing the way relationships are built, business is conducted and even the way people evaluate their self-worth ((Naughton, 2010), (Gordhamer, 2009)). The media-sharing culture also has a significant effect on data communications and in particular secret data exchanges. Neutralising the threat of an unwanted observer accessing secret information has always been a concern wherever data has been swapped, but now more than ever the amount of content that can be exchanged online makes this especially pertinent.

This dissertation explores the topic of *steganography*, which has a role to play in hiding transactions within digital communications and which, although relatively new within the digital domain, is growing rapidly in relevance and complexity (Cole & Krutz, 2003). It involves hiding information in seemingly-innocent transactions so that no-one viewing the exchange suspects this. The rate and ease with which digital media objects can be accessed, created and exchanged over the Internet makes them perfect carriers of secret information. The goal of this research is to address a shortcoming within a particular type of steganographic system (stego-system) that hides data in online transactions. Before this stego-system is referred to specifically, the concept of steganography is introduced within the field of communication security and in modern times.

We start by considering the following example from (Lin K. T., 2011) where a woman named Jane sends an email to her friend Kevin saying:

> *I'm feeling really stuffy. Emily's medicine wasn't strong enough without another febrifuge.*

At first glance, Jane appears to be simply telling Kevin about her illness, however in reality Jane and Kevin are spies arranging a time to meet.

Upon receiving the email, Kevin follows a pre-arranged protocol and extracts the second letter from each word to reveal the following sentence:

Meet me at nine.

Using an innocent-looking and unrelated sentence, Jane has transmitted a secret message to Kevin. Since only Kevin knows to look at the second letter of the words, only he can access the hidden command. Assuming that the transmitted sentence is natural-looking within the context of the usual messages they exchange, anyone seeing the cover sentence would not suspect that it carries a secret message. This is the idea behind a successful stego-system.

Traditionally, steganography is explained in more detail using the prisoners' problem, first introduced by Gustavus Simmons in 1984 (Simmons, 1984):

Consider Alice and Bob, who are both prisoners in separate cells and who wish to hatch a plan to escape. The two prisoners are allowed to communicate but their exchanged messages are monitored by a warden Eve. If Eve finds them communicating an escape plan she will put the prisoners into solitary confinement; so clearly the prisoners cannot speak openly about a plan nor can they communicate in a way that is obviously irregular. The solution is for Alice and Bob to hide messages in innocent-looking exchanges so that to Eve they appear innocuous. If Alice and Bob agree on a particular way of embedding information (i.e. a *key*), only they will know how to extract the hidden message from the innocent-looking exchange. If Eve detects or even suspects that a message has been concealed, the system fails and she will punish the prisoners. Note that it is not necessary for Eve to determine the content of the secret message; a reasonable suspicion of its existence is enough for the prisoners' communication system to fail since the main goal of steganography is concealment of the communication itself.

1.1 Definition of Steganography

Formally, *steganography is the science of hiding information in innocent objects with the objective of avoiding suspicion from anyone viewing these objects*. The strength of a stego-system comes from the extent to which a warden believes that objects containing embedded information are innocent. In other words, the system should make it impossible for an eavesdropper to distinguish between an ordinary object and one that contains secret data.

The concept of steganography is often confused with *cryptography* but they are quite independent ideas. In cryptography, it is accepted that the warden be aware of the secret communication and there is no attempt to disguise it. The goal is to scramble the secret

message in such a way as to make it unintelligible to those who don't possess the secret-key indicating how to unscramble it. The strength of a cryptographic system is indicated by how powerful the scrambling algorithm is in preventing an attacker from deciphering the message. Cryptography has the disadvantage that even if the warden is not able to decipher the message, he/she may delete it or even alter it. A good data hiding system will usually use cryptography as a first layer of security to scramble the secret data and then steganography as a second layer to hide the scrambled data in a cover object.

Another concept similar to and often confused with steganography is *watermarking*. The difference between the concepts of steganography and watermarking lies in their purpose. In steganography, the cover object used to hide the secret message is not necessarily related to the secret message contents, while in watermarking the hidden message is directly related to the chosen cover object. There are two main types of watermarking, classified by the nature of the watermark (Yeung & Yeo, 1998). The first is for the purpose of detecting alteration of the cover object by an unauthorised person and is performed by embedding a *fragile* watermark that it is easily disturbed and so can be used to detect any illicit editing of the media. The second is used in branding to detect copying or fraudulent use and uses a *robust* watermark indicating ownership which cannot be removed without clearly damaging the object.

1.2 History of Steganography

The term *steganography* is derived from the Greek words meaning *covered writing*. Before analogue and digital technologies, communication required the physical transportation of objects between parties and stego-systems were focused on hiding information in these objects inconspicuously.

Steganography is first recorded to have been practiced during the Golden Age in Greece using wax tablets (Herodotus, 1992). The wax would be melted away, the message would be carved into the underlying wood and then covered again using a fresh layer of wax giving the appearance of a new, unused wax tablet that could be innocently transported. In a similar manner, a Roman emperor Histiæus used slaves to transmit secret data by shaving their heads and tattooing messages into their scalp (Herodotus, 1992). Once the slave's hair grew back, he would travel to the required recipient, and shave his head on arrival to reveal the message.

Later during the 14th century, some poets encoded hidden messages into their work as a unique signature; for example the Italian poet and author Boccaccio encoded sonnets into his poetry as initial letters in the work (Wilkins, 1954). In the 16th century, an Italian Renaissance mathematician named Jérôme Cardin (Kahn, 1996) proposed a grid that allowed the letters of

a secret message to be extracted from seemingly-unrelated text by placing the grid over the text which would mask certain letters revealing the secret message.

Steganography became especially useful during wartime; for example, Brewster (Brewster, 1857) proposed the well-known technique of microdots used in many battles during the 19th and 20th centuries. The idea was to shrink the secret message to the size of a speck of dirt that could only be read under high magnification. The small objects were hidden in nostrils, ears or under fingertips and in the corners of postcards. Another, more recent stego-system used invisible inks (Kahn, 1996), the first of which were organic liquids such as milk, urine or vinegar diluted in a honey or sugar solution. The message written in this ink was invisible once the paper had dried, but the intended recipient could retrieve the message by heating the paper. As another example, (Brassil, Low, Maxemchuk, & O'Gorman, 1995) suggested a steganographic principle where data is hidden in text documents by slightly shifting the lines of text up or down by $1/300$ of an inch. These subtle changes aren't visually perceptible but they survive photocopying, allowing the message to be extracted even if the documents have been copied.

Until the early 1900s, steganography was used mainly by spies and the stego-systems were clever tricks like the ones discussed above, with little theoretical basis. With the transition of communication from analogue to digital, steganography has experienced a renaissance and is now highly technical and mathematical. In the late 1990s, digital watermarking dominated research (Fridrich J. , Introduction, 2010) due to numerous lucrative applications such as secure media distribution and authentication. With this interest, came further research into steganography, especially after concerns were raised that it may be used by criminals.

More recently, the rapid growth of the Internet coupled with high bandwidth and low-cost computer hardware has led to the rapid development of a media-sharing culture, as introduced above. This increase in digital information sharing and transfer over the Internet, combined with the seemingly limitless volume of content that can be uploaded, has provided huge potential for covert communication. With regard to steganography in particular, data can be hidden in digital media such as text, images, video and audio. Since electronic communication is susceptible to eavesdropping, security and privacy are more significant today than ever. Stego-systems are also becoming increasingly compact and neat, with new interest in implementing them on mobile and embedded devices, especially cellular phones. In (Stanescu, Stangaciu, & Stratulat, 2010), the authors show results suggesting how steganography can be used in mobile phones and tablets. Given that digital media objects

could also be used to store malicious data such as viruses (Debattista, 2010) or that it is suspected to be used by terrorists to distribute information (McCullagh, 2001), research into steganography is important not only to develop more robust information-transferral techniques but also to increase the ability to detect techniques developed by the enemy.

1.3 Steganalysis

Referring back to the prisoners' problem, (Anderson R. , 1996) defines three different roles that Eve can take on:

- Passive warden

  Eve only inspects exchanges between Alice and Bob but does not interfere.
- Active warden

  If Eve suspects that Alice and Bob are transmitting secret messages, she may preventatively distort the exchanged objects. Unless the stego-system caters for this, some part of the information carried by the object will be lost.
- Malicious warden

  If Eve thinks an active approach will inform Alice and Bob that their transactions are under surveillance, she may instead attempt to guess the steganographic method and impersonate Alice or Bob to intervene and confuse the communications.

Steganalysis refers to how successfully Eve can distinguish between innocent objects and those carrying secret data when she takes on the *passive warden* role. If she can perform this classification with some certainty greater than a random guess simply by observing and analysing the exchanges then the stego-system is considered broken.

Any information that Eve knows about the steganographic system *a- priori* can help her attack. Steganalytic methods can be divided into two primary categories based on the amount of additional information known by the warden about the system: *blind steganalysis* methods and *targeted steganalysis* methods.

Targeted steganalytic techniques are constructed from the knowledge of a particular stego-system and are designed to only detect that system, but with a high success rate. For example, if Eve knows the way in which the object is altered to contain the secret data, then she can search objects for any artefacts that indicate this type of embedding. The advantage is that Eve is more likely to be successful since she knows which embedding artefacts to look for, but if the steganographer changes the scheme, then Eve's analysis method will be useless. Another

difficulty is that Eve needs to know enough information about the embedding method to understand what embedding artefact to look for.

Blind steganalytic techniques in contrast are not devised to detect any particular stego-system, but rather the analyser uses machine learning and self-calibration techniques to analyse selected features of objects and classify them. Eve would need to accept a model of innocent objects using a set of feature vectors. In contrast to the targeted approach where a single feature is deduced to be an accurate detector, the blind approach requires a lot of features because, theoretically, blind steganalysers need to capture all possible patterns followed by innocent objects assuming that any embedding disturbs some of the features making corrupted objects detectable. The primary difficulty in the development of blind steganalytic techniques is deducing which features to include in the determining set, since they need to be noticeably changed due to data hiding but invariant with object content.

Generally, blind analysers detect a wider range of stego-systems but with less success than a targeted steganalyser for any individual stego-system. The primary advantage with blind analysers is that they may also, rather unintentionally, classify objects corrupted from stego-systems not used during training if the new stego-system also happens to disturb some features in the chosen set.

1.4 Digital Image Steganography

As stated above, modern-day stego-systems exist primarily in the digital domain and involve hiding information in media transactions carried over the Internet meaning data is hidden in images, video, text or audio. Out of all digital media objects, digital *image* transactions are the most common on the Internet. On Facebook alone, 2.5 billion photos are uploaded every month ((ReadWrite Cloud, 2010), (Answers.com, 2011)). If secret transactions are to occur as inconspicuously as possible, steganographers should use the most common form of exchanged media as cover objects for communication which are digital images. The predominance of the use of digital images as covers over other media in steganography applications, as of 2008 (Johnson & Sallee, 2008), is shown in Figure 1-1.

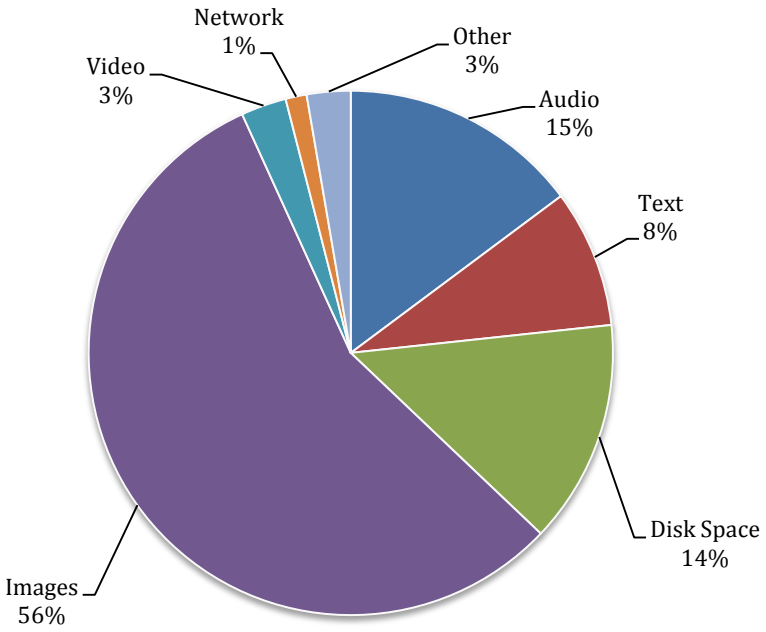

Figure 1-1. Proportion of cover types used in digital stego-applications

Given these statistics, it should be clear why it is appropriate that the research in this dissertation be concerned with *digital image steganography* - steganography focused on embedding secret messages within digital images. Unless otherwise noted, all stego-systems discussed in this document from hereon will refer to digital image stego-systems.

Digital image steganography finds application across many fields, ranging from secret pledges of undying love between a pair of teenagers to the corporate, military and medical fields. A state secret, a command, trade secrets or perhaps private medical information may be transmitted discretely using steganography especially when the transaction occurs over a public channel.

Digital images may be stored and transmitted in either uncompressed or compressed format but given the limited bandwidth of the Internet the uncompressed version is considered wasteful and clumsy. In particular, to provide high levels of compression, the *Joint Photographic Experts Group (JPEG)* developed the JPEG compression standard which has become extremely popular for digital image storage and transmission (Braga, 2010). It is thus evident that for any digital image stego-system to be effective, it should cater for this compression scheme.

JPEG compression is lossy, causing corruption of image data, the extent of which is determined by the amount of compression performed. For stego-systems, this poses a threat when secret

data is embedded into the image prior to compression and thus requires implementation of error correcting codes to compensate for the inevitable data corruption. Unfortunately, this has a negative effect on embedding capacity because error correcting schemes require transmission of redundant overhead bits (that take up space in an image that could be used for secret data) that will be used at the receiver to detect and correct erroneous bits.

A type of stego-system that embeds into digital images and tends to accommodate JPEG compression, called *cell-based systems,* has emerged as particularly secure. These systems confuse blind steganalysers by randomising the areas of the image into which data is embedded. However, as only select areas of the image are used when combined with the requirement for error coding means that the embedding capacity for these systems is comparatively low. However, the data embedding and error correcting schemes used in cell-based systems have not been determined analytically in the literature thus far, and so this research addresses the extent to which these schemes can be chosen more methodically so that embedding capacity is improved while maintaining good security properties.

1.5 Research Problem Statement

With relevant background regarding digital image steganography explained, the main purpose of this research can now be stated.

Given the relevance of cell-based systems in modern digital image steganography, the main issue addressed in this dissertation is how to develop an approach to analytically determine data handling (i.e. data embedding and error coding) schemes for cell-based stego-systems so that embedding capacity is improved and security properties are maintained. This approach should give rise to a set of data handling parameters that can then be implemented in the context of cell-based systems and tested for performance.

1.6 Research Methodology

In order to address the research problem statement, certain steps need to be taken. The research methodology refers to the logical sequence of actions required to gather sufficient knowledge to address the research problem statement and to test the results. The methodology can be broken down into the following four stages:

1. The first stage requires background research to develop an understanding of the field of digital image steganography, including the general philosophies behind design, generic system models and terminology. In the process, an understanding of the context within which cell-based systems were developed and their purpose is acquired.

2. The second stage requires analysis of cell-based systems and identification of potential areas of improvement in terms of data embedding and error correction.
3. The third stage requires implementation of a simulator to re-enact cell-based systems and to analyse the extent to which improvements can be made. This results in the proposition of new data embedding and error coding schemes.
4. In the final stage, the new data handling schemes are placed back into context and are used within cell-based systems that are then tested for security and the extent to which embedding capacity has been improved.

1.7 Dissertation Roadmap

Chapter 2 presents a model of the digital image steganographic systems considered in this dissertation along with relevant terminology and system characteristics. The development of digital image stego-systems is then traced, which provides the context within which cell-based systems were developed. The operational steps of cell-based systems and their varieties are then presented.

Chapter 3 introduces a new approach to embedding data and correcting errors in cell-based systems, based primarily on accommodating the effects of lossy JPEG compression. This approach is explored further and data handling parameters are derived.

Chapter 4 tests the new data embedding and error coding systems with respect to security, embedding rate and error rate requirements.

Chapter 5 summarises the main points of the dissertation and discusses the extent to which the original goals presented in this chapter are addressed. Some suggestions for future work that could build on this research are provided.

1.8 Published Works

The published works based on the research described in the dissertation are:

1. Optimising the Error-Free Embedding Rate in Variable Cell-Size Steganographic Schemes at the Military Information and Communications Symposium of South Africa (MICSSA) 2011
2. Quantifying Steganographic Embedding Capacity in DCT-Based Embedding Schemes at the Southern African Telecommunication Networks and Applications Conference (SATNAC) 2011

Chapter 2. Digital Image Steganographic Systems

So far, the relevance of digital image steganography as a field of research given the predominance of digital image exchanges on the Internet has been discussed. These digital images can be stored in compressed or uncompressed formats but given bandwidth limitations on channels over the Internet plus the significant volume of storage required for the huge number of images, compressed formats are more useful and thus popular and in particular JPEG compression is extremely common.

Within digital image steganographic systems, cell-based systems have emerged as particularly secure and are designed to cater for the likely application of JPEG compression but unfortunately display relatively low embedding capacity properties. However, data embedding and error coding systems have not been determined analytically in the literature thus far, and so there is an opportunity to improve embedding capacity of cell-based systems by determining more effective data handling procedures. This idea forms the foundation for this research which aims to develop an approach to doing this.

Before this approach is developed specifically, this chapter formally defines the relevant properties of digital image steganographic systems, contextualises and motivates cell-based systems within digital image steganography and discusses cell-based systems as they are currently presented in the literature.

2.1 Classification of Steganographic Systems

Many varieties of stego-systems exist and the nature of the systems referred to in this dissertation is now clarified. Stego-systems may be broadly classified according to dependencies between the secret data and cover image, the role of the key and the behaviour of the warden.

2.1.1 Relationship between Secret Message and Cover Image

In the first broad category, stego-systems vary according to the relationship between the secret message and the image into which it is hidden. As presented by (Fridrich J. , 2010), there are three main types of stego-systems based on this:

- Steganography by *cover selection*

  Alice has access to a fixed database of images, and she chooses the one that communicates the required message based on some features such as a certain sequence of colours. This has the disadvantage that Alice may have difficulty finding an appropriate image.

- Steganography by *cover synthesis*

  Alice creates a cover so that it conveys the required message. She can do this, for example, by placing certain objects in the frame of a photograph which she then uses as the cover image. However, this is clumsy and difficult for Alice, who needs to keep setting up frames and taking photos.
- Steganography by *cover modification*

  Alice starts with any cover image and embeds data into it by modifying it according to some protocol. This type of stego-system is the most practical for communicating large amounts of data out of the three categories listed here because Alice can theoretically select any image as a cover. This is the most studied steganographic paradigm.

Since steganography by cover modification is, by far, the most favoured by the research community, this form of steganography is assumed here.

2.1.2 Key Type

The concept of a key was mentioned in Chapter 1 as something shared between the sender and intended recipient only and which provides the specifics of the way in which data is embedded for a particular transaction. For example, in the case of Jane sending her friend Kevin an email arranging a meeting time as in Chapter 1, the stego-system is the embedding of one sentence into another but the key specifies which letters in the transmitted sentence should be extracted to reveal the message. In the example provided, the key for that specific transaction indicated to Kevin to extract the second letter of each word.

In the prisoners' problem, it is assumed that Eve knows the complete steganographic algorithm used by Alice and Bob *with the exception of the transaction-specific key* which was agreed upon by the prisoners before imprisonment. The expectation that the stego-algorithm but not the stego-key be known to Eve is called *Kerckhoffs' principle* which states that security should be maintained not by the secrecy of the system but be based on the key. First articulated in 1883 (Kerckhoffs, 1883), it stems from experience through espionage where the stego-algorithm was usually discovered by the enemy. In this event, the security of the stego-system should not be threatened.

The varying role and nature of the key was first used to classify stego-systems in (Anderson R. , 1996). The given system categories are:

- Pure systems

  No key is used. Once the stego-system itself is known, the hidden message can be extracted. This system does not follow Kerckhoffs' principle and is considered poor.
- Secret-key (Symmetric) systems

  The same key is used to both embed and extract the hidden information from the image and it is assumed that this key is secretly shared between the sender and intended recipient.
- Public-key (Asymmetric) systems

  These systems use two keys – a public key that is openly published and a private key known only to the intended recipient. The information is embedded using a public key and extracted using the private key. Contrary to secret-key systems, these systems exhibit asymmetry in that the key used to embed information in the image is not the same one used to extract that secret information.

Secret-key systems are the most popular in the literature, and this type of system will be assumed in this dissertation.

2.1.3 Role of the Warden

The possibilities of warden behaviour were already described in Chapter 1 as passive, active or malicious. Steganalysis was defined as the science of distinguishing between innocent and corrupt digital images in the case of the passive warden scenario which is by far the most common paradigm in the literature on digital image steganography and hence the passive warden scenario is the assumed model for this work.

2.2 Stego-System Model

A formal stego-system model is shown in Figure 2-1. Figure 2-1 and the terminology explained in this section were agreed upon at the first international workshop on information hiding ((Anderson R. , 1996), (Pfitzmann & Anderson, 1996)).

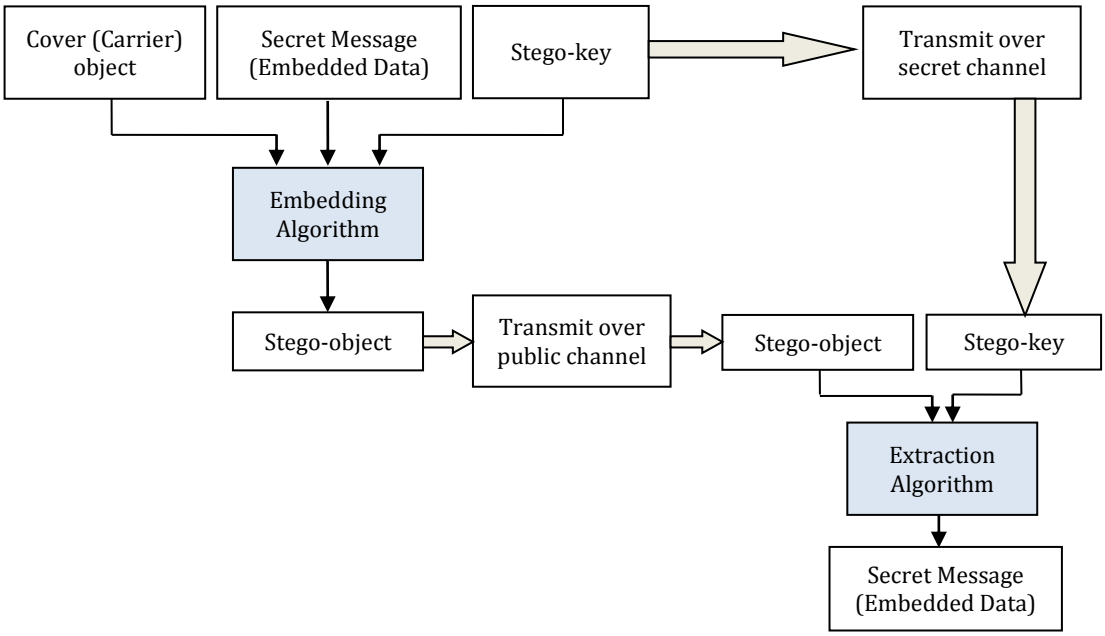

Figure 2-1. Overview of stego-system

Steganography is used when there is a need to transmit a *secret message* which is achieved by hiding it in a *cover image*. It is important that the innocent cover image itself is not publicly available, as this would make steganalysis by the warden a trivial exercise of comparison between a suspect stego-image and its innocent version.

The message is any data represented by a bit stream. In binary digital communications, all information is ultimately represented in bits so there is no requirement that the cover and message objects have the same original form (e.g. audio, video, text). The process with which the message is embedded in its cover is called the *embedding algorithm,* the result of which is called a *stego-image*.

Mathematically, the embedding algorithm can be expressed as shown in Equation 2-1.

$$y = Emb(x, k, m) \quad \textbf{2-1}$$

where y is the stego-object, x is the cover object, k is the secret-key and m is the secret message.

The stego-image is then transmitted across an unsecured, public channel which we assume is error-free (passive warden scenario). If the stego-image is compressed, the compressed version is sent over the channel and may undergo steganalysis.

At the receiver side, the secret message is retrieved using the stego-key and an *extraction algorithm*, shown in Equation 2-2.

$$Ext(y,k) = m$$
$$or\ Ext(Emb(x,k,m),k) = m \qquad \textbf{2-2}$$

The embedding and extraction algorithms may be designed specifically so that the original cover image can be retrieved by the recipient in what is called a *lossless data hiding scheme.* This is not relevant here because the cover image itself is not considered to have any value. A lossless scheme would be more relevant in a watermarking application.

2.3 Pertinent Properties of Stego-Systems

Now that the structure and relevant terminology relating to stego-systems has been described, the next relevant concept is that of performance of stego-systems. The requirement for security against steganalysis has already been mentioned and this section describes two other important performance requirements. It also describes in more detail what is meant by security and resistance to steganalysis.

2.3.1 Primary Attributes

(Smith & Comiskey, 1996) define three primary attributes for an information hiding system; *imperceptibility*, *embedding capacity* and *robustness*:

- Imperceptibility

  The difficulty a warden has in detecting the presence of hidden information or, more specifically, the uncertainty with which a warden can classify corrupt stego-images from innocent cover images. This has already been mentioned under the description of steganalysis.
- Embedding Capacity

  Sometimes referred to as *effective payload* or simply *capacity*, it is the amount of information (excluding any overhead or dummy bits) that can be hidden in a given cover image. The larger the capacity of a stego-system, the better the system.
- Robustness

  The amount of modification the stego-image can undergo before the hidden information becomes irretrievably damaged. Depending on whether the stego-object is likely to undergo alteration this may or may not be a critical attribute.

There is general agreement in the literature that imperceptibility and capacity are the most important of the attributes (e.g. (Luo, Huang, & Huang, 2010), (Smith & Comiskey, 1996)). In other words, a good stego-system should embed as much data as possible and keep distortion as low as possible. It should only be robust when the application requires it. Furthermore, a system is effectively useless if it does not effectively combat steganalytic attacks, no matter how robust or how much capacity it has.

The three properties contradict one another and thus it is impossible to achieve a system that has all three excellent qualities. For example, if the amount of hidden information is increased (i.e. increased capacity), the warden will have more chance of detecting it (i.e. lower imperceptibility) since inevitably more artefacts indicating embedding will be introduced into the cover.

In order to maintain imperceptibility, the stego-system should firstly not introduce any obvious visual artefacts into the stego-image during embedding. The visual imperceptibility associated with a stego-image is often measured in the literature using the *mean square error* (MSE) or *peak signal to noise ratio* (PSNR) that is calculated as the average difference in colours between the innocent cover image and stego-image. However, these measures offer only a limited reflection of imperceptibility. To demonstrate this, consider the two images of Lena shown in Figure 2-2.

(a) (b)

Figure 2-2. Sample image with a clear visual distortion (a) and after JPEG compression (b)

The photograph of Lena on the left is generated by introducing a square of black pixels in the centre of her face, while the photograph on the right has been generated by JPEG-compressing and -decompressing the original photograph of Lena. Even though the JPEG compressed image is more innocent-looking, it has a 20% higher MSE.

The main problem with the MSE is that it measures the *average* difference between the colours of the stego-image and cover image, and so localised distortion on a small scale, even if clearly visible, is not represented. Unfortunately, as it shall be seen, papers on the topic of digital image steganography still use the MSE as a measure of performance. A more useful measure of visual perceptibility would be the success of human suspects categorising innocent and corrupt images visually as done in (Dawoud, 2010).

One additional property of a stego-system apart from the three discussed that merits mentioning is the computational demand in implementing it (Fan & Wediong, 2004). Generally the more complex the embedding scheme, the more secure the system. However, the processing power of modern, commercially-available computers more than suffices for any requirements, even in the most complex of schemes, especially since there are no requirements for ultra-fast real-time implementation. Restrictions in system complexity arise when the scheme is limited to embedded devices as seen in (Stanescu, Stangaciu, & Stratulat, 2010). These types of limitations and applications are not assumed here, so simplicity in algorithm and execution time is not used as a measure of success of a system.

2.3.2 Detectability versus Imperceptibility

Given that most images transmitted over the Internet are displayed at some point if not directly uploaded to a public website, it would be foolish for a stego-system to introduce obvious visual distortion to a stego-image since this would immediately arouse suspicion. Over time the complexity of both steganographic and steganalytic techniques has increased, primarily in response to each other's development in a spiral development pattern. The requirement of visual imperceptibility is no longer sufficient in itself and the combat between data hiding and the attack has moved to a more subtle, statistical level. Modern steganalytic techniques classify images based on changes and boundaries in statistics across an image rather than any visual artefacts (Fridrich & Goljan, 2002). No matter how imperceptible the embedding artefacts visually, appreciable statistical traces of embedding in an image may usually be determined.

At this point an extra attribute is introduced - *detectability* which is used to refer to the extent to which steganalytic techniques detect stego-images through statistical means whereas perceptibility is now re-defined to be limited to the extent to which embedding artefacts are visually clear. Visual embedding artefacts will automatically introduce statistical anomalies (but not vice-versa) therefore a system that is undetectable will also be imperceptible but the opposite is not true. In this dissertation, the term *naïve* will be used to refer to old-fashioned

stego-systems that aim for imperceptibility only and *complex* will be used for modern stego-schemes that aim to avoid detectability.

Generally, the similarity between an innocent cover image and stego-image (visually or otherwise) may be expressed using a property called Transparency (where x is the cover object and y the stego-image):

$$tra(x,y) = 1 \leftrightarrow x = y, and\ for\ x \neq y, 0 \leq\ tra(x,y) < 1 \quad \textbf{2-3}$$

In the case of a secure system, Equation 2-3 can be re-written as shown in Equation 2-4.

$$\mathrm{tra}\left(\mathrm{x}, \left(\mathrm{Emb}(\mathrm{x}, \mathrm{k}, \mathrm{m})\right)\right) \approx 1 \quad \textbf{2-4}$$

A stego-system is secure if a warden can only guess whether an image is corrupt or innocent and equally determines stego-images as innocent and innocent images as stego-images. This can be stated differently as that the warden achieves a *detection rate* of 0.5.

There are more formal definitions of security and one popular definition by Cahin (Cahin, 2004) uses information theory to compare the distribution of innocent cover objects and stego-objects. His definition is given next.

By first defining:

C... Set of cover object $x \in C$

S. ..Set of stego-object for x

$K(x)$... Set of stego-keys for x

$M(x)$ ... Set of all messages that can be communicated in x.

Equations 2-1 and 2-2 can be rewritten as shown in Equations 2-5 and 2-6.

$$Emb: C\ x\ K\ x\ M\ \rightarrow\ S \quad \textbf{2-5}$$

$$Ext: S\ x\ K\ \rightarrow\ M \quad \textbf{2-6}$$

If we observe the transactions between Alice and Bob for long enough, the images chosen as covers would produce a probability distribution P_C in the space of all the covers C. The distribution represents legitimate communication between the two. If Alice and Bob now

embed secret information in the images (i.e. use the images to generate stego-images), if you again observe the transactions over a long enough period of time, the images will follow a different distribution P_S over C. Intuitively, the stego-system should be designed so that P_S is as close as possible to P_C. If P_C and P_S are similar, the warden will make erroneous decisions more often. The two distributions can be compared using the *KL distance* or *relative entropy*, which is a fundamental concept from information theory for measuring the difference between distributions, given in Equation 2-7.

$$D_{KL}(P_C||P_S) = \sum_{x \in C} P_C(x)\, log \frac{P_C(x)}{P_S(x)} \quad \textbf{2-7}$$

A completely secure stego-system is one where the distribution of the resultant stego-objects exactly follows that of innocent cover objects so that the warden cannot distinguish between the two distributions. In this case $P_C = P_S$, and the KL distance is zero. This means that no steganalytic scheme can perform better than a random guess.

If we write:

$$D_{KL}(P_C||P_S) \leq \varepsilon \quad \textbf{2-8}$$

Then we say that the system is *ε-secure*. Through calculations not detailed here but available in (Fridrich J. , 2010), this translates to the fact that if we assume that the warden is not allowed to falsely accuse the prisoners, the smaller the value of ε, the lower the probability of detection. This motivates the use of the KL divergence as a measure of the security of the stego-system.

It is convenient to use KL divergence for comparing two systems. For example, if you have two systems $S^{(1)}$ and $S^{(2)}$, we would say $S^{(1)}$ is more secure that $S^{(2)}$ if:

$$D_{KL}\left(P_C||{P_S}^{(1)}\right) \leq D_{KL}\left(P_C||{P_S}^{(2)}\right) \quad \textbf{2-9}$$

2.4 Taxonomy of Digital Image Steganography

The development of digital image steganographic systems has been fuelled mainly by advances in steganalytic methods for detecting ever more subtle statistical embedding artefacts. Data hiding in the spatial, uncompressed representation of digital images came first followed by the idea of transform-based data hiding. The development of stego-systems from naïve to complex and the context within which cell-based systems were developed is explained in this section. Cell-based systems are then described as they are currently defined in the literature.

2.4.1 Spatial Domain Steganography

The first naïve digital image stego-systems focused on embedding data bits in the spatial domain representation of images with the purpose of avoiding perceptible artefacts. Initially, the idea of transform representation and image compression were not known or referred to. This section explains the spatial domain representation of images and then how spatial stego-systems were designed to operate.

2.4.1.1 Spatial Domain Representation

The spatial domain representation of an image deals with representing the colours of a real-world scene in digital format. Visible light consists of the sum of electromagnetic waves with wavelengths between approximately 280nm and 750nm. A colour is defined by a combination of waves, each one of a particular wavelength and energy. Even though there are infinitely many different colours in the real world, the human eye is capable of distinguishing only a small subset of them.

When digital cameras capture a scene, they must digitise the light information in the frame before storage, the result of which is the digital image. Spatially, a digital image may be defined as a discrete 2-dimensional function $f(x, y)$ where x and y are spatial coordinates and the value of f at point (x, y) is called the *intensity* of that point. Each point in the image is called a pixel.

If an image is monochrome (grey scale), the intensity level refers to how light the pixel is, with the lowest intensity (0) representing black and the highest intensity (usually 255) representing white. Figure 2-3 shows a grey scale image (taken from (Rst, 2010)) and 5x5 pixel segment of this image. The corresponding intensity values for the segment are also shown based on an intensity range of 0-255.

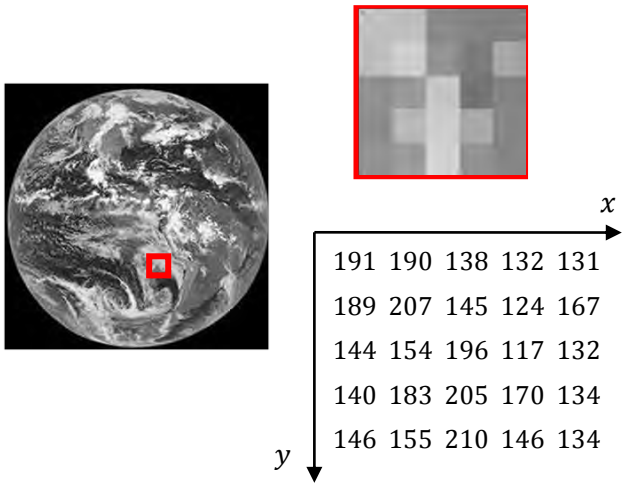

Figure 2-3. Grey scale image and 5x5 pixel segment with corresponding pixel values

A *binary image* is a specific type of grey scale image with only two intensities; 0 for black and 1 for white.

If the image is in colour then it would be sage to represent the colours in a way that is effective according to the characteristics of the human visual system. The human eye contains three receptors called *cones* that have peak sensitivities to red, green and blue light (Rockwell, 2007). The electrical pulses from these cones are fed to the brain giving humans the ability to perceive colour. This idea led to the definition of the *additive colour model* where any colour in an image can be represented by a linear combination of red, blue and green. In RGB image representation each pixel is assigned three values corresponding to the red, green and blue (RGB) components. RGB images are represented by three 2-dimensional planes, one plane for each colour component.

The values of f are not continuous but quantised. The more quantisation levels, the better the quality of the image but since there is an upper limit on the number of colours perceivable by the human eye the number needn't be extremely high. It has already been stated that grey scale image intensities vary between 0 and 255 (represented in binary using 8 bits). Similarly, each of the three colour components in RGB images is commonly represented by the range [0,255] so 256^3 = 16 777 216 different colours can be produced.

Apart from being represented in the RGB space, colour digital images may also be described in other *colour spaces* such as YCbCr and HSV colour spaces. Effectively, colour spaces are just different ways of representing colours and different ones are useful depending on the application. Conversion between colour spaces is performed using linear equations, and all of

them can be derived from the RGB space. The conversion between RGB space and YCbCr (Y meaning luminance and (CbCr) meaning chrominance) space, for example, is given in Equation 2-10 (Gonzalez & Woods, Image Types, 2002).

$$\begin{bmatrix} Y \\ Cb \\ Cr \end{bmatrix} = \begin{bmatrix} 16 \\ 128 \\ 128 \end{bmatrix} + \begin{bmatrix} 65.481 & 128.553 & 24.966 \\ -37.797 & -74.203 & 112.000 \\ 112.000 & -93.786 & -18.214 \end{bmatrix} \begin{bmatrix} R \\ G \\ B \end{bmatrix} \quad \textbf{2-10}$$

Images represented in the manner explained so far are called *intensity images*.

Images may also be represented as *indexed images*. In this format, the image is represented by a data matrix of integers and an associated colour map matrix. The values associated with each pixel act as pointers directly to colours in the map. Indexed images were used to save space by representing each RGB pixel by an 8 bit index into a colour table. The resultant images were of a lower quality than a full colour image and as storage space has become less critical, indexed images have lost favour and are very seldom used anymore. In this dissertation, only RGB and YCbCr images will be used.

2.4.1.2 Naïve Spatial Domain Steganography

The simplest and most-common spatial domain naïve stego-algorithm is *Least Significant Bit (LSB) embedding*. The idea is that changing the LSB in the binary representation of a particular pixel will change its intensity only slightly which is not perceptible, providing an element of redundancy where information can be stored. The process of extracting and embedding in the LSB of a particular pixel is shown in Figure 2-4 (adapted from (Beaullieu, Crissey, & Smith, 2000)).

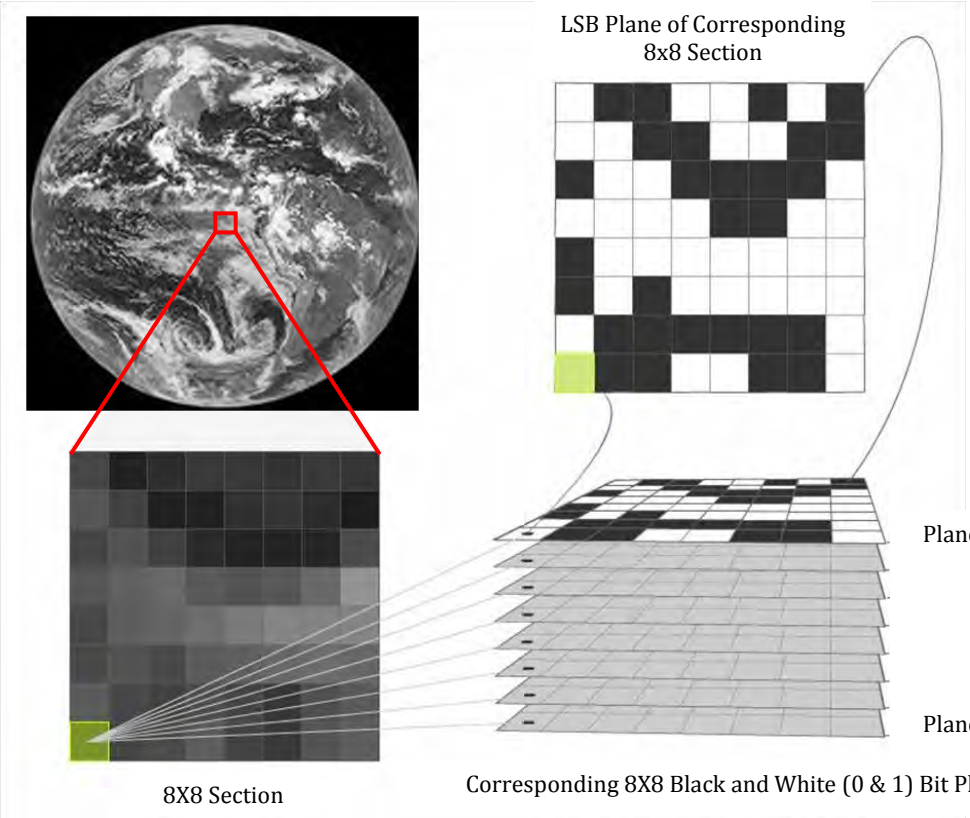

Figure 2-4. LSB embedding

The simplest form of LSB embedding scans through an image column-by-column and changes the LSBs of the cover image to the secret data bits. Consider the secret image (cat + blanket - created by cocor , 2010) and cover image (The President Elect's Favorite Movies and Books, 2008) shown in Figure 2-5. The cover image has the dimensions 480x640 (307 200 pixels), while the smaller secret (data) image has dimensions 110x130 pixels. Since each pixel of the data image is represented by 8 bits, it is described in total using 110x130x8 = 114 400 bits.

(a) (b)

Figure 2-5. Secret image (a) and cover image (b)

If each bit of the secret image is embedded into the LSB of a pixel in the cover image, the secret image fits into a small section of the cover image. If the image is traversed column-by-column, the resultant stego-image is shown in Figure 2-6.

Figure 2-6. Stego-image using LSB embedding with a small secret message

The stego-image appears visually identical to the innocent cover image (making the system imperceptible), but there are clear embedding artefacts if the LSB planes of the images are compared as shown in Figure 2-7. The innocent LSB plane in Figure 2-7 (b) appears as a random variation of black and white dots as is common with natural images while the stego-image plane (a) shows obvious distortion. The clear embedding artefacts in the statistical domain (the statistical distribution of LSBs) show the importance of steganalysis as a statistical analysis process (detectability) rather than a visual one (perceptibility).

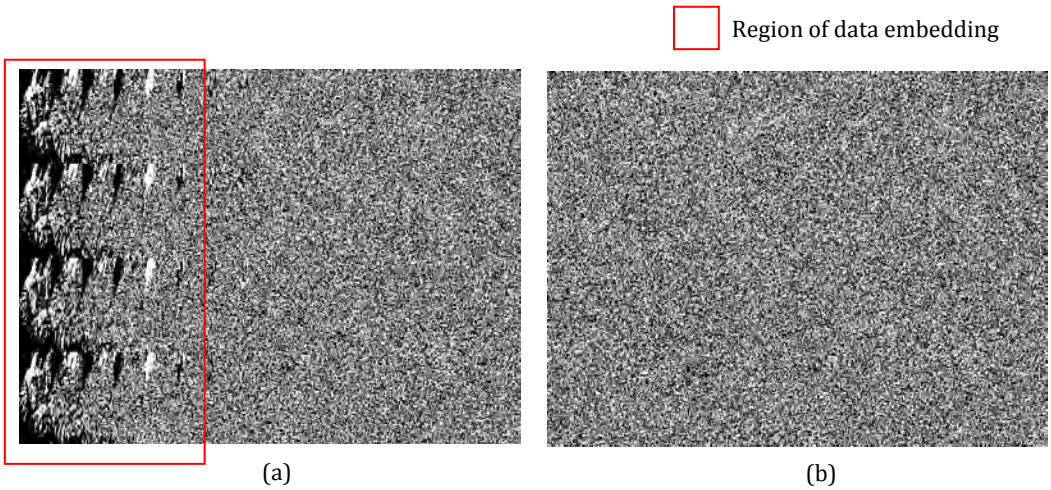

Figure 2-7. LSB plane of stego-image (a) and original cover image (b)

Apart from its high detectability, performing LSB embedding column-by-column has the disadvantage that a key is not required in disagreement with Kerckhoffs' principle, making it a poor system.

An improvement would be to use a pseudo-random number generator (PRNG) to distribute the LSB changes throughout the image spreading the artefacts over the entire plane and making them less obvious. The system now also follows Kerckhoffs' principle since the receiver would not know the path with which data was embedded without the key to the PRNG. However, even this type of LSB embedding has a significant effect on the histogram of the image and can be detected using a histogram attack, also known as a *chi-squared attack* (Westfeld & Pfitzmann, 1999). The effect of LSB embedding on the image histogram is shown in Figure 2-8. LSB embedding has the tendency of evening out adjacent bin heights.

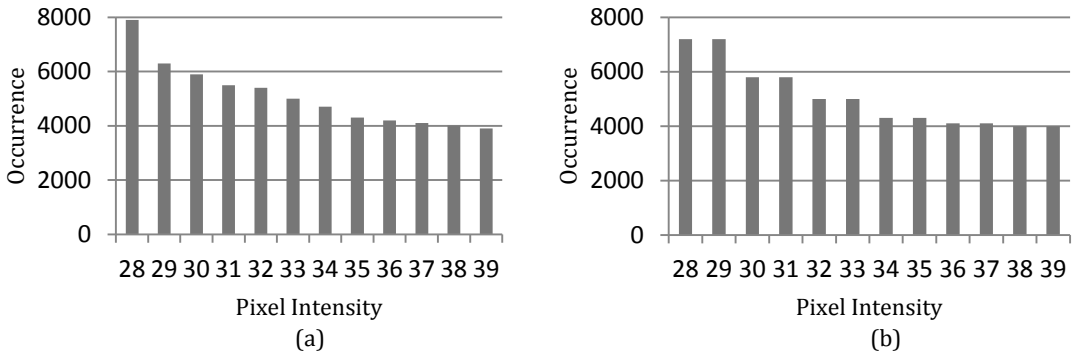

Figure 2-8. Portion of image histogram before (a) and after (b) LSB embedding

One may ask about embedding in bits other than the LSB. Apart from causing more noticeable statistical artefacts, aggressive embedding in higher order bits causes visual problems, namely the *bleeding effect* where the image appears shadow-like due to the obvious changes in pixel intensity. This is shown in Figure 2-9 where five least significant bits are used to carry secret data.

(a) (b)

Figure 2-9. Original cover image (a) and 'bleeding effect' due to too aggressive embedding (b)

Apart from LSB embedding, the second major segment of naïve digital image steganographic methods in the spatial domain involves embedding data while converting true-colour images into palette images using quantisation and dithering (Fridrich & Du, 1999). This concept is powerful but limited since palette images are generally used for computer-generated images where embedding changes can be easily perceived visually. For example, the plain colouring in the eye of Figure 2-10 (taken from (Fridrich & Du, 1999)) shows effects of simple embedding while dithering. Spots of grey and blue can be seen in the white part of the eye on the right.

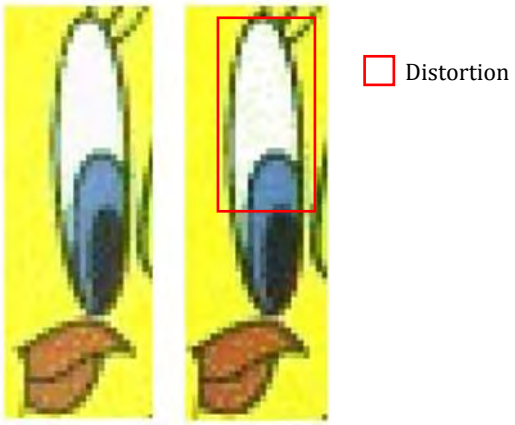

(a) (b)

Figure 2-10. Original image (a) and non-adaptive dithering (b)

While this topic has been extended to more adaptive methods in the papers quoted, it does not appear popular among the research community in recent literature.

2.4.1.3 Complex Spatial Domain Steganography

After naïve steganography became obsolete, the goal of stego-systems became to preserve the statistical distribution of cover images in line with the definition of security by Cahin

(Section 2.3.2). One of the first attempts to do this was to try to camouflage statistical data embedding artefacts by making them mimic the artefacts of some natural processing. The idea is that if the effects of embedding were identical to a natural process, the stego-images would have the same statistical distribution as cover images satisfying the requirement for a perfectly secure system.

One popular example is a stego-system that tries to mimic the multiple noise sources that affect a digital image during acquisition by a camera and which vary from camera to camera (e.g. (Franz & Schneidewind, 2005), (Fridrich & Goljan, 2003)). In this case, it turns out that normally the noise is injected into the images before the analogue to digital converter of the camera. Adding noise to the final image does not have the same effect because the image would already have many complex dependencies among neighbouring pixels as a result of in-camera processing (such as de-mosaicing, colour correction and filtering). These types of problems are common with these systems and are no longer commonly researched.

To attempt to maintain some random statistical properties of a cover image, other popular spatial-domain stego-systems were developed that use secret matrices as keys to scramble and translate the pixels in the spatial domain (e.g. (Tseng, Chen, & Pan, 2002), (Lin & Delp, 1999)). These papers also only measure performance in terms of MSE and are more just randomly-implemented scrambling methods rather than mathematically-justified systems.

Instead of trying to camouflage overall statistical embedding artefacts, techniques emerged from LSB embedding that, rather than blindly inserting data into all pixels, attempted to address common specific statistical artefacts used by steganalysers. For example, one of the most blatant faults of simple LSB embedding used by steganalysers is the inherent asymmetry that shows in the image histogram because an even-valued pixel will always either keep its value or be incremented by one and never decremented, and the converse is true for an odd-valued pixel. Examples of systems that aim to rectify this are presented in (Mielkainen, 2006); namely, *LSB Matching* (*LSBM*) which randomly adds +1 or -1 depending on the message stream, and *LSB Matching Revisited* (*LSBMR*) which uses a pair of pixels to carry information. Both systems provide only a slight to moderate increase in system security. Another system that built on the LSB matching algorithm is introduced in (Negrat, Smko, & Almarimi, 2010). Here, LSB replacement is performed in the YCbCr space rather than the RGB space stemming from the idea that the human eye is much more sensitive to luminance and so the secret message is only embedded in the chrominance portion. While this idea appears to have some

merit, the paper only measures the difference between the stego-image and cover image using the MSE and is thus presented as more naïve rather than realistic.

LSB embedding has experienced renewed popularity as a research topic in *adaptive systems* (also known as *statistics-aware* or *masking*) that attempt to minimise statistical embedding artefacts in an optimised image-by-image manner (e.g. (Yang, Weng, Tso, & Wang, 2011), (Hsiao & Chang, 2011), (Luo, Huang, & Huang, 2010)). The idea is that a given image will have certain areas with a lot of detail and texture, such as those located along edges, with statistical properties similar to those of random data and hence provides redundancy for data embedding. Conversely, there will be image areas that are smooth with consistent statistical trends where embedding will easily disturb the statistics. As explained in (Luo, Huang, & Huang, 2010), simply performing general LSB embedding using a pseudo-random number generator does not consider the relationship between the embedding and the image content and so smooth regions in the cover image will certainly be contaminated after embedding, even at a low embedding rate. In an adaptive system the embedding can be performed optimally in sharp regions for a low to moderate payload, with edges being released adaptively for embedding if necessary. For a very high payload, adaptive systems will begin to use less favourable, smoother regions.

In order to select appropriate regions in the image for embedding, a metric needs to be compiled that measures the favourability of a particular group of pixels. This property is measured against a particular threshold on both the transmitter and receiver side and should take into account correlation between neighbouring pixels and the contents of various lengths of secret data bits. A sizeable amount of literature has been written on the topic of this metric and popularly a measure of complexity (and thus favourability) of a region is taken as the number of different colours it contains, or the number of non-zero DCT coefficients (and hence the energy of the DCT coefficients) ((Solanki, Jacobsen, Madhow, Manjunath, & Chandrasekaran, 2004), (Hedieh & Jamzad, 2010), (Velasco, Nakano, Perez, Martinez, & Yamaguchi, 2009)). Alternatively the idea of using edge detection to identify favourable areas has been presented substantially ((Solanki, Jacobsen, Madhow, Manjunath, & Chandrasekaran, 2004), (Luo, Huang, & Huang, 2010), (Sun, Qiu, Ma, Yan, & Dai, 2010), (Sajedi & Jamzad, 2010)).

One well-accepted adaptive system is called *Bit Plane Complexity Steganography* (BPCS) (Kawaguchi & Eason, 1998). In this technique, the cover image is divided into segments that are classified as *informative* or *noise-like*. Noise-like blocks are ones with a lot of variation

between pixels and are replaced by blocks of secret data. Leading on from this idea, (Kermani & Jamzad, 2005) replaced similar 4x4 blocks in the cover image with secret blocks. The problem with this simplistic approach is that it only analyses a particular block/region itself without looking at surrounding pixels. Therefore, by simply replacing the blocks, virtual edges and corners appear that present detectable global statistical irregularities. In (Sajedi & Jamzad, 2008) this is addressed by considering block texture and neighbourhood information in the metric so that there is less distortion. The papers on these topics, however, tend to focus on minimising the visual distortion and do not test the system performance against steganalysers.

One may wonder how the feature selection criterion for a particular adaptive system is transmitted to the intended receiver. One possibility is to assume that for a particular property, the value of that property compared to a set threshold is what decides whether or not some section of the image is appropriate for embedding. Both the sender and receiver could use this threshold as a test while embedding and extracting. However, it is not guaranteed that the property of the segment after embedding will still lie on the same side of the threshold. Systems assume that this will probably be the case. If not, then the embedded block is left as is, and the same data is embedded into the next block until the embedded segment lies on the same side of the threshold (Luo, Huang, & Huang, 2010). An alternative would be to use what is called *wet paper codes*, introduced in (Fridrich J. , Goljan, Lisoňek, & Soukal, 2004) and used in situations where the recipient is not aware of where data was embedded. In other words, we assume that that the selection rules used by the sender based on side information is not available to an attacker or the recipient. The metaphor of “writing on wet paper” is explained by imagining that some water drops have fallen onto a piece of paper. The sender can only modify the dry regions, but once the paper has dried, the recipient cannot tell which regions were used by the sender. These codes are valuable because they are more secure than systems where the selection rules are publicly available. Apart from adaptive systems, there may be certain areas of a cover image in, for example, sensitive medical or military applications, which cannot be edited. Wet paper codes use a principle from error-correcting in digital communications called *syndrome coding*. The mathematical theory is for this is not explained here but may be read in (Fridrich J. , Goljan, Lisoňek, & Soukal, 2004).

In addition to adapting the stego-algorithm according to the cover image, it may be useful to choose, within reason, the most appropriate cover images from a set. Images with low variation and a low number of colours are poor choices. For example, an image of a cloudless sky over a plain, snowy landscape would be a particularly poor choice as there is hardly any natural statistical variation and statistical anomalies due to embedding would be easily

introduced. Images that are commonly found on the Internet and other public sources are also not favourable as covers as the attacker will have the advantage of being able to compare the stego-object to the original cover object which will inevitably provide the most certain of steganalysis tests. (Hedieh & Jamzad, 2008) emphasise that the ability of steganographers to select an appropriate cover image is an advantage associated with steganography (versus watermarking for example). (Hedieh & Jamzad, 2010) suggest choosing cover images with maximum contrast from the database and even implementing image pre-processing such as sharpening and contrast-improvement on the cover image before data embedding to increase statistical variation. The paper finds that performing pre-processing has an acknowledgeable effect on security for the same level of embedding with security being measured as the resistance of stego-images to detection by a selected handful of blind steganalysers.

2.4.2 Transform Domain Steganography

With time, steganalysis tools became more intelligent and ensuring visual imperceptibility was no longer sufficient to maintain security. In addition to this, image compression became a likely eventuality for cover images especially if they are transmitted using the Internet. Transform domain stego-systems embed into the transform domain representation of images and take both of these factors in account and thus emerged as more relevant than spatial domain systems. This section describes transform domain image representation and, as a side note, covers JPEG compression preliminarily before reviewing transform-based stego-systems as they exist in the literature. The literature review provides a short history and context which then shows the motivation for the creation of cell-based systems.

2.4.2.1 Transform Domain Representation

Instead of representing digital images spatially, they may be represented in some transform domain, the most common of these being the frequency domain. This is analogous to a time domain signal being represented by its constituent frequencies using the Fourier transform. The most commonly-used image transformation between the spatial and frequency domains is the 2-dimensional *Discrete Cosine Transform* (DCT) which is computed over a rectangular group of pixels.

The transform is defined as follows:

Let $f(x,y)$ denote an MxN image segment with x = 0, 1, 2, ..., M-1 and y = 0, 1, 2, ..., N-1. Then the 2-D DCT of f, denoted by F, is defined as:

$$F(u,v) = \sum_{x=0}^{M-1}\sum_{y=0}^{N-1} f(x,y)e^{-j2\pi(\frac{ux}{M}+\frac{vy}{N})} \quad \textbf{2-11}$$

For u = 0, 1, 2,..., M-1 and v = 0, 1, 2,..., N-1 and $(j^2 = -1)$. The frequency domain is simply a coordinate system spanned by $F(u,v)$ with u and v being the frequency variables, analogous to x and y being the spatial variables.

The inverse DCT (IDCT) is defined as:

$$f(x,y) = \frac{1}{MN}\sum_{u=0}^{M-1}\sum_{v=0}^{N-1} F(u,v)e^{j2\pi(\frac{ux}{M}+\frac{vy}{N})} \quad \textbf{2-12}$$

The 5x5-pixel segment of Figure 2-3 and its DCT are shown in Figure 2-11. The DCT coefficients are rounded to the nearest integer.

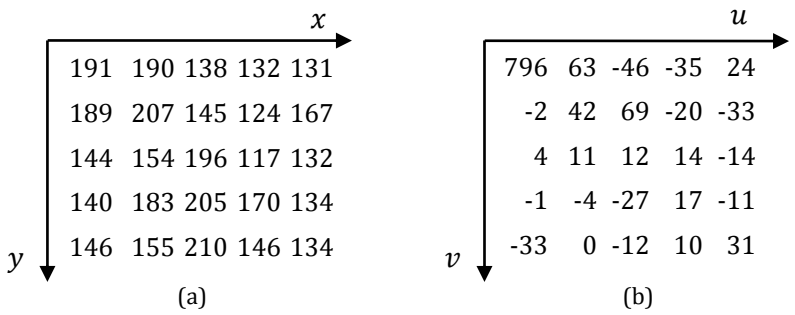

Figure 2-11. 5x5 pixel block in spatial domain (a) and its DCT (b)

The physical significance of the DCT is shown in Figure 2-12 (adapted from (JPEG, 2011)) using an 8x8 block. While in the case of the spatial domain the value in the matrix at each coordinate represents something about colour, in the frequency domain each element represents the extent to which there is variation in pixel intensity values at a particular frequency and direction.

As shown in Figure 2-12, the horizontal and vertical frequencies increase in steps from the left to right and from the top to bottom, respectively. Each step is an increase in frequency by half

a cycle. The top left corner represents the average value of the entire block, commonly termed the *DC coefficient*, with the other coefficients termed the *AC coefficients*. The bottom right coefficient represents the energy in the highest horizontal and vertical frequencies.

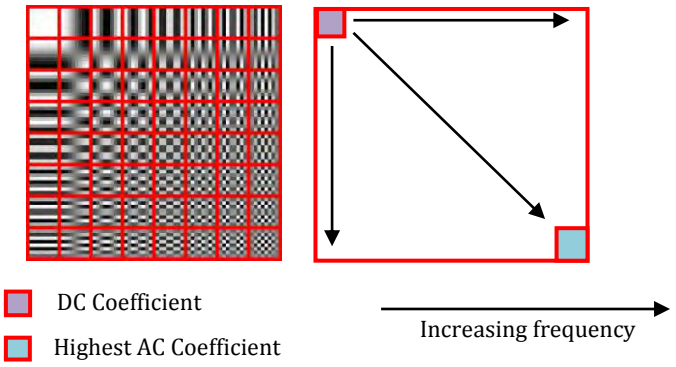

Figure 2-12. Illustration of physical significance of DCT

Effectively, the higher frequency values represent the *detail* in a particular block, whereas the lower frequency values represent the larger-scale features of the block.

This has two primary consequences:

1. Since the larger-scale features are usually more prominent in an image segment, the lower frequency DCT coefficients tend to be larger in size than the higher frequency ones but this depends on the image segment content.
2. Altering low frequency DCT coefficients is more noticeable visually and statistically than high frequency coefficients. Take as an example the three images in Figure 2-14 which shows versions of the earth in Figure 2-13 where DCT information has been altered. First, assuming the entire image to be one block, the DCT is taken. The size of the image is 225x225. Taking the bottom right 80x80 block of DCT coefficients and setting them to 0 corresponds to removing around 13% of the high frequency detail of the image and results in (a) which is visually indistinguishable from the original because the human eye is insensitive to the detail in the image. Image (b) results when the bottom right 200x200 block of DCT coefficients is set to 0 which corresponds roughly to removing 80% of detail. The main effect is that the image becomes more blurry but is still relatively natural looking. In image (c), the top left 2x2 square of high frequency DCT coefficients are reduced by 10 which results in a dramatic effect on the image colouring.

Figure 2-13. Original example image

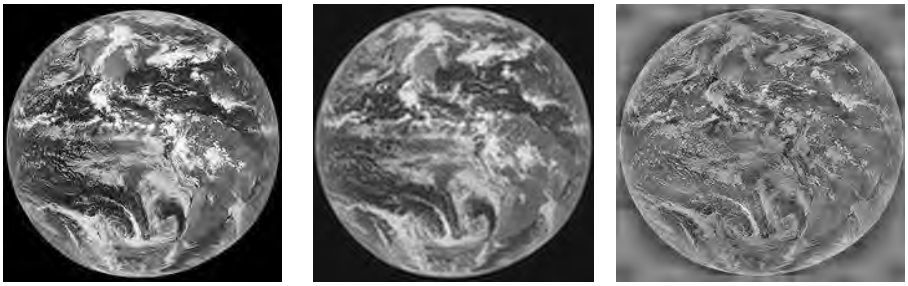

(a) (b) (c)

Figure 2-14. Example image Figure 2-13 with 13% of highest frequency DCT coefficients set to 0 (a), 80% of highest frequency DCT coefficients set to 0 (b) and 4 lowest frequency DCT coefficients reduced by 10 (c)

Even relatively small changes in lower frequency coefficients are noticeable and the lower the frequency of coefficients being altered the more obvious the alterations.

It is important that the reader understand that the DCT is an operation whose result represents the characteristics of a block as a whole. It is not in any way a mapping between a spatial intensity at a particular coordinate and a DCT coefficient and depends on the block over which the DCT is taken. For example, as illustrated in Figure 2-15, if the DCT of blocks A and B are taken individually, the DCT coefficients in the region of overlap will not be the same, because the transform does not associate a particular transform value to a spatial coordinate.

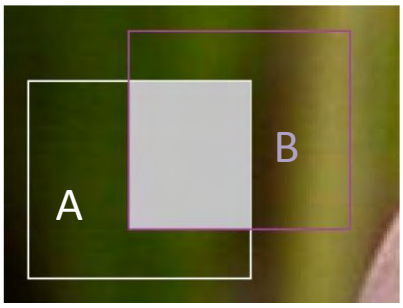

Figure 2-15. Sample of an image with two overlapping blocks over which the DCT could be taken

Similarly, changing a single coefficient in the transform domain representation will affect the entire block in the spatial domain. The idea that embedding in the transform domain spreads

the embedding effects over an image spatially was one of the main reasons that lead to the development of transform-based data hiding.

Finally, it should be noted that when there is any conversion between the spatial and transform domain of an image or image segment, if any decimal places occur (which they usually do) rounding has to take place because only integer values are accommodated resulting in the DCT and IDCT of an image not being exactly reversible processes.

2.4.2.2 JPEG Compression

The DCT has a direct connection to JPEG compression and a small detour is now made to explain the compression algorithm, required by the reader to follow the discussion on transform-based stego-systems.

The human visual system is insensitive to changes in the detail of an image (as seen in Figure 2-14) and the JPEG compression schemes takes advantage of this. It first uses the DCT to separate out the detail in an image from the macro visual characteristics. The use of the DCT then allows the JPEG scheme to remove detail from the image thus compressing it with minimal visual effect.

The steps of JPEG compression are:

1. **Colour transformation**

   If the image is grey scale, no colour transformation is performed. If the image is RGB, then it is converted to the YCbCr space using Equation 2-10.

2. **Division into blocks**

   Recall that grey scale images have only one plane whereas YCbCr images will have three image planes. Each plane is compressed separately and first subdivided into non-overlapping 8x8 pixel-size blocks as shown in Figure 2-16.

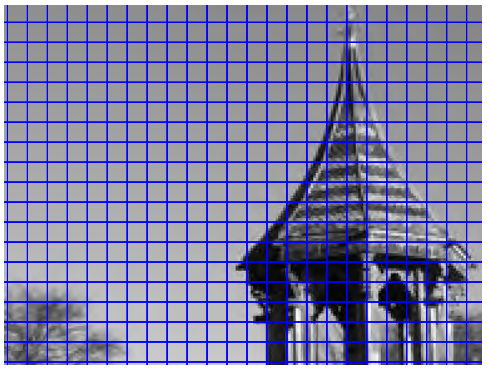

Figure 2-16. Image showing 8x8 grid blocks used during JPEG compression

3. **Scaling**

   If m is the number of bits used to represent each pixel (usually 8), each pixel intensity value is shifted down by subtracting 2^{m-1}. This reduces the average intensity of the block making the DC DCT coefficient smaller and assisting in compression.

4. **DCT Transform**

   The 2-D DCT of each block is taken. The convention taken here is that the DCT coefficients are rounded to the nearest integer since an image is normally represented by only integers.

5. **Quantisation**

   The DCT coefficients are quantised by dividing them by an integer and rounding the result. This is the step where data corruption occurs since loss due to rounding cannot be retrieved again.

6. **Encoding and lossless compression**

   The elements in each 2-D 8x8 grid block are then reordered according to a zigzag pattern shown in Figure 2-17.

1.	2.	6.	7.	15.	16.	28.	29.
3.	5.	8.	14.	17.	27.	30.	43.
4.	9.	13.	18.	26.	31.	42.	44.
10.	12.	19.	25.	32.	41.	45.	54.
11.	20.	24.	33.	40.	46.	53.	55.
21.	23.	34.	39.	47.	52.	56.	61.
22.	35.	38.	48.	51.	57.	60.	62.
36.	37.	49.	50.	58.	59.	63.	64.

Figure 2-17. Zigzag ordering used during JPEG

   The resultant 1-D array then undergoes run-length encoding and Huffman encoding.

The integer value by which a DCT coefficient is divided in step (5.) above is given by an 8x8 quantisation matrix $Z(u, v)$. The JPEG standard (JPEG, 2007) published an empirically-determined standard 8x8 quantisation matrix shown in Figure 2-18. The quantisation matrix is shared by the transmitter and the receiver as part of the final compressed file.

16	11	10	16	24	40	51	61
12	12	14	19	26	58	60	55
14	13	16	24	40	57	69	56
14	17	22	29	51	87	80	62
18	22	37	56	68	109	103	77
24	35	55	64	81	104	113	92
49	64	78	87	103	121	120	101
72	92	95	198	112	100	103	99

Figure 2-18. Standard JPEG quantisation matrix ($Z(u,v)$)

The process of scaling and quantising is described in Equation 2-13.

$$\hat{T}(u,v) = round\left(\frac{T(u,v)}{Z(u,v)}\right) \qquad \textbf{2-13}$$

where $T(u,v)$ is an 8x8 integer matrix of the original DCT coefficients in the image block. The function $round(x)$ represents the operation of mapping x to its nearest integer. $\hat{T}(u,v)$ is a matrix of the resultant coefficients at each location (u,v) within the block after scaling and rounding. Define $z(u,v)$ to be an element from $Z(u,v)$, $t(u,v)$ to be an element from $T(u,v)$ and $\hat{t}(u,v)$ to be an element from $\widehat{T}(u,v)$.

In the case that the input image is colour, it is always transformed to the YCrCb colour space and the Y (luminance) plane is compressed using the above quantisation matrix while the Cb and Cr (chrominance) planes use a different quantisation matrix. Whereas in RGB images the human eye is equally sensitive to all three colour components, the human eye is much more sensitive to luminance than chrominance. Therefore, converting the image to YCbCr space allows more compression because the two chrominance planes can be compressed much more than the luminance plane.

As discussed earlier in this section, it is expected that for higher frequency coefficients, $t(u,v)$ will be smaller than for low frequency coefficients. Further, since $z(u,v)$ increases as frequency increases, high frequency $\hat{t}(u,v)$ will tend to be small (usually 0) because in Equation 2-13 the numerator will be small while the denominator will be large. The reason for reordering the array in step (6.) is so that the resulting array is qualitatively ordered in increasing spatial frequency and thus it is expected that long runs of zeros will exist at the end of it. Run-length encoding takes advantage of this because it does not store the 0's. The result

after run-length encoding then also undergoes Huffman coding which provides further compression.

To decompress the image, the operations described for compression are reversed with the exception of de-quantisation where Equation 2-14 is applied.

$$T'(u,v) = \hat{T}(u,v).Z(u,v) \quad \textbf{2-14}$$

where $T'(u,v)$ is the matrix of retrieved estimates of the original DCT coefficients. The information lost during rounding in Equation 2-13 cannot be recovered, making JPEG compression lossy.

A DCT coefficient $t(u,v)$ will be unchanged (i.e. $t'(u,v) = t(u,v)$) only if it is originally an integer multiple of $z(u,v)$ and therefore no rounding occurs for that coefficient.

The amount of loss experienced by each DCT coefficient due to rounding is at most $\lfloor z(u,v)/2 \rfloor$, i.e.

$$|t'(u,v) - t(u,v)| \leq \lfloor z(u,v)/2 \rfloor \quad \textbf{2-15}$$

To illustrate this, consider the case of $z(u,v)$ being even e.g. 10. If the value of the DCT coefficient is divided by 10, the remainder will be in the range [1-9]. For remainders [1-4], the value of the DCT coefficient will be rounded down giving a rounding loss of up to 4. For remainders [5-9], the DCT coefficient value will be rounded up by up to 5 by the compression process. It is clear then, how the movement in the coefficient value is limited to the maximum amount by which it can be rounded up or down, which is half of number you are dividing by. If $z(u,v)$ is odd e.g. 11, for remainders [1-5], the coefficient will be rounded down, and for remainders [6-10], the coefficient will be rounded up. Overall, the maximum movement from the original value is limited by 5. The extent to which an image is compressed (which also corresponds to the extent to which the compression process is lossy) depends on the size of $z(u,v)$. Because $z(u,v)$ is larger for higher frequency DCT coefficients, these coefficients tend to undergo larger changes in value due to JPEG compression than lower frequency ones.

The JPEG compression standard allows for a quality factor Q_{JPEG} $(1 \leq Q_{JPEG} \leq 100)$ which corresponds to the amount of compression an image undergoes. The lower the quality factor, the higher the level of compression and the smaller the resultant file size, but the more

noticeable the visual artefacts after decompression. The level of compression is related to $Z(u,v)$ and associated with each quality factor is a particular quantisation matrix.

At $Q_{JPEG} = 50$, the quantisation matrix used is the standard one given in Figure 2-16. Apart from the quantisation matrix in Figure 2-16, the JPEG standard does not explicitly define the quantisation matrices for each quality factor; rather, this is left to the discretion of the designer and varies between image processing programs (Hass, 2008). The guidelines for designing the quantisation matrix are that the values in the matrix should be such that the required grade of compression is achieved with minimum visual distortion, which means that the higher frequency $z(u,v)$ should be larger so that those coefficients are reduced more ruthlessly. In this dissertation, the library used to provide quantisation matrices is taken from the commonly used (Sallee P. , 2003). To contrast with the standard quantisation matrix, two more at quality factors of 70 and 30 are shown in Figure 2-19. Notice that for a smaller quality factor $z(u,v)$ is larger at all frequencies.

10	7	6	10	14	15	31	37	27	18	17	27	40	67	85	102
7	7	8	11	16	35	36	33	20	20	23	32	43	97	100	92
8	8	10	14	24	34	41	34	23	22	27	40	67	95	115	93
8	10	13	17	31	52	48	37	23	28	37	48	85	145	133	103
11	13	22	34	41	65	62	46	30	37	62	93	113	182	172	128
14	21	33	38	49	62	68	55	40	58	92	107	135	173	188	153
29	38	47	52	62	73	72	61	82	107	130	145	172	202	200	168
43	55	57	59	67	60	62	59	120	153	158	163	187	167	172	165
			(a)								(b)				

Figure 2-19. JPEG quantisation Q_{JPEG}=70 (a) and Q_{JPEG}=30 (b)

To illustrate the effectiveness of JPEG compression, consider the image of the cameraman given in Figure 2-20. If the image is compressed and subsequently decompressed for Q_{JPEG} = 80, 10 and 5, the results are shown in Figure 2-21. The ratios of the size (in bytes of data) required to represent the decompressed image, to the size of the original image, are given in Table 2-1.

Figure 2-20. Sample image

(a) (b) (c)

Figure 2-21. Decompressed images using JPEG compression with Q_{JPEG}= 80 (a), 10 (b), 5 (c)

Table 2-1. Compression ratio corresponding to a JPEG quality factor

Q_{JPEG}	$\frac{Number\ of\ Bytes\ Required\ to\ Represent\ Compressed\ Image}{Number\ of\ Bytes\ Required\ to\ Represent\ Original\ Image}$
80	0.1376
10	0.0303
5	0.0182

Table 2-1 and Figure 2-21 show that even when compressing the image to less than one seventh of its original size as in the case of $Q_{JPEG} = 80$, there is no recognisable visual distortion.

Depending on the stage in which data is embedded in a JPEG image, error coding may or may not be required. If the data is hidden in the DCT coefficients after they are quantised during JPEG compression, then there will be no loss in the hidden message and no error coding requirement. If data is hidden in the image before lossy quantisation, error coding will be necessary.

A more recent version of JPEG compression called *JPEG2000* uses the discrete wavelet transform (DWT) instead of the DCT. As explained in (Su & Kuo, 2003) and (Cheddad, Condell, Curran, & McKevitt, 2010), this method of compression is more efficient and outperforms the DCT in many aspects. However, the papers introducing this concept date to before 2003 and no significant amount of research has since been output in this field. This may be credited to

the fact that DCT-domain JPEG compression is well-established, suffices for many applications and is the predominant form of JPEG compression on the Internet.

2.4.2.3 Complex Transform Domain Steganography

Now that transform domain image representation and JPEG compression have been covered, a review of transform domain steganography can be performed. Although spatial domain digital image steganography is still being investigated in the literature, it is not as relevant anymore because spatial domain schemes do not cater for the likely event of an image undergoing JPEG compression. Since JPEG compression involves the generation and manipulation of DCT coefficients, transform-based stego-systems that embed in the DCT coefficients of an image lend themselves naturally to catering for possible JPEG compression and in fact the first transform-based systems were designed specifically to embed into JPEG images.

The first stego-systems developed to embed into images during the JPEG compression process did so after quantisation so there was no error coding requirement. The first of this kind was *Jsteg* (Upham, 1993). Extending on LSB embedding, it hides information by performing LSB embedding in quantised DCT coefficients after step (5.) in Section 2.4.2.2, with the exception of embedding into 0's, 1's and DC coefficients as doing this introduces disturbing statistical artefacts used commonly by steganalysers. Editing the LSBs indiscriminately changes the marginal statistics (histograms) of the DCT coefficients in the same way as explained in Section 2.4.1.2 for the spatial domain and is detected using the chi-squared attack. This is documented by (Chandramouli & Subbalakshmi, 2003).

A method that was developed next to overcome this shortcoming is called *F5 embedding* (Westfeld, 2001). Instead of LSB flipping, the absolute value of the quantised DCT coefficient is decremented by one along a pseudo-random path through the cover image. By changing the absolute value of the image rather than blindly tweaking the LSB, the natural shape of the DCT histogram is preserved and the cover image appears, after embedding, simply as if it was initially compressed with a lower quality factor. In addition to this, F5 also uses *matrix embedding* which implements a block-code-type system to minimise the number of embedding changes made to the cover image with the trade-off that relative payload decreases. There exists a matrix embedding theorem that states how to transform any linear code into a matrix embedding scheme, the details of which are beyond the scope of this dissertation and are not explained here. This approach is more resistant to visual and first-order statistical attacks as it preserves the natural distribution of the DCT coefficients, and allows higher capacity for the same security when compared to Jsteg. However, F5 still

changes the histogram in a detectable way as shown by (Fridrich, Goljan, & Hogea, 2003) and (Dabeer, Sullivan, Madhow, Chandrasekaran, & Manjunath, 2004) and can be detected by comparing the stego-image histogram to an estimate of the original histogram. The original histogram is estimated using a self-calibrating method: the JPEG stego-image is decompressed and cropped by a few pixel rows or columns in order to desynchronise it from the original JPEG grid. If this cropped image is then recompressed, the statistical properties of the resultant image are similar to those of the original cover image and can be compared to the suspicious stego-image (Fridrich, Goljan, & Hogea, 2003).

Another system, *OutGuess* (Provos, 2000), was the first system whose goal was specifically to match the DCT histogram of the cover image. It embeds messages into the cover image by slightly changing the quantized DCT coefficients using two runs. Firstly, the message bits are embedded into a pseudo-random set of DCT coefficients. In the second run, corrections are made to other DCT coefficients in order to match the stego-image histogram with that of the cover image. So if a particular coefficient is changed from histogram bin A to B during embedding, the correction for this would be to move another coefficient from bin B to A. OutGuess uses about half of the coefficients for embedding and the other half for correcting statistical deviations. This technique is effective in maintaining the DCT coefficient histogram but reduces the effective capacity by half and can be broken by second order statistical analysis (Hetzl & Mutzel, 2005).

Steghide, introduced in (Hetzl & Mutzel, 2005), also preserves global first-order statistics of DCT coefficients using a different mechanism to OutGuess. Coefficients are swapped rather than having their LSB modified.

Another proposed system is called *Model-Based Steganography* (Sallee P. , 2004) which assumes a more abstract mathematical approach that edits coefficient values with the primary goal of maintaining the original statistical composition of the coefficients. (Fridrich J. , Goljan, Lisoňek, & Soukal, 2004) present an approach that uses *perturbed quantisation* where the way in which quantisation of the DCT coefficients occurs is slightly perturbed to embed secret message bits. (Solanki K. , Sullivan, Madhow, Manjunath, & Chandrasekaran, 2005) and (Solanki K. , Sullivan, Madhow, Manjunath, & Chandrasekaran, 2006) introduce mathematical schemes that match the DCT histogram of the stego-image to that of the cover image exactly, providing provable security only if the steganalyst uses properties of the DCT histogram for detection.

Adaptive embedding in the frequency domain developed from the discussed schemes is not a well-developed topic in contrast to the spatial domain. Typical examples include (Kumar, Raja, Chhotaray, & Pattnaik, 2010) where varying amounts of bits are embedded in coefficients depending on their size, and (Velasco, Nakano, Perez, Martinez, & Yamaguchi, 2009) which uses the energy of the DCT coefficients as a metric.

Stego-systems may also use the compression process itself to embed information. For example, (Guo & Le, 2010) uses various quantisation tables for different regions of the JPEG-compressed image to provide information that achieves satisfactory performance while simplifying the embedding process.

2.4.2.4 Cell-Based Systems

So far, the stego-systems have focused on hiding data with the purpose of camouflaging some statistical artefacts of embedding. In general, blind statistical steganalysis schemes have been very successful in detecting these types of stego-systems.

As explained in (Solanki, Sarkar, & Manjunath, 2007), the elements that contribute to the success of blind steganalysers are:

- **Self-calibration mechanism**

  With this mechanism, the blind steganalysers make an estimate of the original statistics of the cover image. In the case of JPEG images, the self-calibration technique of cropping and recompressing the image mentioned earlier is used.
- **Features capturing cover memory**

  Some steganographic systems hide data symbols rather than individual bits and the blind steganalyser can use any known statistical properties of the symbol bits to detect trends in statistical changes. Cover memory has been shown to be an important feature (Sullivan, Madhow, Chandrasekaran, & Manjunath, 2006) and has been incorporated into the feature vector for training (e.g. (Fu, Shi, Zou, & Xuan, 2006), (Shi, Chen, & Chen, 2006)).
- **Powerful machine learning**

  The existence of powerful machine learning techniques combined with training over several thousand images often ensures even slight statistical variations become learned by the analyser.

The most prominent of the above elements is the ability of the blind analyser to use certain assumptions about the image to get a model of the innocent cover image despite not having access to it and even though no universal statistical model for images exists.

To address this, (Solanki, Sarkar, & Manjunath, 2007) suggest that instead of the approach used by stego-systems so far to try to *maintain* statistical features of the cover image, a steganographer can take the approach of attempting to *distort* the blind steganalyst's estimate of the innocent cover image statistics in two ways:

1. **Hiding with high embedding strength**

   Instead of minimising embedding artefacts, if embedding is performed so that the cover image is so distorted that cover image statistics can no longer be derived then detection will be more difficult for the blind steganalyser. (Kharrazi, Sencar, & Memon, 2006) show that this is possible.

2. **Randomised hiding**

   If the embedding approach is randomised then the steganalyst cannot make any consistent assumptions regarding how data has been hidden even if the stego-algorithm is known as per Kerckhoffs' principle.

The danger of the first approach above is that the likelihood of embedding artefacts being visually perceptible is high and it's possible the image can be detected by a steganalyst with a universal image model even if it is very rough. The second approach is more appealing and (Solanki, Sarkar, & Manjunath, 2007) explore the first simplest implementation of this by randomising the locations where data is hidden in an image. This implementation is called *Yet Another Steganographic System* (YASS) and is the earliest of the *cell-based systems* so called because embedding occurs in certain randomly-selected blocks/cells in an image.

In addition to the randomised approach to embedding, cell-based systems embed into an image before the lossy stage of JPEG compression which further disguises embedding artefacts since the analyser would examine the stego-image after compression. This also means error coding is required to cater for lossy JPEG compression. (Huang, Huang, & Qing Shi, 2010) and (Fridrich & Kodovsky, 2008) say YASS is arguably one of the most promising transform domain-based systems to date and the security of this method against advanced blind steganalysis systems has gained attention in the research community in the past two years (e.g. (Li, Huang, & Shi, 2009), (Huang, Huang, & Shi, 2010)). Only one other paper (Sajedi & Jamzad, 2010) was found that uses the philosophy of randomising where data is hidden but YASS has gained much more interest and is the focus here.

The input image to YASS is grey scale or, if not, the Y plane is extracted and used to carry secret data since it is the least-aggressively compressed plane during JPEG compression resulting in lower errors.

An overview of the steps of YASS is:

1. **Error Coding of Secret Message**

   The secret message bits are first encoded using a repeat-accumulate (RA) code. RA coding is explained further later.

2. **Blocking of the Image**

   The image in the spatial domain is divided into blocks called *B-blocks* of size BxB, B>8. B is random across images but is fixed for any given image. B ranges typically from 9 to 14 but there are no limitations set explicitly by the literature. Within each B-block, an 8x8 *E-block* is chosen, the position of which is selected pseudo-randomly. The location of these sub-blocks is transmitted in the key along with the value of B. Figure 2-22 shows this for an image segment where B=10. In this dissertation, this procedure will be called the BLOCKING phase.

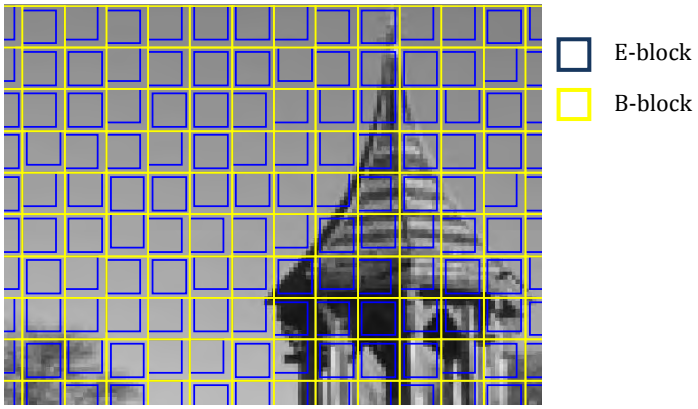

Figure 2-22. YASS grid

3. **DCT Transform**

   The 2-D DCT of each E-block is performed. Any resultant DCT coefficients with decimal places are rounded.

4. **Embedding of Secret Message**

   The encoded message bits are embedded in the DCT coefficients of the E-blocks using Quantisation Index Modulation (QIM). QIM is explained further later. Only the first 19 AC DCT coefficients (labelled in zigzag order) are candidates to carry data. All DCT coefficients that could become 0 as a result of embedding are skipped.

5. **IDCT Transform and Block Replacement**

   Once the DCT coefficients have been altered to contain data bits, the 2-D IDCT of the E-blocks is taken. Any resultant pixel intensities with decimal places are rounded. The E-blocks are replaced back in the image. Steps (3.) to (5.) together form the EMBED phase.

The image is then expected to be compressed using JPEG with an advertised quality factor Q_a to obtain the stego-image. This will be referred to as the COMPRESSION phase. This expectation is not part of the steganography, it is merely an expectation that the embedding scheme anticipates and accommodates.

Figure 2-23 shows again the steps of data embedding in E-blocks in YASS.

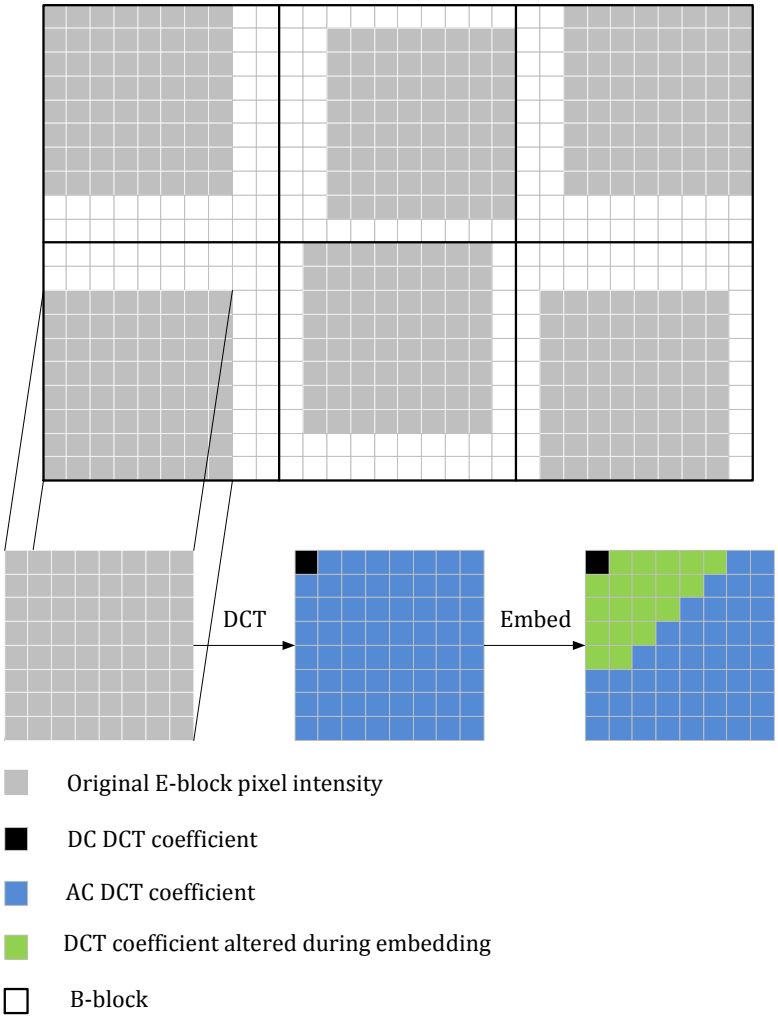

Figure 2-23. BLOCKING and EMBED phases

Further explanation regarding the details of data embedding and error correcting in steps (1.) and (4.) are given next.

Error Coding of Secret Message

In step (1.) above, RA coding is incorporated to cater for lossy JPEG compression. It is a simple coding scheme where the input message (a finite length bit stream) is repeated N times, scrambled in a pseudo-random way and then encoded using an accumulated sum.

This means, if the repeated, scrambled bit stream is $u_1 u_2 \dots u_K$ the output accumulated bit stream t is

$$\begin{aligned} t_1 &= u_1 \\ t_2 &= t_1 \oplus u_2 \\ t_n &= t_{n-1} \oplus u_n \end{aligned} \qquad \textbf{2-16}$$

The code is normally decoded in what is known as a sum-product algorithm in a factor graph which is beyond the scope of this dissertation. The ratio of the number of data bits versus the total amount of bits being transmitted is known as the code rate and in the case of RA codes is $1/N$. In (Solanki, Sarkar, & Manjunath, 2007), a repetition of between 10 and 40 is used for the image database on which testing for YASS was done. Errors are detected and corrected by analysing the bit values across the various iterations.

Embedding of Secret Message

In step (4.) above, QIM (Chen & Wornell, 2011) is used to embed data into the DCT coefficients. Mathematically, the value of the coefficient after QIM is given by Equation 2-17.

Let $F(u, v)$ be the value of the E-block DCT coefficient,

$$QIM\big(F(u,v)\big) = \begin{cases} 2\Delta \left\lfloor \dfrac{F(u,v) + \Delta}{2\Delta} \right\rfloor for\ embedding\ '1' \\ 2\Delta \left\lfloor \dfrac{F(u,v)}{2\Delta} \right\rfloor + \Delta\ for\ embedding\ '0' \end{cases} \qquad \textbf{2-17}$$

QIM is easier to understand visually. It involves creating overlapping quantisers as shown in Figure 2-24. Each quantiser represents a bit value ('0' or '1'). During embedding, the DCT coefficient is rounded to the nearest point from the quantiser of the bit to be embedded. The spacing between two points of the same lattice is delta (Δ). A DCT coefficient value can be changed by up to delta during embedding and so qualitatively we can see that delta should be kept as small as possible to prevent large changes to DCT coefficients and embedding artefacts.

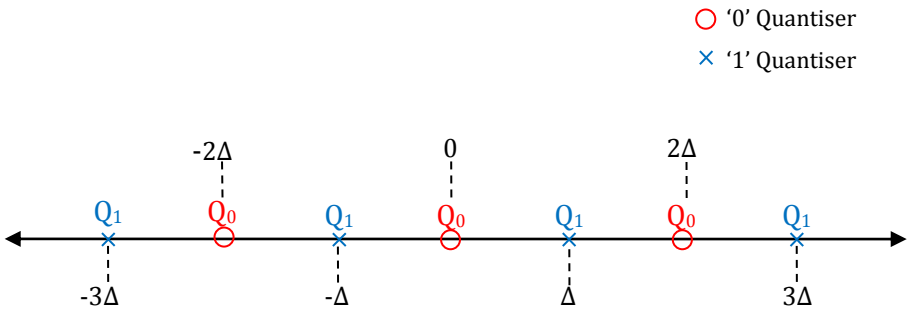

Figure 2-24. Lattices to embed one-bit data using QIM

While the DCT coefficient values before embedding exist on a continuous scale, after embedding they exist at lattice points. During subsequent lossy JPEG compression and decompression it is expected that the DCT coefficient values will change from their embedded values as shown in Figure 2-25.

The receiver makes a decision on the message bit hidden in a particular DCT coefficient by assuming that the DCT coefficient value changed such that out of all lattice points it still remains closest to its original embedded value. So it makes a decision based on the proximity of the retrieved coefficient value to a lattice point. For example, if it is closer to a lattice '0' point, it is assumed that a '0' was embedded. Thus, the correct message bit is extracted from a coefficient provided that the coefficient has shifted during the JPEG compression/decompression by less than Δ / 2 from its original value. Therefore, Δ must be chosen to be large enough so that movement is accommodated by the lattice spacing.

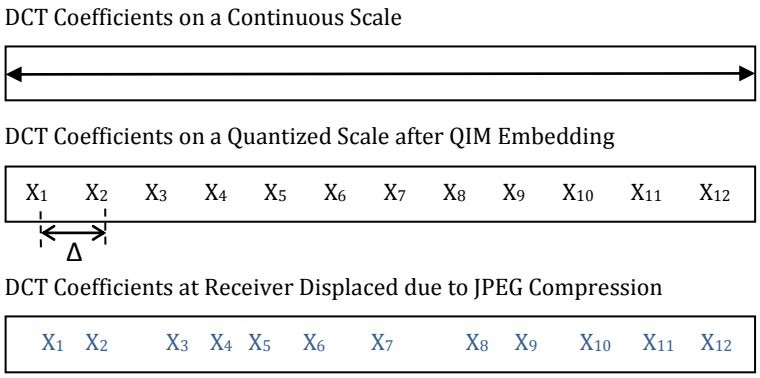

Figure 2-25. QIM data embedding and retrieval

The change in data carrying E-block DCT coefficient value between QIM embedding and QIM de-embedding is caused by two things:

1. Rounding after each conversion between the transform and spatial domains during the EMBED phase. This is because the image representation does not accommodate decimal places.
2. The effects of JPEG compression during the COMPRESSION phase, namely the harsher treatment of higher frequency coefficients.

Out of the two causes of change in value of the data carrying DCT coefficients, rounding can cause absolute value change of 1, while the effects of JPEG compression are much more profound. The exact extent to which JPEG compression causes the data carrying DCT coefficient value to change is required to determine an appropriate QIM system and is investigated in Chapter 3.

Roughly speaking, since higher frequency coefficients experience more error (change in value) due to JPEG compression, it would make sense to use a larger delta for these coefficients than for low frequency ones. The values of delta used by YASS have purposefully not been explained here because some further knowledge is required before this is understood by the reader and therefore will be referred to in the next chapter where for now only the concept is important.

It was stated that during the EMBED phase, not all of the 19 candidate AC DCT coefficients in an E-block are necessarily used to carry data. Specifically, candidate coefficients in the range $(-\Delta, \Delta)$ are at risk of being quantised to 0 during embedding and so are rejected. This is to prevent the embedding scheme from changing the number and distribution of DCT coefficients of value 0 which has been used previously as a statistical artefact for detection by steganalysers. In this dissertation, the requirement that a candidate E-block DCT coefficient be outside the range $(-\Delta, \Delta)$ in order to be selected to carry data will be referred to as *selection criteria*.

Embedding into the DC DCT coefficient is also forbidden to prevent statistical boundaries in variation of average colour that can be easily detected by analysers. In Figure 2-26, the DC coefficient in a block was decreased by 10, and clear visual (and thus also statistical) boundaries exist, providing an obvious give-away embedding artefact that should be avoided.

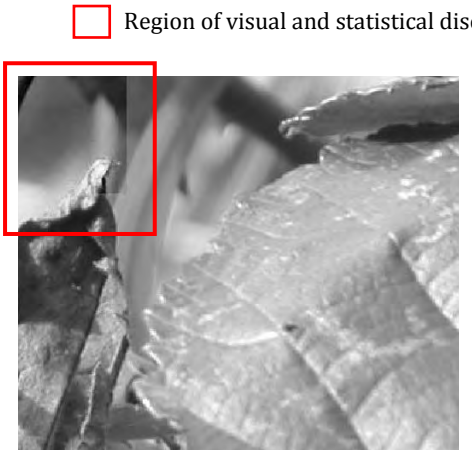

Figure 2-26. Sample image with clear artefacts of alteration of DC DCT coefficient

Even though it has many good properties, YASS has certain shortcomings:

1. While YASS has good strength against blind steganalysers, it has since been cracked using a targeted approach ((Li, Huang, & Shi, 2009), (Xiaoyi & Babaguchi, 2008)). This is because a steganalyser can calculate the possible positions of an E-block within its parent cell, especially if B is known. In addition to this, two blind steganalysers have been developed that can detect YASS ((Pevny & Fridrich, 2007), (Pevny & Fridrich, 2006)).
2. YASS has a low embedding capacity, firstly because a significantly smaller portion of the image is used for embedding (19 or less coefficients out of a possible 64 in each E-block) and secondly because using RA coding requires a high number of redundant bits. The purpose of YASS was not to address data embedding and error correcting schemes in detail but rather to present the idea of randomised embedding for increased security.

As an improvement to YASS, (Sarkar, Solanki, & Manjunath, 2008) suggest changing embedding parameters and testing security assuming the JPEG decorrelation mode of attack iteratively until parameters are found that minimise error rate thus maximising embedding capacity. The success of this approach is studied in (Huang, Huang, & Shi, 2010) and it is found to provide only moderate improvement in security and embedding capacity. It is also clumsy and time-consuming for the steganographer.

To further improve security, (Yu, Zhao, Ni, & Shi, 2010) present a YASS-like system with one extra degree of randomisation, namely where B can vary within an image thus introducing more uncertainty in E-block position which reduces the detection rate. (Dawoud, 2010) takes the idea of variable cell size even further by randomising the size of both the B-blocks and the

E-blocks as shown in Figure 2-27. At this point we define E-blocks to be of size ExE, and for this stego-system 8<E<12 and 9<B<14.

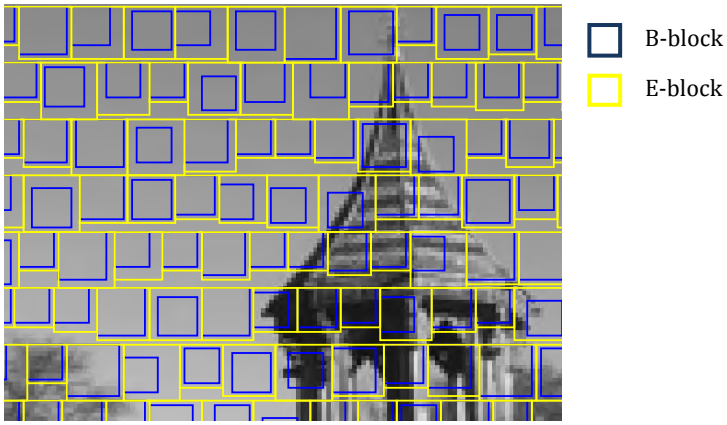

Figure 2-27. MULTI grid

(Dawoud, 2010) calls this the *MULTI* scheme and it is the most general and secure of the cell-based systems. The complexity of steganalysis is increased by two orders over YASS because the large block size, B, is unknown. (Dawoud, 2010) shows that for conditions where YASS is detectable, the detection rate of MULTI is reduced to close to 0.5, making it highly secure even against the most advanced blind analysing system. The MULTI scheme has not yet been published formally or successfully attacked.

2.5 Discussion of Cell-Based Systems

Cell-based systems are distinguished from previous stego-systems by the concept of randomisation for security to confuse blind steganalysers rather than attempting to camouflage embedding artefacts. MULTI is more secure compared to YASS because the blocking scheme is more random, reducing the certainty with which a blind steganalyser makes assumptions regarding the embedding process. Even though MULTI addresses security requirements, it has not rigorously addressed the relatively low embedding capacity associated with all stego-systems in the cell-based system family.

The two primary elements that detract from embedding capacity are:

1. The entire image is not used for embedding, but only image areas in the E-blocks. Within an E-block, only the lowest 19 AC DCT coefficients that meet selection criteria are used to carry data.
2. Due to lossy JPEG compression, the image data will be corrupted which could result in the retrieval of incorrect secret message bits. To cater for this, error correcting codes need to be applied which use redundant overhead bits to detect and correct erroneous bits. The

inclusion of these overhead bits further reduces the number of information bits that can be accommodated.

The two data handling issues presented above have not been rigorously addressed in the literature so far. It should be noted that the focus of the literature around cell-based systems has not been on embedding capacity in particular and so no claims have been made that the used data handling systems are optimal.

In particular, the values of delta using during QIM for YASS and MULTI have been estimated simplistically. Given the effect of JPEG compression, it is expected that as coefficients increase in frequency a larger delta for QIM would be required since they are likely to experience more error. YASS does use larger delta for higher frequency coefficients (the details will be referred to in Chapter 3) but the suitability of the delta values was not analysed.

Regarding the number of DCT coefficients considered for embedding, there is no evidence that only the first 19 low frequency coefficients are appropriate, and it is viable to suspect more vulnerable higher frequency coefficients may provide increased embedding capacity if the correct error coding is used. (Sarkar, Nataraj, Manjunath, & Madhow, 2008) suggest analysing the potential of different E-block coefficients to carry data but do not take the idea further.

There is no evidence that RA coding is the most efficient in terms of embedding capacity and to the contrary the code rates appear low compared to other possible coding schemes. The choice of code rates is also made based on characteristics of image segments or entire images which considering the effect of JPEG compression appears to be inefficient. To illustrate this, consider that within any image segment, different frequencies of DCT coefficients will be treated differently by JPEG compression. More specifically, higher frequency DCT coefficients will experience more change in value due to JPEG compression than lower frequency coefficients according to the principles of JPEG that state the visual integrity of the image should be preserved. Therefore, the likelihood and concentrations of errors in the DCT coefficients will vary across a segment. At first sight it seems inefficient to design one coding scheme to cater for the wide range of error in different parts of the image segment. These issues regarding effective data embedding and error coding are discussed in detail in the next chapter.

2.6 Summary

This chapter has described the assumed restrictions on stego-systems considered in this research and presented a system model with related terminology. In particular, a private-key

stego-system by cover modification with a passive warden is assumed. The characteristics of a successful stego-system, namely perceptibility, robustness and capacity are described. Although initially visual perceptibility was a pertinent characteristic, the field has developed such that the battle between steganography and steganalysis exists now on a more subtle, statistical level. The term detectability is defined to mean susceptibility of a scheme to statistical analysis whereas perceptibility is defined to be limited to the extent to which embedding artefacts are visible.

The development of steganography and steganalysis can be traced from naïve and focused on perceptibility to more complex and focused on detectability. In particular, naïve stego-systems were based in the spatial domain and over time developed into more adaptive systems. With the advent of effective image compression techniques, digital images are seldom transmitted in the spatial domain anymore but in compressed versions where the image has been transformed into the frequency (transform) domain. Within the field of transform-based stego-systems, cell-based systems distinguish themselves from previous JPEG stego-systems by embedding not with the purpose of maintaining cover image properties, but by randomising the embedding process so that blind steganalysers aren't able to estimate original cover image properties. Cell-based systems are able to achieve high security by randomising embedding locations and by hiding data before lossy JPEG compression, with the disadvantage that embedding capacity is compromised. The lack of analytic reasoning in the selection of coefficients for embedding, delta for QIM and error coding provides opportunity for research.

Chapter 3. Formalising and Quantifying the Embedding Process

Digital image steganographic systems have developed from naïve and spatially-based to complex and transform-based and the major milestones of this development have been reviewed in Chapter 2. Within transform domain steganography, cell-based systems have emerged and their relevance lies in their good security properties and the fact that they are designed to cater for the likely event that the stego-image undergoes JPEG compression, with the disadvantage that the embedding capacity is relatively low.

By analysing some major elements of cell-based systems, it has become evident that a research opportunity exists in improving embedding capacity in cell-based systems by determining data embedding and error coding (i.e. data handling) schemes more analytically than in previous literature. In particular, the idea that JPEG compression affects E-block DCT coefficients of different frequencies in different ways can be used to implement more targeted data embedding and error coding. These ideas form the main thrust behind the research presented in this dissertation and this chapter discusses the steps of a new approach to determining better data handling schemes and the final results of this approach.

3.1 The Channel Concept

If the data embedding and error coding requirements for cell-based stego-systems are going to be deduced, first the specifics of what constitutes a data carrying *channel* in cell-based systems are required and then the nature of the channel must be understood. By nature it is meant the likelihood that an erroneous bit is retrieved at the recipient side of the channel (error rate) and the ability of the channel to carry data (embedding rate). A particular channel, when understood, can be assigned its own appropriate data handling schemes which are composed of a choice of delta for QIM (data embedding) and an error coding scheme. This section discusses what constitutes a channel in a stego-image traditionally in the literature and proposes a new channel model that allows more efficient data handling.

Start by considering the case of time-based communication systems where the channel may be some physical medium such as wireless (air) and the channel characteristics are measured over a particular time period. For example, an error rate corresponds to the likelihood of an error being incurred at any particular *time* instance.

In cell-based stego-systems, there is no time base and *the channel is constituted by the data carrying E-block DCT coefficients strung together*. The secret data bits are thus distributed spatially over an image and carried by the values of the relevant DCT coefficients, and so now

the error rate, for example, corresponds to the likelihood of an error being incurred in some DCT coefficient at some location spatially in the stego-image. We assume that we assign one data embedding scheme (delta value for QIM) and one error coding scheme per channel.

According to the traditional model, all of the data carrying E-block DCT coefficients in an image are taken as one channel, so only one channel exists per stego-image. This is shown in Figure 3-1. The block structure (E- and B- blocks) for YASS is shown. In this dissertation we are challenging the requirement that only the first 19 AC DCT coefficients of each E-block be considered for data embedding and so to maintain generality and for simplicity we start with a more inclusive model that assumes all of the DCT coefficients can be used.

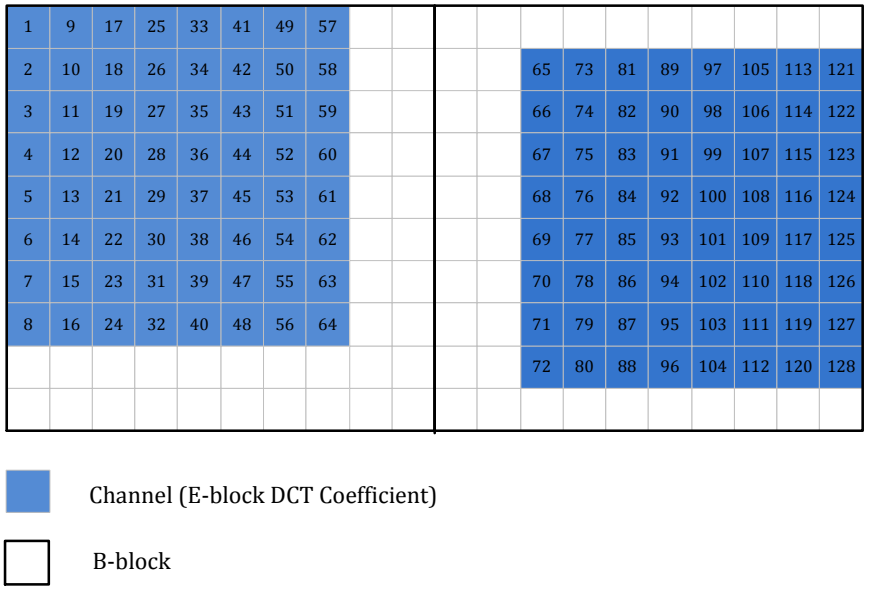

Figure 3-1. Traditional channel model in YASS

The numbers in Figure 3-1 represent an arbitrary column wise order with which the E-block DCT coefficients are strung together. Reordering the DCT coefficients results in the 1-D channel array shown in Figure 3-2.

Figure 3-2. Traditional channel model in YASS reordered column-by-column

Taking the example of error rate again, it is defined in cell-based systems as the likelihood of a data carrying DCT coefficient at any position in the channel in Figure 3-2 changing in value in such a way that during QIM de-embedding the incorrect bit would be retrieved from it.

Reviewing the steps of cell-based stego-systems as explained in Chapter 2, the two factors that cause change in value of the data carrying DCT coefficients between data embedding and retrieval are:

1. During the EMBED phase, each time an image segment is converted between the spatial and transform domains, the resultant pixel intensities or DCT coefficients are rounded because image representation doesn't allow for decimal places.
2. During the COMPRESSION phase, the image undergoes JPEG compression and subsequently JPEG decompression which is lossy causing corruption of image data.

Rounding effects cause image data to vary only slightly (±1) and so the dominant factor in change in value of DCT coefficients is (2.) from the list above during the COMPRESSION phase. Recall from Chapter 2 that the JPEG compression process is trying to compress the image while maintaining visual quality of the image, therefore more error will be introduced in higher frequency DCT coefficients (detailed image regions) than in lower frequency ones.

The problem with the traditional single channel model is that it does not consider the significantly different error rates that different frequency DCT coefficients in the stego-image are subject to in the COMPRESSION phase. For example, in Figure 3-2, the likely error in low frequency DCT coefficients (2, 3, 4) will be less than in high frequency coefficients (6, 7, 8). Attempting to design one delta value and one error coding system to cater for this wide variation in concentrations of error is inefficient and thus has a negative effect on embedding capacity. In the case that average error is catered for, DCT coefficients at higher frequencies will experience high concentrations of error that won't be corrected. In the case that worst-case error is catered for, the error correcting scheme will be devised to address the higher concentration of errors for high frequency components and will grossly overcompensate for more rare errors in low frequency coefficients.

It would be better to group DCT coefficients that are likely to undergo similar effects together producing many separate channels with each channel having more focused characteristics, and deducing different data handling procedures that optimise embedding capacity for each of these channels. Because we know that the primary source of error in data carrying DCT coefficients is the COMPRESSION phase and that JPEG compression incurs different grades of error on different frequencies of DCT coefficients, a novel channel model is thus proposed where *DCT coefficients in a particular position (frequency) in an E-block are grouped together to form one channel*.

In this case, one image now has many channels with each channel containing all the DCT coefficients at a particular position (frequency) in the E-blocks. Each channel can now be given an appropriate delta value for QIM and an error coding system that are best adapted for the nature of the channel and which optimise embedding capacity.

Figure 3-3 illustrates this new multi-channel model for the YASS system. All DCT coefficients at a particular matrix position (frequency) are considered to constitute a single channel, so one stego-image now contains many parallel channels. Five parallel channels are shown, each indicated by a different colour.

The DC coefficient in each E-block is blacked out because it is definitely not used during embedding to prevent artefacts and each E-block contributes one candidate DCT coefficient to the channels. If the candidate DCT coefficient meets selection criteria based on the QIM delta for that channel it will be used in the channel to carry a secret data bit and if not it will not be used as part of the channel. Assuming for simplicity that all candidate DCT coefficients meet selection criteria in Figure 3-3, each channel is shown as the string of its DCT coefficients at the bottom of Figure 3-3. The secret message data would need to be broken up and distributed over each channel separately.

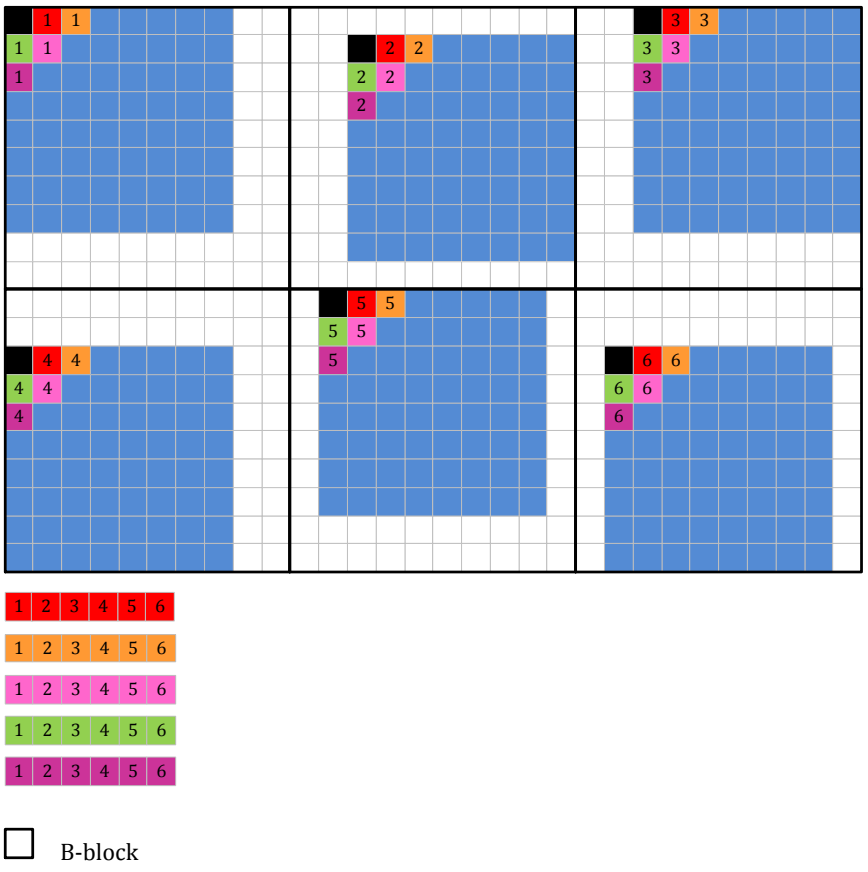

Figure 3-3. Proposed channel model in YASS

The new channel model for the more general case of MULTI is the same as for YASS except that an image may now contain up to 144 channels (since E-blocks in MULTI are specified to be up to 12x12 in size). Some of the channels constituted by the string of E-block DCT coefficients are shown in Figure 3-4.

The main difference in channel structure in MULTI from YASS is that not every E-block in MULTI contributes a candidate DCT coefficient to a channel. For example, the DCT coefficient shown in the position (frequency) marked in brown only exists when the generated E-block is 9x9 or greater. Therefore, for a given number of E-blocks, the number of candidate coefficients in a channel is not the same as the number of E-blocks for those DCT coefficients that lie outside the top left 8x8 block.

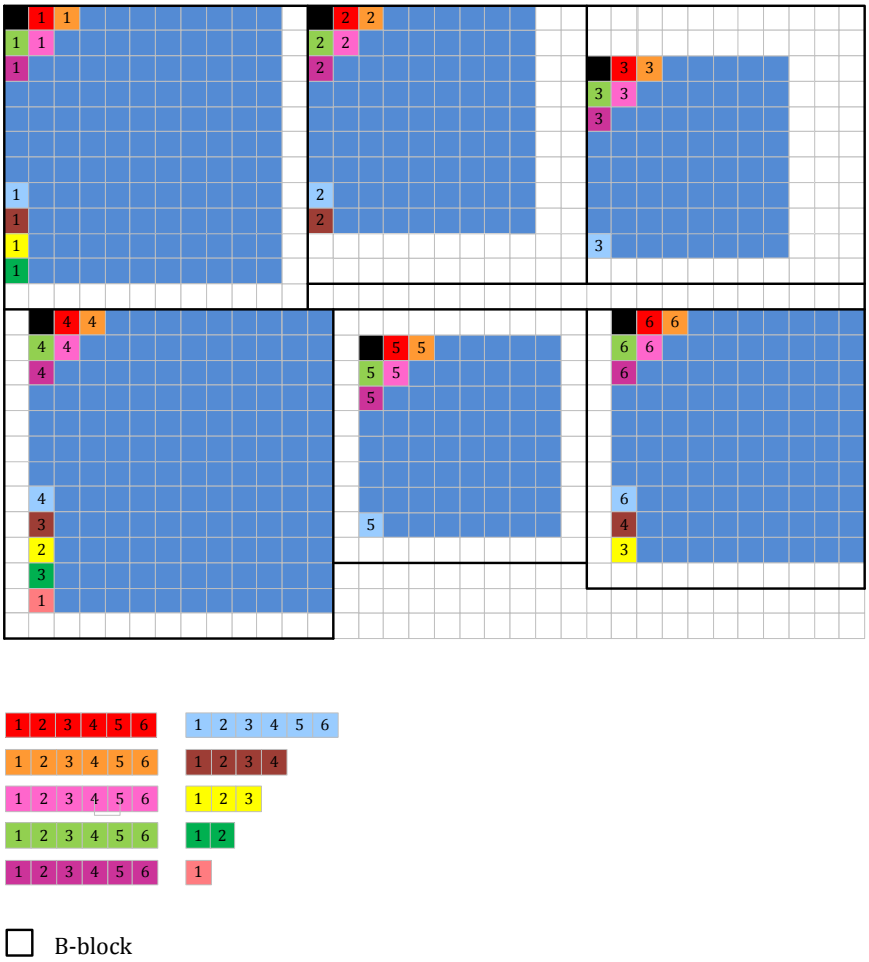

Figure 3-4. Proposed channel model in MULTI

Again, each channel has its own QIM delta and error coding (i.e. data handling) schemes. The new channel model will be assumed by default from now on.

Now that the channel model has been defined, the specific characteristics of each channel need to be determined. The rest of the chapter will be concerned with how to determine relevant channel characteristics and how to use these characteristics to derive data handling schemes that improve embedding capacity in cell-based stego-systems.

3.2 Coefficient Movement & Previous Delta Values

Although so far the concept of the change in value of data carrying DCT coefficients between QIM data embedding and retrieval has been referred to, and it has been shown that JPEG compression is the main factor controlling this change, the exact effects of JPEG compression have not been discussed. For brevity, the change in value of E-block DCT coefficients between data embedding and retrieval will be referred to as DCT *coefficient movement.* When we speak about movement, we will refer to the absolute value of the change in DCT coefficient value. Understanding what causes DCT coefficient movement and quantifying how coefficients move is important in order to gain insight on how to select the best data handling parameters so that embedding capacity is improved.

This section describes the causes of coefficient movement and presents an analysis of the characteristics of movement. It also digresses slightly to show a specific case where delta values have a profound effect on coefficient movement and how this case was used in the literature to provide delta parameters previously.

3.2.1 Coefficient Movement

So far, the concept that JPEG compression affects E-block DCT coefficients at different frequencies differently has been referred to, but the amount of error induced in the DCT coefficients as a result has not be described specifically. This section deals with coefficient movement more specifically for different cell-based systems.

3.2.1.1 Movement in JPEG-GRID

As a start consider a very extreme cell-based system where the B- and E-blocks coincide at a size of 8; i.e. B=E=8, shown in Figure 3-5. This is not a practical system but is useful for the purposes of explaining coefficient movement initially, and will be referred to in this dissertation as *JPEG-GRID*. As we will see, the movement in value that a DCT coefficient is likely to undergo between JPEG compression and de-compression is related to the JPEG quantisation matrix.

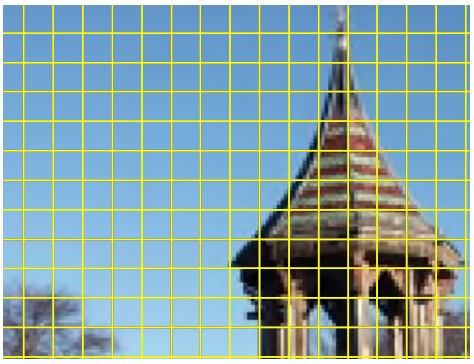

Figure 3-5. JPEG-GRID block grid

In this specific case, the DCT coefficients of the E-blocks coincide with those of the 8x8 grid used during JPEG compression. The E-block DCT coefficients are altered twice in cell-based systems: firstly during the EMBED phase and then secondly in the COMPRESSION phase. These two phases are shown in Figure 3-6 and Figure 3-7. For the purposes of illustration, consider the top left E-block in an image as a sample E-block.

During the EMBED phase, the E-block is translated from the spatial domain to the frequency domain using the DCT (shown in blue in Figure 3-6). The resultant DCT coefficients are then altered using QIM and the secret bit stream to produce a new E-block (shown in orange in Figure 3-6). This DCT E-block is converted back into the spatial domain and replaced in its original position.

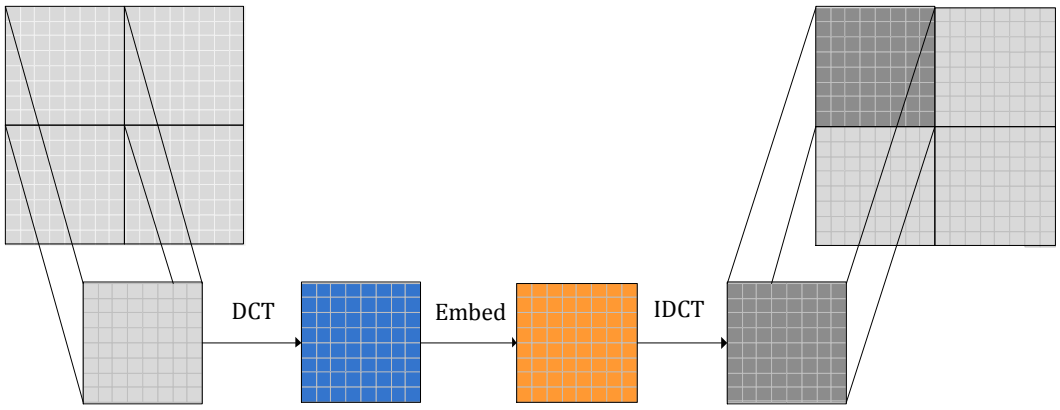

Figure 3-6. EMBED phase for JPEG-GRID

During the COMPRESSION phase, the image is divided into 8x8 blocks and each block is operated upon in turn by the JPEG compression algorithm which involves taking the DCT (shown in orange in Figure 3-7), dividing by $Z(u, v)$ and rounding.

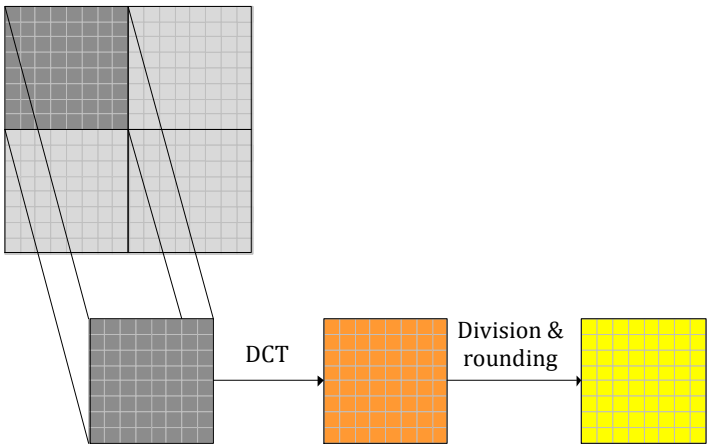

Figure 3-7. Portion of COMPRESSION phase for JPEG-GRID

As discussed in Chapter 2, the DCT is not an element-wise mapping but DCT coefficient values depend on the size of the area being converted to the transform domain. Taking the top left 8x8 block as an example - because the grid block used during COMPRESSION exactly coincides with the E-block used during EMBED, when the DCT is taken during the COMPRESSION phase you recreate exactly the same 8x8 E-block that existed after embedding (shown in orange in Figure 3-7). The DCT coefficients ($t(u,v)$ in Equation 2-15 and Equation 3-1 below) in the block are exactly those that were manipulated using QIM during embedding and which will now be divided and rounded. In essence, replacing the E-block after embedding and then retrieving it again before compression are reverse operations.

As explained in Chapter 2, the DCT coefficients in the 8x8 blocks during JPEG compression will be subject to an absolute change in value of $\leq \lfloor z(u,v) \,/\, 2 \rfloor$ over the course of lossy compression, i.e.

$$|t'(u,v) - t(u,v)| \leq \lfloor z(u,v)/2 \rfloor \qquad \textbf{3-1}$$

Because the DCT coefficients $t(u,v)$ in the 8x8 grid blocks during JPEG compression are exactly those used during embedding we can say with certainty that the data carrying DCT coefficients will experience a movement of $\leq \lfloor z(u,v) \,/\, 2 \rfloor$. Recall that some small errors may be introduced by rounding during conversions between the spatial and transform domains but these are neglected since they are not significant compared to coefficient movement caused by JPEG compression.

To get an overview for the limits on movements for each DCT coefficient in a block, a Matlab program was written to plot $\lfloor z(u,v) \,/\, 2 \rfloor$ in the case that an advertised JPEG compression quality factor Q_a of 50 is used. Although the coefficient value may move in the positive or

negative direction, the direction of movement is not important. For the purposes of QIM, we are only concerned with the absolute value of displacement from the original lattice point value after embedding.

Plotting the absolute value of the maximum coefficient movement at each frequency moving *column-by-column* through an E-block results in the awkward plot shown in Figure 3-8.

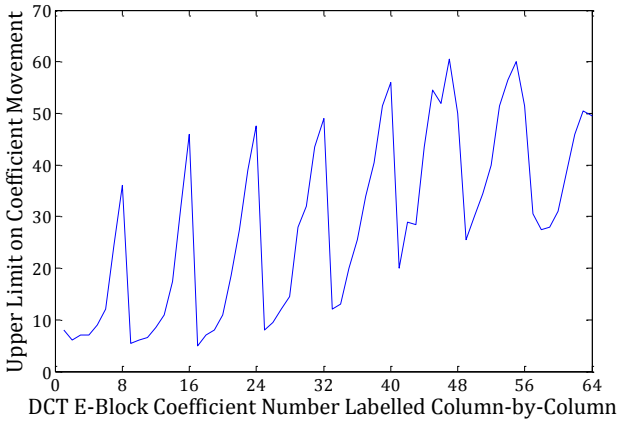

Figure 3-8. Upper limit on DCT coefficient movement using Q_a=50 plotted column-by-column

For the purposes of illustration, a more intuitive plot results if channels are labelled in a zigzag fashion as during JPEG compression, thus reordering them in qualitatively increasing spatial frequency. This is shown in Figure 3-9.

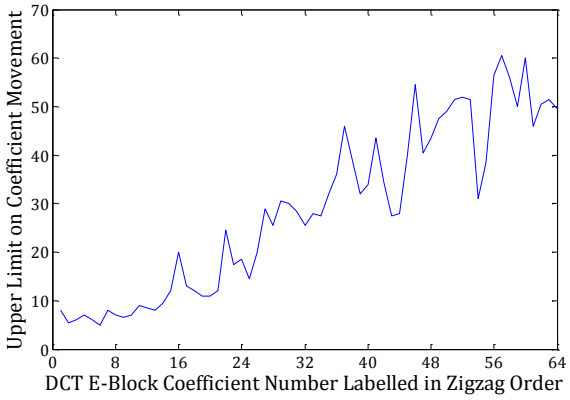

Figure 3-9. Upper limit on DCT coefficient movement using Q_a=50 plotted in a zigzag order

By drawing graphs in this way, it is easier to see which coefficients appear more vulnerable to movement than others, and how they are ordered roughly in increasing risk of movement although there is not a smooth increase in DCT coefficient movement with spatial frequency because $Z(u, v)$ was determined empirically in the original standard (JPEG, 2007). From this point onwards, channels will be labelled within an E-block according to the zigzag order.

3.2.1.2 Movement in YASS and MULTI

While coefficient movement can be determined easily in JPEG-GRID, JPEG-GRID is too simplistic to be a useful stego-system and YASS and MULTI are the important cell-based systems. JPEG-GRID was discussed only to introduce zigzag channel numbering and to provide a build-up to the discussion regarding coefficient movement in YASS and MULTI which is performed in this section of the chapter.

In the case of YASS and MULTI, the DCT coefficients of the E-blocks do not coincide with those of JPEG-GRID. The EMBED and COMPRESSION phases are shown in Figure 3-10 and Figure 3-11 for the most general case of MULTI.

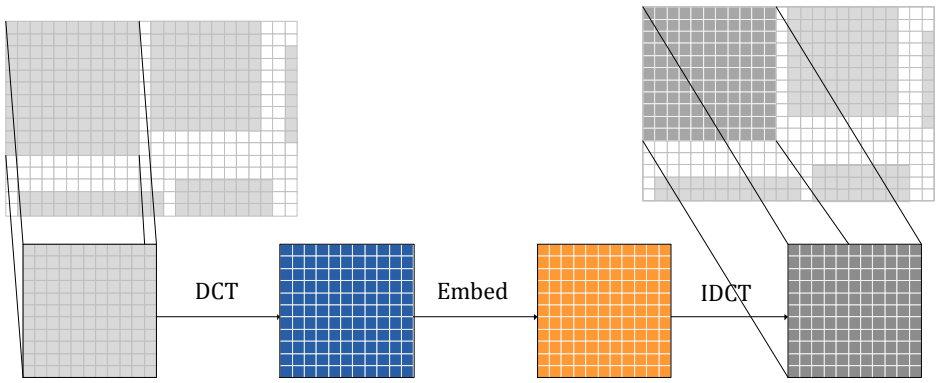

Figure 3-10. EMBED phase for MULTI

During the EMBED phase an E-block is extracted which may not be 8x8 or positioned in the extreme top left of an image. In Figure 3-10, the first E-block is 11x11 and positioned in the top left of the stego-image. The DCT of the E-block is taken and data is embedded into it before converting the E-block back into the spatial domain and replacing it in the image as previously described for JPEG-GRID.

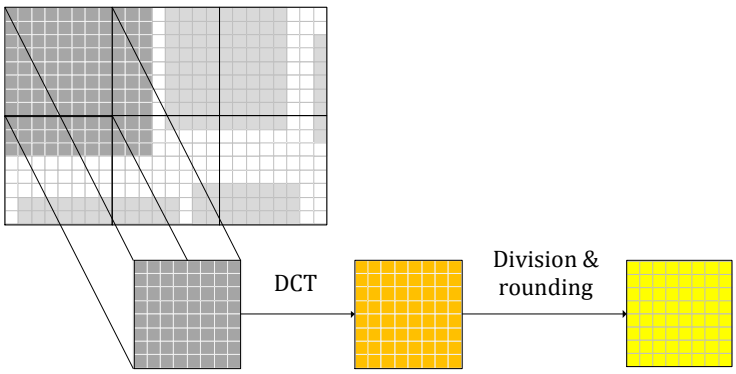

Figure 3-11. COMPRESSION phase for MULTI

The main difference between the more general case of YASS and MULTI and that of JPEG-GRID is that generally the 8x8 grid block used during JPEG compression is not the same in location and size as the E-block used during the EMBED phase. In other words, the grid used during the COMPRESSION phase is not the same as the grid of E-blocks used during the EMBED phase. Therefore, when the DCT of the top left 8x8 block is taken during JPEG compression, the data carrying DCT coefficients are not retrieved (i.e. they are not $t(u, v)$).

In Figure 3-11, the retrieved 8x8 DCT block is shown in a different shade of orange to the E-block after embedding in Figure 3-10. The 8x8 block will have similar frequency characteristics since it lies in the same area as the E-block spatially but division and rounding operations during JPEG compression will not act directly on the values of the data carrying E-block DCT coefficients because they are not retrieved as $t(u, v)$.

The general frequency characteristics of the image area will be altered with higher frequency coefficients likely to undergo more movement than lower frequency coefficients but the exact effect on the data carrying DCT coefficients of the E-block cannot be directly derived from $z(u, v)$.

To further clarify this point, consider the matrices below. Let's say after embedding the example 11x11 E-block in Figure 3-10 appears as shown in Figure 3-12. Once it is converted back to the spatial domain, it has the appearance of Figure 3-13. This 11x11 matrix would then be replaced back in the stego-image. The E-block doesn't coincide exactly with an 8x8 block during the COMPRESSION phase and in fact covers three adjacent 8x8 blocks. For the first 8x8 block, only the top left 8x8 pixel intensities are taken (indicated by the black square) and when the DCT is performed on this block the result $T(u, v)$ is shown in Figure 3-14. The DCT coefficient values ($t(u, v)$ in Equation 3-1) are not the same as the embedded ones (the top 8x8 coefficient values in Figure 3-12) and the net effect on E-block DCT coefficients is not obvious (not dictated by Equation 3-1) although we know that some detail in that image area will be removed by JPEG compression.

1409	-12	-14	-10	-2	4	-4	-2	0	-1	-4
31	11	-8	3	-1	4	0	1	-3	1	1
10	-5	3	-3	4	-6	5	-1	-1	0	1
1	3	-2	2	-3	3	-4	1	1	1	-1
-2	1	0	0	-1	0	0	0	0	1	0
2	2	0	-1	1	-1	1	-1	-1	1	1
1	1	0	-1	0	0	1	0	-1	0	1
-1	0	0	1	0	0	-1	0	0	0	-1
-1	0	0	1	-1	1	-1	0	0	0	0
1	0	0	0	0	0	0	0	-1	0	0
1	0	0	0	1	-1	1	0	-1	1	1

Figure 3-12. Example 11x11 DCT Coefficients of E-block

130	132	133	136	138	136	134	134	132	132	130
128	130	131	135	136	135	133	133	132	132	130
127	129	129	133	134	134	132	132	132	132	130
126	128	128	132	133	132	130	130	130	130	128
125	127	128	131	133	130	128	129	128	128	127
122	125	126	128	128	131	124	126	130	128	121
121	124	125	127	127	130	124	126	129	128	122
121	124	125	127	27	129	124	126	129	128	125
120	123	124	126	126	128	125	126	127	128	129
119	122	123	125	125	127	125	126	126	128	133
118	121	122	125	124	125	125	126	125	128	136

Figure 3-13. Spatial representation of 11x11 E-block

1034	-11	-14	1	1	-4	1	-4
25	-1	0	0	2	1	-3	2
1	0	0	0	-1	0	1	-1
1	1	-1	0	0	-1	1	0
3	1	0	-1	1	0	-1	2
-1	0	1	1	-1	0	0	-1
0	0	0	0	-1	0	1	-1
1	0	0	0	1	0	-1	1

Figure 3-14. DCT of top left 8x8 segment of E-block

The main consequence is that change in the data-carrying E-block DCT coefficients due to lossy compression can no longer be accurately predicted as $\leq \lfloor z(u,v) \,/\, 2 \rfloor$ as was the case for JPEG-GRID.

However, it can be argued that a good estimate of the movement of the coefficients in a particular channel (and channel characteristics in general) can be made by taking measurements over a sufficiently large and varied image data set so that the characteristics converge. This will be the main idea behind characterising the channels in the more general YASS and MULTI systems later in this chapter. Before these measurements are performed, the theories stated here regarding coefficient movement are tested practically in Matlab over a few images.

3.2.1.3 Matlab Simulation & Image Database

To demonstrate the extent to which DCT coefficient values in each channel change, a simple experiment was implemented in Matlab. Code which maps out E- and B-blocks for the MULTI and YASS schemes was provided by (Dawoud, 2010), and additional code was written to record the changes in value of the E-block DCT coefficients in each channel as the images were passed through a JPEG compression/decompression process. This was done by saving coefficient values for each channel before and after JPEG compression and recording the difference for all the coefficients in each channel.

In-built JPEG compression provided by Matlab is not accompanied by any documentation regarding the quantisation matrices used for each quality factor. Because the specifics of the quantisation matrices $Z(u,v)$ are important in this research, instead of using in-built Matlab JPEG compression functions, code from (Gonzalez & Woods, JPEG, 2002) that manually performs the compression and decompression was edited to use the quantisation matrices defined in the toolbox by (Sallee P. , 2003).

Since this is the first time the simulator has been mentioned in this dissertation, it is an appropriate point to briefly introduce the reader to the image database that will be used for all simulations. The image database chosen in this research is from (Schaefer & Stich, 2004) and contains 1338 TIFF images in their uncompressed forms which can be resized as required. To give the reader an idea of the variety of the images in the database, a random sample of sixteen images is shown in Figure 3-15. This database was chosen because the images contain a wide combination of organic and manmade objects, highly textured and plain, taken at various angles and zoomed to several degrees. The colours of the images are diverse, as are the textures of the elements in the pictures.

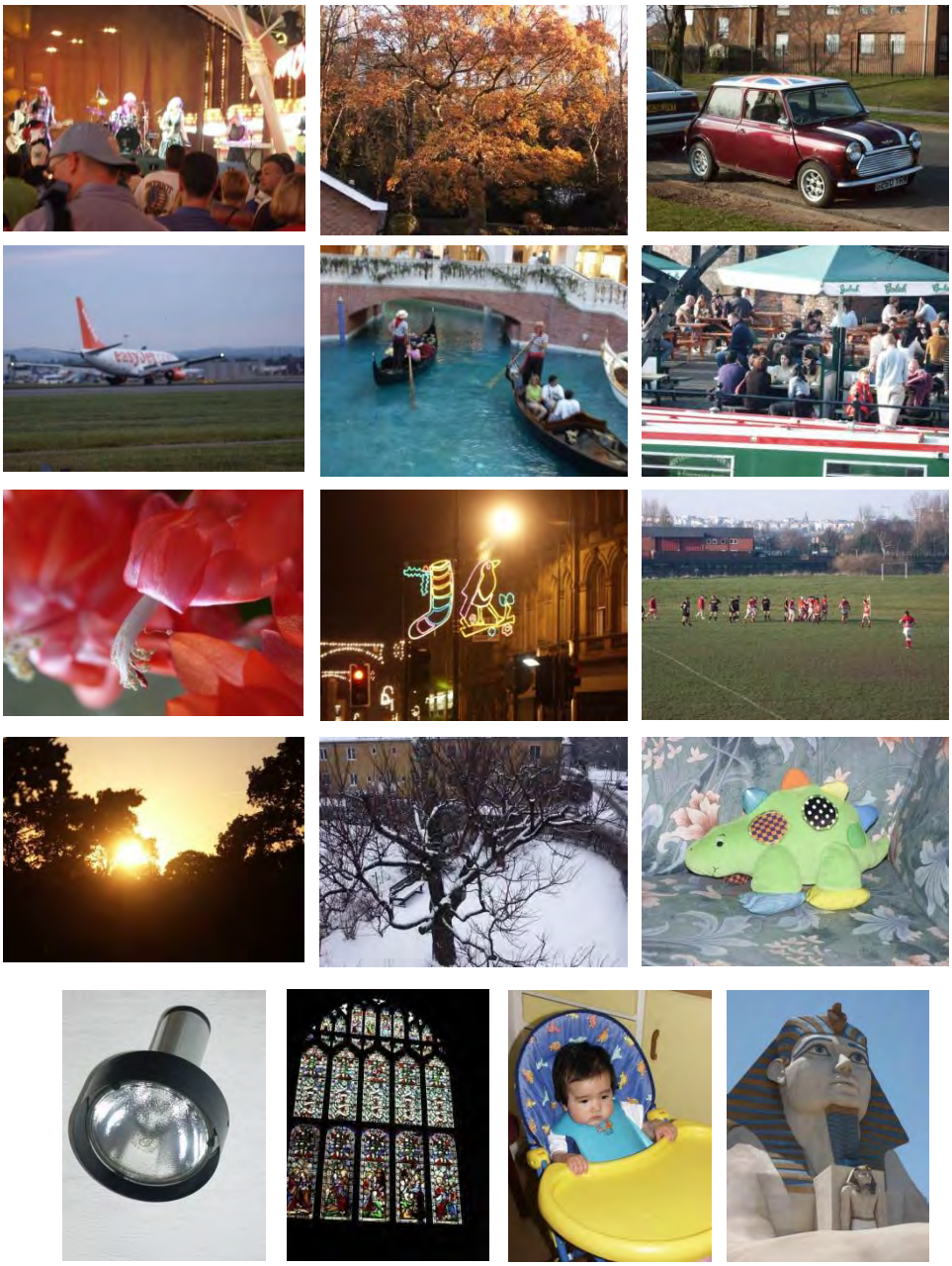

Figure 3-15. Random sample of 16 images taken from image database

Returning to the simulation, the movement in coefficient value for the channels was recorded over five images randomly sampled from the database, shown in Figure 3-16.

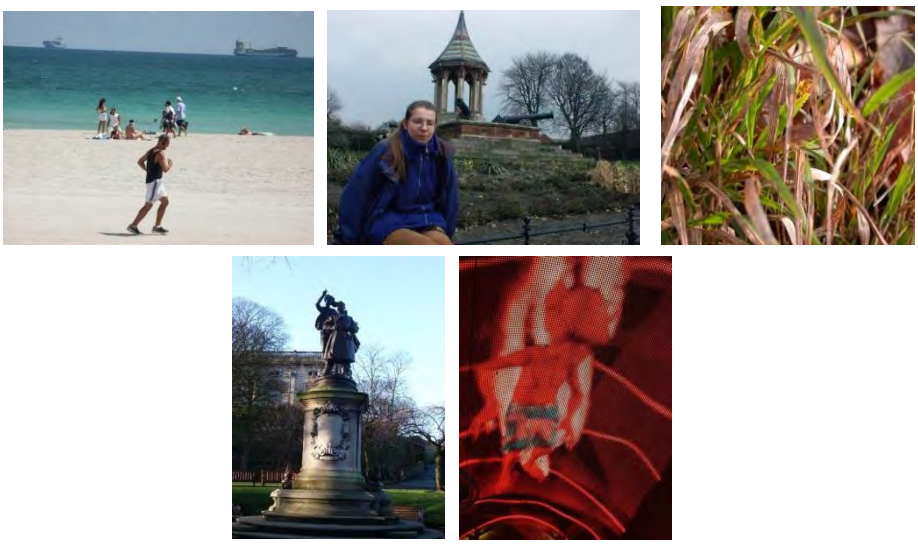

Figure 3-16. Images used to produce results in Figure 3-18 and Figure 3-19

For these five images, a JPEG quality factor of 80 was used for compression. The corresponding quantisation matrix from (Sallee P. , 2003) is given in Figure 3-17.

6	4	4	6	10	16	20	24
5	5	6	8	10	23	24	22
6	5	6	10	16	23	28	22
6	7	9	12	20	35	32	25
7	9	15	22	27	44	41	31
10	14	22	26	32	42	45	37
20	26	31	35	41	48	48	40
29	37	38	39	45	40	41	40

Figure 3-17. Quantisation matrix for a quality factor of 80

Using these images, the histograms of DCT coefficient movement for channels 2 and 15 were plotted (with channels labelled in a zigzag order as explained previously) for JPEG-GRID and MULTI. $z(u, v)$ for the two channels is highlighted in blue in Figure 3-17. Across the five images, a total of 7220 E-blocks are created.

The histograms in Figure 3-18 show that the coefficient values for JPEG-GRID in position 2 are more stable than those in position 15 as expected. In the case of JPEG-GRID, the movement is also limited to $\leq \lfloor z(u, v) \,/\, 2 \rfloor$ (2 and 5 for channels 2 and 15 respectively). Rarely, movement of the coefficient is measured as beyond $\lfloor z(u, v) \,/\, 2 \rfloor$ due to rounding errors while converting between the spatial and transform domains in the EMBED phase but as the histograms show this is a minor effect.

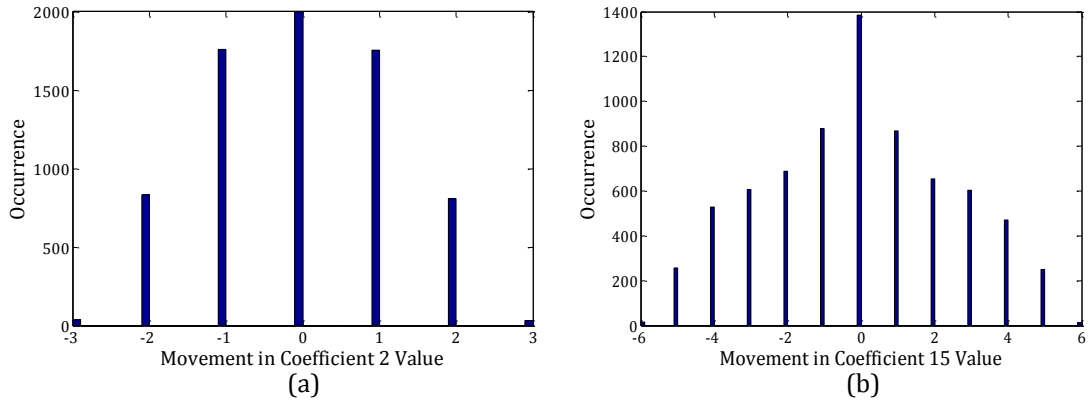

Figure 3-18. Histograms of coefficient movement for channels 2 (a) and 15 (b) for Q_a=80 for JPEG-GRID

Figure 3-19 shows the movement of coefficients for MULTI for the same channels over the same five images where now 3120 E-blocks are generated. The trend that higher frequency channels experience more widespread movement is shown to still hold true however the limits on movement can no longer be predicted using $z(u, v)$.

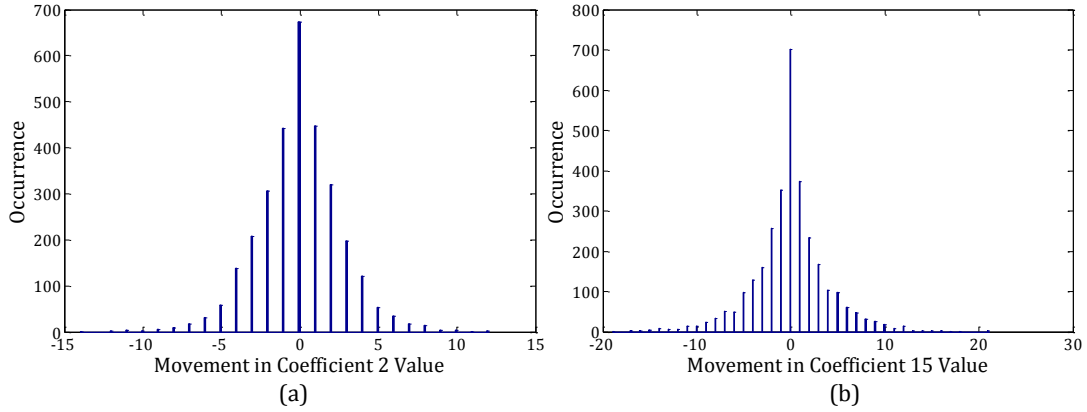

Figure 3-19. Histograms of coefficient movement for channels 2 (a) and 15 (b) for Q_a=80 for MULTI

Thus far we have seen that in the case of YASS and MULTI, the coefficient movement for each channel cannot be determined analytically but must be deduced using extensive measurements. The channel characteristics regarding coefficient movement will be useful when determining data handling procedures and will be referred to again later in the chapter. For now the concept of relative coefficient movement in the channels is important.

3.2.2 Delta Values used in YASS/MULTI

Given the newly acquired knowledge about DCT coefficient movement in cell-based systems, the reader is now sufficiently informed to understand how data embedding parameters have been determined in cell-based systems thus far and this section describes this.

With regard to the statistical distribution of the movement in DCT coefficient values for the channels, embedding should not alter any significant properties of the distribution and thus embedding hasn't been mentioned so far.

There is, however, one special case where embedding has a significant effect on coefficient movement and this is now discussed because it explains what delta values cell-based systems have used up until now and why. Recall that delta is the value with which the DCT coefficient is quantised by during the QIM process.

In the case of JPEG-GRID, let's assume that the delta value used during QIM is the same as the corresponding $z(u, v)$ during JPEG compression for a channel.

Recall $Z(u, v)$ was defined to be the JPEG quantisation matrix used during compression, and $z(u, v)$ to be an element from $Z(u, v)$.

Define:

$$z(u, v) = L \qquad \textbf{3-2}$$

where L is an integer from position (u, v) in $Z(u, v)$.

In the QIM system for this channel, define:

$$\Delta = L \qquad \textbf{3-3}$$

Recall $T(u, v)$ was defined to be an 8x8 matrix of the DCT coefficients in the E-block after embedding using QIM before lossy JPEG compression and $t(u, v)$ is an element of $T(u, v)$. After QIM embedding, the resultant value of the DCT coefficient is shown in Equation 3-4.

$$t(u, v) = s.L \qquad \textbf{3-4}$$

where s is a random integer correlated to the lattice point to which the DCT coefficient is moved during embedding.

Recall $\hat{T}(u, v)$ was defined to be an 8x8 matrix of the data carrying DCT coefficients after quantisation during JPEG compression and $\hat{t}(u, v)$ are elements from $\hat{T}(u, v)$. The operation of quantisation during JPEG compression is shown in Equation 3-5. Recall that Equation 3-5 was previously given as Equation 2-13.

$$\hat{T}(u,v) = round\left(\frac{T(u,v)}{Z(u,v)}\right) \quad \textbf{3-5}$$

Element-wise, Equation 3-5 can be rewritten as Equation 3-6.

$$\hat{t}(u,v) = round\left(\frac{t(u,v)}{z(u,v)}\right) \quad \textbf{3-6}$$

By substituting Equation 3-4 in Equation 3-6, you get Equation 3-7.

$$\hat{t}(u,v) = round\left(\frac{t(u,v)}{z(u,v)}\right) = \frac{s.L}{L} = s \quad \textbf{3-7}$$

Because the quotient in Equation 3-7 is an integer, there is no rounding and JPEG compression is no longer lossy.

To see this, consider the step of retrieving the DCT coefficient value during de-compression in Equation 3-8 where $t'(u,v)$ is the recovered DCT coefficient.

$$t'(u,v) = \hat{t}(u,v).z(u,v) = s.L = t(u,v) \quad \textbf{3-8}$$

The final effect is:

$$t'(u,v) = t(u,v) \quad \textbf{3-9}$$

This means that if the delta value for a channel is the same as $z(u,v)$ for that channel, then there should be no errors in the data retrieved since *JPEG compression has been made lossless.*

The cell-based systems thus far have used JPEG quantisation matrices $Z(u,v)$ at different quality factors as values of delta during QIM. The reasons for this choice are not specified in the original literature but it is suggested that it was a basic extension of the optimal case just explained.

As a rough estimate, the delta matrix has a correct look since delta values would be expected to be larger for higher frequency channels to tolerate more coefficient movement, and as we have just seen more movement does occur in higher frequency channels. However, there is no justification for why these values specifically would work well during YASS or MULTI where E-blocks do not align with grid blocks. MULTI (Dawoud, 2010) crudely extends the JPEG quantisation matrix to make a 12x12 matrix to accommodate the larger E-block sizes.

While using different deltas for DCT coefficients at different frequencies suggests a channel model as explained earlier in Section 3.1, the literature thus far has not been close to defining it and error coding has been used across blocks, which has been explained to be inefficient.

In Chapter 2, the term advertised quality factor Q_a was used to refer to the factor with which the quantisation matrix used during JPEG compression is chosen. We now define a second quality factor - a hiding quality factor Q_h as the factor to choose the JPEG quantisation matrix used to provide delta values for embedding during QIM in YASS and MULTI literature so far. This chapter will present an approach to choosing delta and error coding schemes more analytically than done previously.

3.3 Determining Channel Data Handling Parameters Graphically

So far, a new channel model has been deduced and the reasoning for the new channel model has been validated by exploring more specifically the properties of coefficient movement. It was stated that the coefficient movement in the more general cases of YASS and MULTI cannot be derived analytically as in the case of JPEG-GRID, but that through extensive measurements can be characterised.

We know that we will need to use the channel characteristics somehow with data embedding and error coding procedures to optimise embedding capacity in each channel but the exact nature of how to do this has not been explored. Therefore, before acquiring the channel characteristics, it is worth taking a step back and getting an overview of how we will be able to combine channel characteristics with our understanding of data handling procedures to derive better data handling parameters that will hopefully address the relatively low embedding capacity of cell-based systems (in effect the main research problem statement in this dissertation).

The main players in embedding capacity are selection criteria and error coding which are both connected to the value of QIM delta. This section discusses these broad issues.

If error coding is ignored for the moment, the effect of the choice of delta on error in a channel can be explained. Consider the histogram of movement in channel 15 in JPEG-GRID for a JPEG quality factor of 80 taken from Figure 3-18(b), repeated in Figure 3-20. Assuming as an example the use of a delta of 10 for this channel, tolerance boundaries representing the limit on coefficient movement for correct data retrieval (Δ / 2) can be superimposed on this histogram as shown.

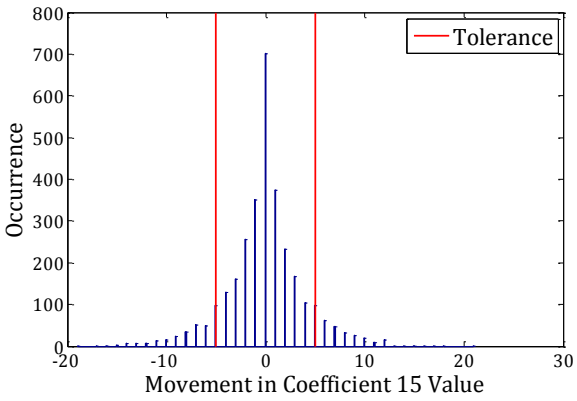

Figure 3-20. Histogram of channel 15 movement for Q_a=80 for JPEG-GRID

From this, the probability of error can be calculated as the ratio of the sum of the heights of the bins *outside* the boundaries to the total number of coefficients for that channel. Therefore, as delta is increased one can imagine the tolerance lines moving outwards and the likelihood of error decreasing.

In Chapter 1, the basic idea of error correcting was introduced which is the inclusion of overhead bits in the transmitted bit stream that are then used at the receiver to detect and correct erroneous bits. Generally speaking, the higher the error rate required to be corrected for the more overhead bits required. Therefore, delta will have an indirect effect on embedding capacity through the error rate due to the associated overhead bits. As delta decreases, the error rate will increase and more overhead bits will be required reducing embedding capacity.

The question of the appropriate value for delta then arises. So far, the value of delta has been related to embedding capacity in two ways:

1. It has just been shown that an increase in delta corresponds to reduction in error in a channel which requires fewer overhead bits. For small delta more overhead bits are required.
2. In Chapter 2, a selection criterion was explained. In order not to risk changing the number and distribution of zero-valued DCT coefficients in an image, no DCT coefficient in the range $(-\Delta, \Delta)$ is used to carry data. Therefore, as delta increases, so does the number of DCT coefficients that will not be used for embedding.

Overall, it can be said that for smaller delta there is a large error rate, more aggressive error correcting is required and the embedding capacity is reduced by the amount of overhead bits,

whereas for larger delta less aggressive error correction is required but now fewer coefficients outside the range $(-\Delta, \Delta)$ are selected for embedding and capacity is again reduced.

The two effects of delta on embedding capacity for a channel are summarised in Figure 3-21. The factor that reduces embedding capacity is printed in red whereas the factor the increases embedding capacity is printed in green.

Figure 3-21. Overview of effects on embedding capacity versus delta

Because there are two separate factors influencing embedding capacity over opposite ranges of delta, Figure 3-21 suggests that if net embedding capacity is plotted for a range of delta, there should be some moderate delta where the effects of error-coding and selection criteria are such that embedding capacity is optimal in the channel.

For a particular delta, the error rate and embedding rate (i.e. effect of selection criteria) for a channel in YASS and MULTI cannot be determined analytically but can be deduced through extensive measurements as explained earlier. These two properties will be referred to as *channel characteristics*. Given that the channel characteristics are known, the plot of net embedding capacity can be generated in the following way:

1. At each delta, if the error rate is known (from channel characteristics), then the amount of overhead required to correct for it can be determined.
2. At each delta, if the effects of selection criteria on the proportion of coefficients used are also known (from channel characteristics), then the effect of embedding capacity reduction due to selection could be factored in with the embedding capacity reduction due to error coding overhead (which you would know from the choice of error code in (1.) above) and for each delta a net embedding capacity value would be calculated.
3. By doing this over all delta values a plot of net embedding capacity would be acquired. This would have to be repeated for each channel.

Recall that data handling refers to data embedding (QIM which is characterised by delta) and error coding schemes. Once the embedding capacity plot is drawn for a channel and the maximum embedding capacity point is found, the data handling schemes for that point could

be deduced by reading the QIM delta value off of the x-axis and determining the error coding scheme that was implemented at the maximum capacity point.

It can now be seen that *this type of plot holds the key to deriving optimal data handling schemes for a channel* and the focus of this work now shifts to determining this type of plot for the defined channels.

One final factor related to delta not yet mentioned but worth consideration is that the larger the delta, the greater the embedding artefacts which may increase detectability. In cell-based systems, the random nature of embedding is the most important aspect in ensuring security therefore it is assumed for now that the random nature of embedding should guarantee adequate resistance against steganalysis even if the delta values for the channels deduced here are higher than those in the literature previously. It is expected, however, that the delta values derived here will be similar to existing ones. This assumption will be tested in Chapter 4.

Now that we have a global view of what is required to find data handling parameters for each channel, the rest of this chapter deals with deducing channel characteristics and consolidating them with error coding systems to give this net embedding capacity plot and hence deriving data handling schemes.

3.4 Channel Characterisation

In order to plot the net embedding capacity curve, first the channels in YASS and MULTI need to be characterised which can only be done empirically through extensive measurements. Specifically, the error rate and effects of selection criteria (embedding rate) for each delta for each channel need to be determined. This section formally defines the channel characteristics of interest and how the measurements are conducted, as well as presents some final channel characteristics and comments.

3.4.1 Determining Channel Characteristics Empirically

In order to plot net embedding capacity versus delta, the characteristics of the channels need to be known first. The idea here is to gather statistics of the channel for each delta regarding the proportion of channel coefficients that meet selection criteria and the error rate a correction code would be required to cater for. For the moment, we ignore error coding requirements.

It has already been seen that the DCT coefficients in the E-blocks of MULTI and YASS are not directly correlated to the JPEG quantisation matrix values $z(u, v)$ as in the case of JPEG-GRID. To solve this problem, an assumption is made that *if channel characteristics are measured over*

a sufficiently large and variable set of images for the most general case of MULTI until the characteristics converge, the characteristics will be a good representation of the channel properties in any image likely to be used as a cover image.

The channel characteristics deduced in this section will be for the 144 channels in the MULTI system. These characteristics will be representative of all cell-based systems since they all generate E-blocks randomly in an image. Statistically speaking, the only real difference then between YASS and MULTI is the number of channels, but the channels in the top left 8x8 segment of the MULTI E-blocks will have the same statistical properties as those of YASS E-blocks. All of the AC channels are considered for data carrying and not only the first 19 as originally presented in the literature.

In order to plot the embedding capacity against delta, for each value of delta the proportion of DCT coefficients in the channel that meet selection criteria needs to be known, and the error rate needs to be known so that the amount of overhead related to coding can be found. Although already introduced, these two critical characterising factors for a channel are defined formally next.

i. Embedding Rate

The average embedding rate for a block of data bits is defined in Equation 3-10.

$$Embedding\ Rate = \frac{Number\ of\ DCT\ Coefficients\ Used\ For\ Embedding}{Total\ Number\ of\ Candidate\ DCT\ Coefficients} \quad \textbf{3-10}$$

The embedding rate represents the proportion of the candidate coefficients in each channel that are deemed acceptable to carry information by selection criteria. Taken as an average over a channel, it also represents how appropriate a particular channel is to carry data with regard to the security of the system.

ii. Error Rate

The average error rate for a block of data bits is defined in Equation 3-11.

$$Error\ Rate = \frac{Number\ of\ Errors\ in\ Retrieved\ Data}{Total\ Number\ of\ Data\ Bits\ Embedded} \quad \textbf{3-11}$$

The error rate represents the likelihood of error in a particular group of embedded message bits, based on some observed input and output bit stream. More specifically, given the selection criteria, the error rate indicates the extent to which the surviving coefficients are

appropriate for data embedding for a given delta and advertised quality factor Q_a used for JPEG compression of the stego-image.

To measure these rates, a large image database and simulator are required. The simulator should, for each image, and for each delta for each channel, determine the embedding rate and error rate using the MULTI system.

The image database has already been introduced in Section 3.2.1.3 and the simulator was implemented in Matlab. While the code received from (Dawoud, 2010) generated the E- and B- blocks in an image for YASS and MULTI, there was no functionality accommodating a channel model such as the one presented here since this is original to this dissertation. Recall that the module recording movement in E-block DCT coefficient values between before and after JPEG compression was added on previously. Some pertinent elements of the simulator and further modules added onto it at this point are:

- The original code of (Dawoud, 2010) allowed for pseudo-random data bits to be embedded into the E-block DCT coefficients. This is a good approximation for the nature of the data a steganographer would embed since the data is likely to have undergone cryptographic scrambling and error correcting coding.
- The number of bits embedded into each channel corresponds to the number of DCT coefficients used for data carrying in a channel after selection criteria and the required number of data bits can only be determined once the embedding rate is known. To determine this number, an image undergoes a preliminary stage of processing before data generation and embedding.
- The code of (Dawoud, 2010) only implemented LSB embedding. The code was extended to perform QIM embedding at the transmitter side and QIM de-embedding at the receiver side with a different delta specified for each channel.
- The code of (Dawoud, 2010) embedded data for the purposes of generating stego-images that could be visually and statistically analysed. Modules were added to record the input and retrieved secret message bit streams for each channel used to analyse the error rate and distribution of errors in a channel.

Before acquiring channel characteristics, the advertised JPEG compression quality factor Q_a must be decided upon for 2 reasons:

- The greater the amount of compression, the more likely the movement in the E-block DCT coefficient due to the compression process and this effects all of the parameters for data embedding and error correcting.
- In the eyes of a steganalyser, it cannot distinguish between distortion due to the embedding process or due to heavy quantisation of the JPEG compression process. Therefore, a more heavily compressed image containing data will be more resistant to steganalysis than a stego-image that is more lightly compressed.

All other literature on cell-based systems uses Q_a=75 and to conform to this 75 is also used here.

There is also a more subtle point to be made regarding measurement of the error and embedding rates. In communication channels, the characteristics of a channel can be measured over some time in batches. Given a time segment, there will be certain statistics regarding the behaviour of the channel determined from previous observations. In characterising the channels in cell-based stego-systems, it has already been explained that a time base is not used, but rather the bits are embedded spatially. In the same way that a signal can be analysed over a specific time segment, we need to examine the channel over a certain number (batch) of coefficients (each coefficient retrieved from an E-block in sequence as shown in Figure 3-4).

The number of coefficients in a batch depends on the accuracy with which the embedding and error rates are required to be measured. If we take the batch to be one coefficient, then at any time the channel can have either 0% or 100% embedding or error rates which is not a realistic measurement because this case is so limited. As the number of coefficients in a batch is increased, the accuracy with which we can record the rates increases. Using a batch of 100 coefficients, we can get accuracy in rates of up to 1% which suffices for this application.

To summarise then, the specifics of acquiring error and embedding rate statistics with regard to these batches (accommodated by the above-stated simulator properties) are:

1. Divide the channel coefficients into batches of 100 (ignore any residual coefficients after batching).
2. For each batch: Check how many meet selection criteria based on the delta value for that channel. This proportion is noted as an embedding rate measurement.

3. For each batch: For those coefficients that meet selection criteria, embed data into them and, after the JPEG compression/decompression process, retrieve data from them. How many correct data bits were retrieved? This fraction is noted as an error rate measurement.

As an example of the resultant plots, the embedding and error rates for these batches in channel 3 for delta values from 1 to 40 are plotted in a scatter diagram as shown in Figure 3-22 and Figure 3-23. Figure 3-22 shows the scatter of the rates within one image, whereas Figure 3-23 shows the scatter of the rates over twenty images.

As the number of batches increases the scatter plots become more occupied and trends begin to show. In particular, a concentrated cloud of error rates form that represents the general trend. As the number of batches seen increases further, the shape of the cloud does not change and only scattered outliers appear. For the purposes of determining channel characteristics, our concern is to use as many images as required to gather the statistics from an increasing number of batches until the trend in the scatter plots become sufficiently static and converged so that using any more batches does not make any substantial difference to the channel characteristics.

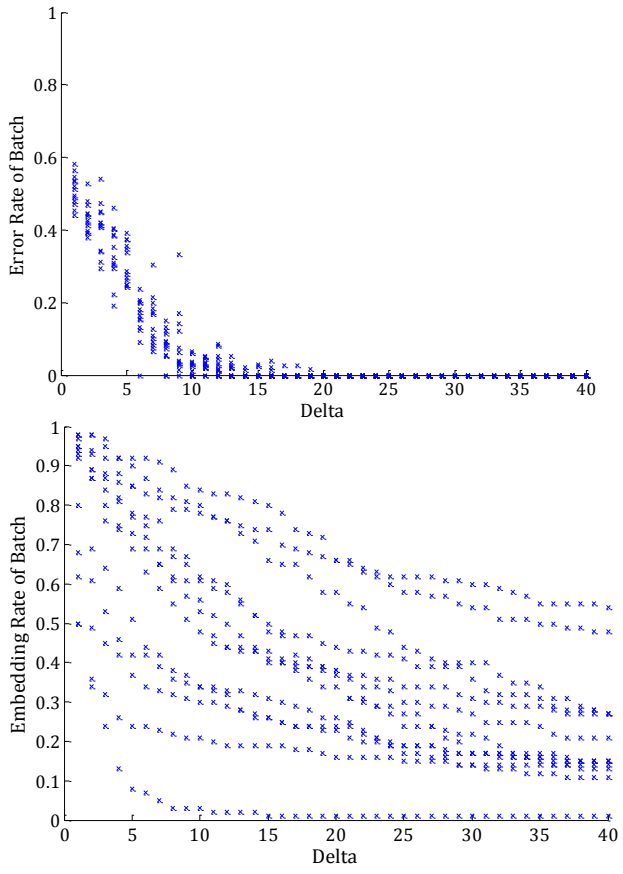

Figure 3-22. Scatter plot for channel 3 error rate and embedding rate over 1334 E-blocks

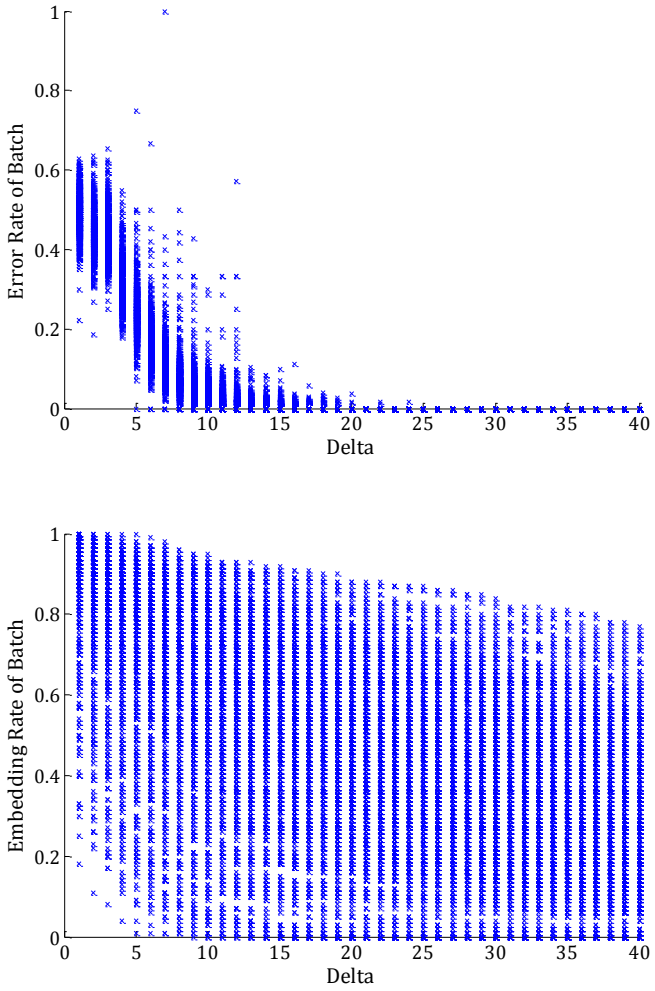

Figure 3-23. Scatter plot for channel 3 error rate and embedding rate over 26680 E-blocks

From Figure 3-23, the embedding capacity of the batches is spread evenly for a given range for each delta and no thick cloud of scatter points is visible. Over a batch, the embedding rate for that batch depends on the segment of image from which those coefficients are taken. This is because embedding rate represents the extent to which the batch coefficients are large enough to be acceptable to carry data. Over a batch, the image area covered can be infinitely variable from plain sky to textured shrubbery and there is an even spread overall of good and bad image areas. Interestingly, Figure 3-23 shows that from a delta of 5 onwards batches may be observed that provide no usable DCT coefficients for data carrying (embedding rate = 0).

The scatter plots for channel 20 are shown in Figure 3-24. Compared to the plot for channel 3 in Figure 3-23, at any given delta the error rate is higher and the embedding rate is lower, implying that generally DCT coefficient values are smaller and more prone to movement as a result of lossy JPEG compression. There are also more extreme error rate outliers than in channels of lower frequency indicating the volatility of the channel.

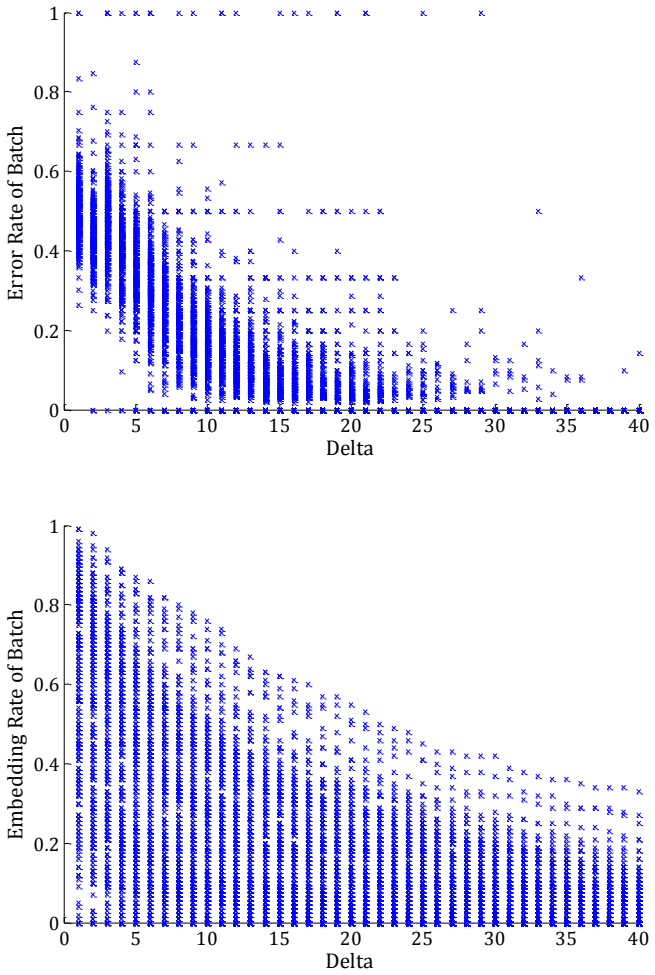

Figure 3-24. Scatter plot for channel 20 error rate and embedding rate over 26680 E-blocks

In order to monitor the convergence of the channel characteristics, trend lines can be derived from the scatter plots. In particular, trend lines can be drawn that link values of rates below which a certain fraction of observed values exist. In this report, these will be referred to as *tolerance lines* which can be drawn on both error rate and embedding rate scatter plots. For example, the 98% error rate tolerance line goes through the error rate value for each delta below which 98% of observed rates exist. These tolerance lines give an indication of the shape and values of the trends from the scatter plots. Various tolerance lines for error rate in channel 3 are shown in Figure 3-25.

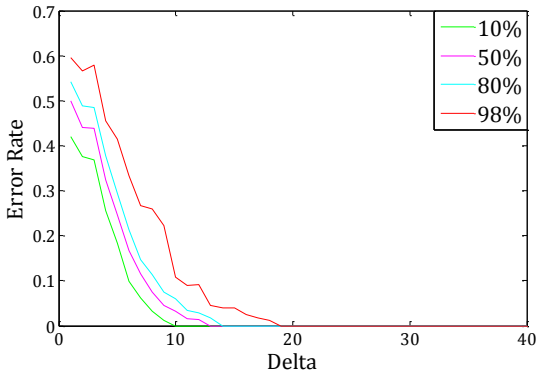

Figure 3-25. Error rate tolerance lines for channel 3

In order for the channel characteristics to converge, the number of images over which batch measurements were taken was increased and the tolerance lines were analysed for movement. The average rates and 98% tolerance lines for error rate in channel 3 are shown in Figure 3-26 and Figure 3-27 for 1, 10, 20 and 30 images respectively.

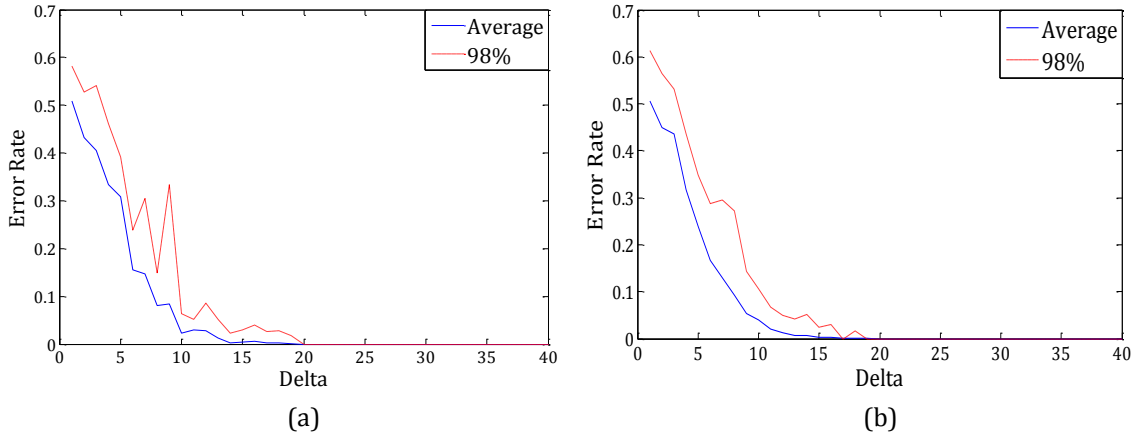

Figure 3-26. Channel 3 characteristics for one image (1334 E-blocks) (a) and for ten images (13340 E-blocks) (b)

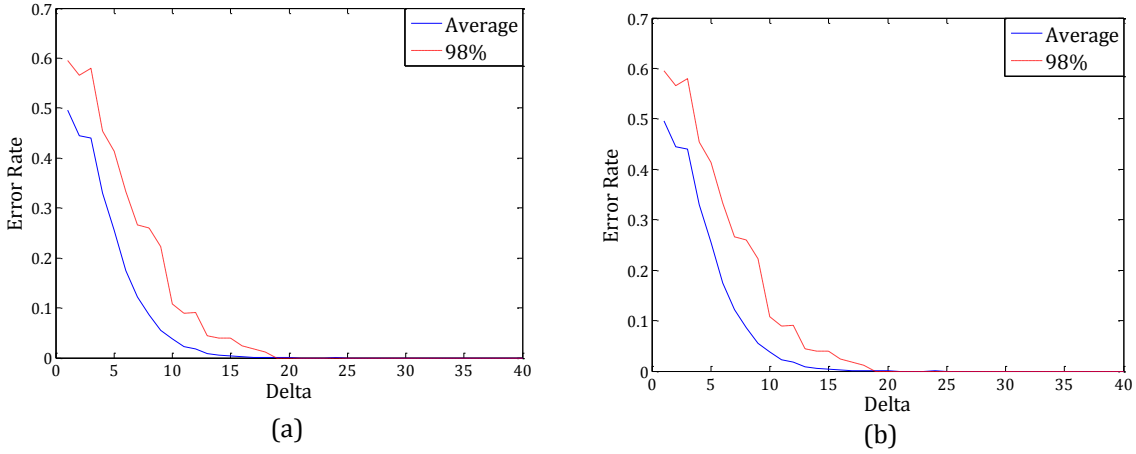

Figure 3-27. Channel 3 characteristics for twenty images (26680 E-blocks) (a) and for thirty images (40020 E-blocks) (b)

As the number of images is increased, the channel characteristic tolerance lines become smoother. It can be seen that after 20 images, the shape of the tolerance line does not change visibly, with all values in tolerance lines agreeing in the case of twenty and thirty images to within 0.05%.

The channel characteristics for channel 20 and 60 after convergence are shown in Figure 3-28 and Figure 3-29. The 98% tolerance line is also shown for embedding capacity just to give the reader an idea of shape of the trend. As the frequency of the channel increases, the tolerance lines for error rate become more erratic and sit higher overall. In Figure 3-29, the tolerance line shows an error rate consistently very close to 100% starting from moderate delta. The error rate tolerance lines are less smooth than those of lower frequency channels because, as explained, higher frequency coefficients tend to be smaller in value and so fewer are selected for embedding. Since error rate is calculated as a fraction of a smaller number of coefficients the trend lines are not as smooth.

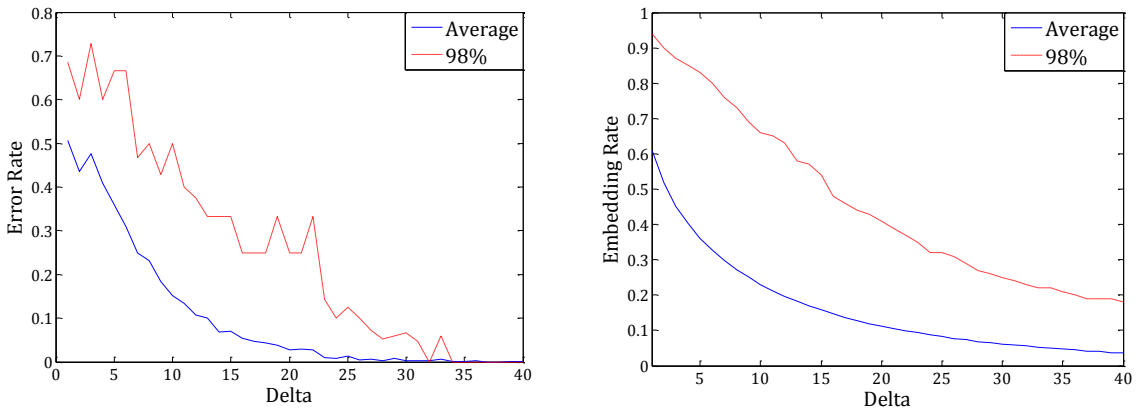

Figure 3-28. Channel 20 characteristics for thirty images (40020 E-blocks)

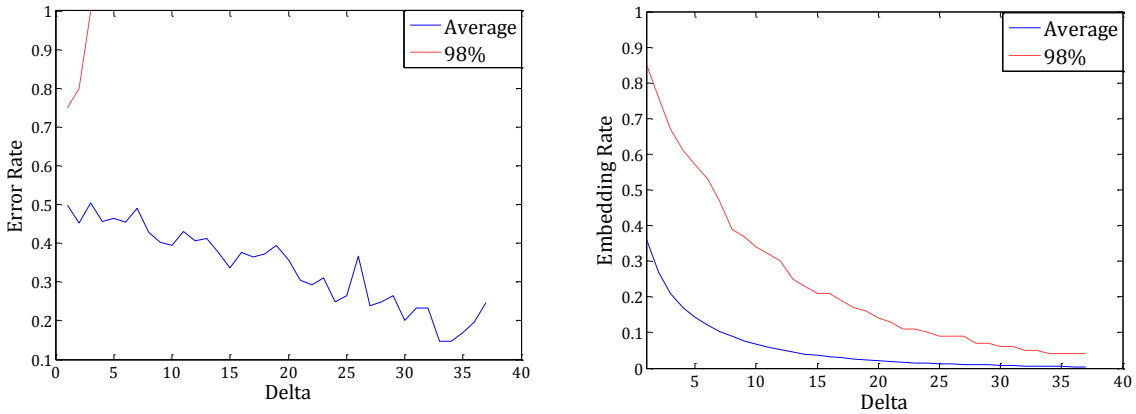

Figure 3-29. Channel 60 characteristics for thirty images (40020 E-blocks)

In Figure 3-29, the channel characteristics 'end' at a delta value of 37. This is because at larger delta, of the 40 020 actual E-blocks, after the selection criteria no usable coefficients were retrieved from the channel and the channel is not considered usable after this point.

3.5 Per Channel Determination of Optimal Delta

Now that the channel characteristics have been determined, the next step towards plotting net embedding capacity curves is the inclusion of error coding parameters. We anticipate that this net embedding capacity plot will have a maximum embedding capacity point at which security and error correcting effects combine optimally.

Before deciding on the specific error coding systems, this section tests the hypothesis that error coding when combined with the channel characteristics just derived does indeed provide a point of optimal embedding capacity.

To recap how the net embedding capacity plot is drawn, the inclusion of the effect of coding is done, for each delta, by finding the specific error correction code that corrects (or just overcorrects) for the corresponding error rate and by simultaneously finding the new net payload by including the proportional reduction in effective embedding capacity due to the inclusion of overhead bits. In this way, the embedding rate graph is altered by multiplying by the proportional loss due to error coding at each delta.

Since the channel characteristics are scatter plots with not one rate value per delta, the error rate for which the coding system would cater can be read off of a particular tolerance line. The choice of tolerance limit depends on the degree to which error is acceptable in the system. For example, if we correct for the noted error rate at the 98% tolerance line then 98% of the batches should end up error free. The embedding rate used in the calculation of the net embedding rate can also be read off of a particular tolerance line. Given the close to uniform distribution of embedding rate scatter plots, it doesn't matter which embedding rate tolerance line is used as they are all very close to integer multiples of each other and so when multiplied by the error coding overhead effect will all provide the same optimal point. Here and for the rest of this dissertation the 98% tolerance line for embedding capacity is chosen.

The repercussions of a particular choice of error rate tolerance line are discussed later in Section 3.6. For now, only the concept of generating the net embedding capacity plot is important.

For the moment the specifics of the error correcting scheme is not crucial since they all have similar characteristics, we just wish to confirm that the net embedding capacity plots will have

the maximum embedding capacity points as expected. Using a simple error block code, three net embedding capacity plots are generated for channels 2, 5 and 11 taking the 98% error rate tolerance and are shown in Figure 3-30. As expected, points of maximum net embedding capacity emerge.

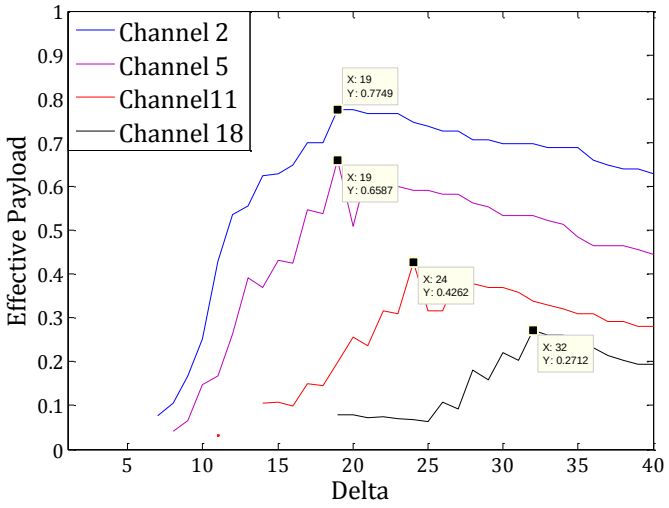

Figure 3-30. Net payload including BCH coding for various channels

These plots provide the following information relevant to the maximum embedding capacity point:

- The corresponding delta value for best embedding capacity for that channel can be read off the x-axis of the plot.
- The corresponding error coding parameters can be retrieved by seeing which error code was used to correct the error rate at that delta.

Thus for each channel the QIM lattices and error correcting parameters can be determined as required.

Regarding the properties of the maximum embedding capacity point for the channels, notice that the retrievable embedding capacity for the channels decreases and delta increases as the frequency of the channel increases, indicating that lower frequency channels are more appropriate for data carrying.

That being said, it was discussed in Chapter 2 that embedding into the low frequency coefficients increases the chances of detection. So the previous statement regarding appropriateness for data carrying should be restated as: low frequency coefficients are better

for data carrying in terms of the amount of data they can carry provided that the value of delta isn't so large that a steganalyser can detect the embedding artefacts.

It is assumed that the random nature of embedding in itself will secure resistance to steganalysis even if the values of delta for lower frequency channels are determined to be slightly higher than those used in the quantisation matrix for hiding quality factor Q_f. This will be assumed for now and checked in Chapter 4 where performance of the determined system is examined.

3.6 Compensation for Errors

Now that channel characteristics have been determined and that it has been confirmed that consolidating channel characteristics with error coding parameters does provide data embedding and error coding parameters that give optimal embedding capacity, the exact nature of the error coding scheme to be implemented needs to be discussed and once this has been decided, similar plots as shown in Figure 3-30 can be deduced which, with some reasoning, should provide a solution.

Previous literature on cell-based systems has used RA coding. In terms of embedding capacity RA coding is inefficient because of the high number of redundant bits. This section works on the premise that a better coding system can be found. A comparison between the performances of the new system versus the old one is then provided in Chapter 4.

It should be mentioned that, depending on the application, errors may be allowed in a secret message. For example, if the message is text or voice, then corruption of some letters or distortion in the voice probably won't prevent the receiver from understanding what was meant. However, if the secret message data is a bank balance, then the movement of a decimal place will have a dramatic impact on how the retrieved message is interpreted by the intended recipient. In this dissertation, no strict limitations are placed on application and it is assumed that the designer would want as close to error-free transmission as possible to satisfy the more strict case. Also, should an error occur, there should be a mechanism in place so that the recipient will realise this and request a re-transmission if desired and possible.

3.6.1 Error Correction Selection

Given a channel subject to errors, error coding can be approached in a few ways. The one way is to not perform error correction but only perform the significantly simpler task of error detection. Should an error be detected at the receiver, a request is sent using a feedback channel to the transmitter to re-transmit the data in a different cover image. This is not

practical in stego-systems because there is no intuitive feedback channel and the requirement that the transmitter regularly re-transmit messages could arouse suspicion from a warden.

A more practical approach is the use of *forward error correcting (FEC) codes*. In this scheme, redundancy is introduced by interleaving the data to be transmitted with check bits (overhead) that are used at the receiver to correct errors. Initially, FEC codes were unpopular due to their high complexity, but since this is now less of a problem following the development of many powerful electronic systems, the effectiveness often outweighs other schemes.

The choice of FEC code is governed by three factors:

- The nature of the errors (i.e. random or burst).
- The degree to which the errors occur.

  In the case of random errors, it is assumed that each bit has the same likelihood of error, independent of any other bits, and so the average error rate represents the likelihood of any bit being in error at any time. In the case of burst errors, the longest burst expected in the channel needs to be quantised.
- Whether the length of data to be transmitted is known in advance and can be broken down into blocks, or whether a continuous stream of data of unknown length needs to be accommodated.

A reasonable cover image will contain regions of varying texture and suitability to carry data. Consider the simple case where a message is hidden in channel coefficients sequentially in adjacent E-blocks as shown in Figure 3-3 and Figure 3-4; if there happens to be an image region that is particularly error-prone then a substantial burst of error will occur. Due to the massive variety in image content, it would be difficult to predict the extent of the error burstiness. This problem can be avoided by embedding data in a pseudo-random order around an image rather than sequentially in adjacent E-blocks. By doing this, the probabilities of adjacent data bits being in error are decorrelated and the nature of the error becomes random (Vaudenay, 2002). The statistics relating to this type of error can be derived directly from the error rate tolerance lines of the channel error characteristics. The scattering of data around the image can be done simply using a pseudo-random number generator, the key to which can be shared in the stego-key.

Given that the purpose of this work is to improve embedding capacity, we will narrow our focus of error correcting schemes to moderate ones that correct for small to moderate amounts of error and which have minimal overhead. Correcting for channels and delta values

with very high error rates is possible with aggressive coding schemes, but goes against the main goal of this work since the heavy overhead requirements would offset any benefit of using the channel to contribute substantially to net embedding capacity.

Within the field of light random error correcting coding, the two primary candidates are *convolutional codes* and *Bose, Chaudhuri and Hocquenghem (BCH) codes* (Lin & Costello, 1983). BCH codes are a type of block code that divide the input bit stream into blocks of fixed size that are then padded with overhead parity bits mapping an input block into a code word. Convolutional codes also convert the input message stream into code words, but do not divide the stream into blocks. Rather, it outputs a code word based on a set of current input bits and previous input bits stored in memory. Convolutional codes are used in real-time applications when the length of the input stream is not known prior to encoding. With regard to stego-systems, there is no reason why the cover image and input bit streams would not be known in advance, making the system more suitable for BCH codes.

BCH codes are a popular generalisation of the well-known Hamming codes. They are highly flexible, allowing variation in block size and overhead within certain error thresholds and mathematical constraints.

As defined in (Lin & Costello, 1983):

Given any positive integers m and t, with $(m \geq 3)$ and $(t < 2^{m-1})$, there exists a binary BCH code with the following parameters:

$$n = 2^m - 1 \quad \textbf{3-12}$$

$$n - k \leq mt \quad \textbf{3-13}$$

$$d_{min} \geq 2t + 1 \quad \textbf{3-14}$$

where t represents the number of errors that can be corrected, n represents the length of the final codeword and k represents the size of the input block of message bits. A table documenting values of (n, k, t) that exist can be found in (Proakis & Salehi, 2002). The possible values of n are 7, 15, 31, 63, 127, 255, 511 and 1023. For a given error rate, a BCH code with smaller block length has a better code rate (k/n). BCH codes can correct for errors up to approximately 25% of the entire block (including overhead bits).

A disadvantage in using BCH codes is that some bits may need to be rejected after blocking if the number of coefficients in a channel is not an integer multiple of n, with an average $n/2$ bits being lost per channel. However, the simplicity and effectiveness of the codes combined with the likelihood that proportionally only a small number of bits will be lost makes BCH codes a good choice.

With regard to the simulator, further modules were added at the front and back ends to provide BCH encoding before embedding and decoding after retrieval. The front end is shown in Figure 3-31. Given an initial secret message bit stream (110010100001101…), each channel has capacity to carry X_{ch} bits after selection criteria (determined using a preliminary stage in the Matlab simulator as explained in Section 3.4.1). Recall channel 1 is not used because it consists of all the E-block DC DCT coefficients. X_{ch} is the total number of bits (information bits and overhead) that can be accommodated into a channel and it is expected that $X_n > X_{n+1}$ since as the frequency of the channel increases it will tend to have a greater number of smaller DCT coefficients that do not meet selection criteria. This is shown in step (1.) in Figure 3-31 for channels 2 and 3. Once X_{ch} is known, at the receiver side:

1. Taking the example of channel 2 further, X_2 is divided into m_2 blocks according to the chosen BCH block size n_2. Any residual bits after blocking ($X_2 - (m_2 * n_2)$) are filled with dummy random bits (not information bits). This is shown in step (2.).
2. Each block is then filled with ($k_2 = n_2 - t_2$) secret message bits and t_2 overhead bits are appending to form a complete block. BCH coding is performed using the function *bchenc* (MathWorks, 2011).This is shown for one block in step (3.).
3. The m_2 blocks of encoded secret message data with the random dummy bits form the complete X_2-bit data block which can then be embedded into channel 2. Before embedding, the block shown in step (4.) is scrambled using a PRNG to remove burst errors (the key to which is transported using the stego-key) and saved in the channel using QIM.

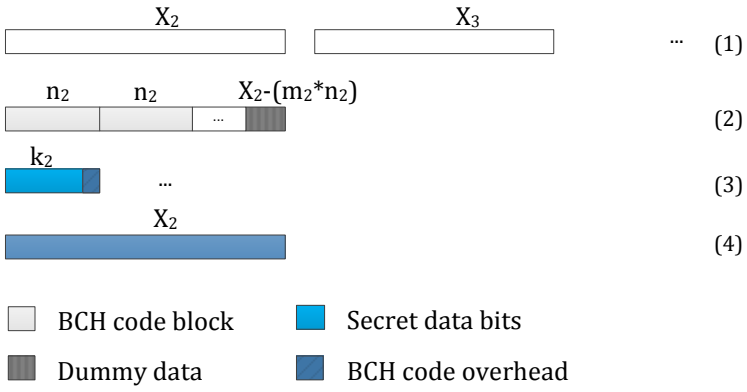

Figure 3-31. Channel-wise BCH encoding

The stego-image then undergoes JPEG compression and decompression.

At the receiver side:

1. The bits are retrieved from each channel using QIM de-embedding and descrambled using a key to a PRNG that is transported in the stego-key.
2. The dummy bits in the residual channel spaces after blocking are rejected and the remaining bits undergo BCH decoding to remove overhead and correct any corrupted data. This is facilitated by function *bchdec* (MathWorks, 2011).

Now that the specifics with regard to the channel error correcting have been decided upon, it is possible to compose an expression for the embedding capacity. At this point it should be reiterated that the term embedding capacity refers to the number of secret message bits *excluding* overhead or dummy bits that can be transported using an image.

Let's define γ_{ch} as the proportion of the total number of DCT coefficients in a channel that meet selection criteria.

Thus, if N_{ch} is the raw number of DCT coefficients in a channel, X_{ch} can be expressed as in Equation 3-15.

$$X_{ch} = N_{ch} * \gamma_{ch} \qquad \textbf{3-15}$$

γ_{ch} cannot be derived analytically but is represented by the embedding rate channel characteristics.

If n_{ch} is the BCH code block length used for a particular channel, the number of blocks in a channel corresponds to the number of batches of n_{ch} that fit completely into X_{ch}. This is shown in Equation 3-16.

$$No.blocks = floor\left(\frac{N_{ch}.\gamma_{ch}}{n_{ch}}\right) \quad \textbf{3-16}$$

where $floor(x)$ maps x to the largest integer that does not exceed x.

In each block there are k_{ch} secret message bits. Therefore, the number of secret message bits (not overhead bits or dummy bits) in a channel is given in Equation 3-17.

$$Emb.Cap.in\ Channel = floor\left(\frac{N_{ch}.\gamma_{ch}}{n_{ch}}\right).k_{ch} \quad \textbf{3-17}$$

The total number of secret message bits that can be accommodated in the image across all channels, which we call embedding capacity, is given in Equation 3-18.

$$Emb.Cap = \sum_{channel} floor\left(\frac{N_{ch}.\gamma_{ch}}{n_{ch}}\right).k_{ch} \quad \textbf{3-18}$$

3.6.2 Usable Channels & Per Channel Error Correction

So far, it has been confirmed that using channel characteristics and error code properties, data handling parameters that give best embedding capacity for a channel can be derived. Now that BCH coding has been decided upon and the embedding capacity can be derived, n_{ch} and k_{ch} need to be considered more carefully and selected to maximise embedding capacity in each channel.

First, a tolerance line needs to be selected to represent the error rate at each delta for which error correcting will cater. Theoretically, if the values of delta and error correcting parameters are derived according to 100% error rate tolerance lines then no errors should ever be observed and error coding would not be required. In reality, it is possible that an outlier was not characterised and rare errors may occur. Using a tolerance limit less than 100% would certainly require error coding. Recall the 98% tolerance line for embedding rate was already selected in Section 3.5.

The tolerance line for which error is corrected can be chosen at the discretion of the designer and will depend on the amount of allowable error in a given channel. Before making the final decision on what tolerance line to use, we can say that the 95% error rate tolerance line is a reasonable boundary for the lowest tolerance percentage a moderate channel error correcting scheme would cater for. Recall the 95% tolerance level for error rate represents the value of error rate below which 95% of observable batch error rates have occurred.

Having defined a lower limit on what error rate tolerance limit to use, we can now consider which channels are usable and which are not. We know that channels where the error rate is consistently above ~25% cannot be corrected for using BCH codes and correcting for high error rates would go against the principle of attempting to increase embedding capacity since a strong coding scheme and significant overhead would be required compromising embedding capacity, bringing into doubt whether the channel should be used at all.

Not all channels have 95% tolerance lines indicating an error rate below 25%, and those that do not are rejected for embedding according to the condition that only moderate error correction is worthwhile. The channels that are deemed usable are highlighted in blue in Figure 3-32.

The 12x12 matrix contains the channel numbers taken in zigzag order in MULTI. It is evident now that 30 channels are usable in an E-block in conjunction with moderate error correction contradicting the assumptions made in the literature previously that only the first 19 are usable. Recall that the corresponding matrix for any E-block smaller than 12x12 can be extracted by taking the required square from the top left hand corner of the matrix in Figure 3-32. All of the channels but one lie in the top left 8x8 segment of the E-blocks and so each E-block will contribute one candidate coefficient towards these channels.

1	2	6	7	15	16	28	29	45	46	66	67
3	5	8	14	17	27	30	44	47	65	68	89
4	9	13	18	26	31	43	48	64	69	88	90
10	12	19	25	32	42	49	63	70	87	91	108
11	20	24	33	41	50	62	71	86	92	107	109
21	23	34	40	51	61	72	85	93	106	110	123
22	35	39	52	60	73	84	94	105	111	122	124
36	38	53	59	74	83	95	104	112	121	125	134
37	54	58	75	82	96	103	113	120	126	133	135
55	57	76	81	97	102	114	119	127	132	136	141
56	77	80	98	101	115	118	128	131	137	140	142
78	79	99	100	116	117	129	130	138	139	143	144

Figure 3-32. 12x12 matrix showing channels appropriate for data carrying

Now that we understand which channels are usable, the embedding capacity plot versus delta can be drawn and the best data handling schemes derived. At this point, we review the sequence of events required to determine these schemes:

Firstly, the tolerance level of error rate and n_{ch} are selected for the channel. Then for each delta, the required k_{ch} for the BCH code is chosen to correct the error rate and correspondingly the embedding rate is consolidated with the reduction in embedding capacity due to coding overhead bits to produce a net embedding capacity value for that delta. Done for all deltas, this generates the net embedding capacity plot for the channel which provides a maximum point from which delta (Δ_{ch}) can be read off of the x-axis and k_{ch} can be read as explained in Section 3.5.

The first step in determining data handling parameters is deciding on the error rate tolerance level and the n_{ch}. We are assuming we use one tolerance level across all channels. Once the n_{ch}, k_{ch} and $\bar{\Delta}_{ch}$ have been determined for all the channels, we can summarise them in 12x12 matrices $\bar{n}_{ch}$, $\bar{k}_{ch}$ and $\bar{\Delta}_{ch}$ with each element representing the respective parameters for each channel. For example, $\bar{n}_{ch}$ is populated with n_{ch} for all channels situated in their respective positions (frequencies) within the 12x12 E-block. For an E-block smaller than 12x12, the matrices n_{ch}, k_{ch} and $\bar{\Delta}_{ch}$ are determined by taking the top left block of size ExE from the 12x12 matrix.

The data embedding and error coding requirements for any one scenario can be summarised by the notation $(tol., \bar{n}_{ch}, \bar{k}_{ch}, \bar{\Delta}_{ch})$. $tol.$ represents the error rate tolerance line chosen.

As a start, the choice of n_{ch} for each channel is not obvious. If two plots for channel 3 are performed with $n_{ch} = 63$ and $n_{ch} = 255$ in Figure 3-33, there is an apparent slight benefit in using a larger n_{ch}.

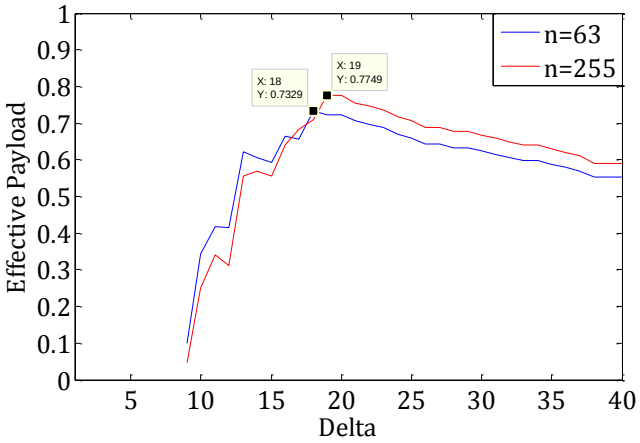

Figure 3-33. Net payload for channel 3 given BCH codes at n_3=63 and n_3=255

This increase is due to a fundamental property of BCH codes. As the error rate that can be corrected (t / n) goes down, the data rate (k / n) goes up. Codes of higher n can correct down to much smaller error rates, as shown in a sample of the BCH codes table in Table 3-1.

Table 3-1. Six BCH code combinations

n	k	t	k / n	t / n
15	11	1	73%	7%
	7	2	47%	13%
	5	3	33%	20%
127	120	1	94%	1%
	113	2	89%	2%
	106	3	83%	2%

Therefore, when the channel characteristics become such that the error rate is very small (which is the case in Figure 3-33 after delta of 15) then using a code with a larger n continues to follow the error rate more closely where the code with a smaller n will hit a floor in minimum error correcting capabilities. So for very small error rates, the larger block length code won't overcompensate for error rate like the smaller block length code, and will continue to offer small improvements in embedding capacity whereas the smaller block length code will have hit a ceiling.

Whether this minor advantage can compensate for the larger average $n / 2$ bits lost at the end of the channel due to blocking will be seen shortly. Nevertheless, this result suggests that where very small amounts of error correction are required, it is better to use schemes with higher block lengths whereas at levels where both codes operate comfortably it is better to use more efficient smaller block length codes. Also visible in Figure 3-33 is that $n_{ch} = 63$ gives better embedding capacity for larger deltas whereas $n_{ch} = 255$ results in better embedding capacity for smaller deltas.

With regard to choosing error rate tolerance limits, we defined a reasonable lower boundary for moderate error correction as 95% in this section thus already accepting a significant likelihood of error in each channel. The more error allowed in the system, the less the embedding capacity is compromised and so we can see using the 100% tolerance line probably won't be a good choice.

At this point, we could ignore the fact that errors may be inevitable and delve further into the question of selecting delta values and an error rate tolerance limit but the fact that some error will probably need to be accepted in the system should be addressed first. With channel error correcting alone, it is not possible to guarantee a low *image* error rate (i.e. the percentage of stego-images that will provide erroneous data during QIM de-embedding) because we have no control on when errors occur simultaneously in different channels.

In particular, this work is trying to keep error to an absolute minimum and since channel-wise error correcting alone has limitations, this leads to the idea of implementing another layer of error correction that can catch any errors that may occur in the channels and further minimise error. This idea is discussed in the next section.

3.6.3 Image-Global Error Coding

It has already been discussed that a particular tolerance level of error rate under 100% would probably need to be selected for the purposes of error correcting on a per channel basis. The implication is then that with only the scheme described some degree of error is inevitable, and we don't have control over when channel errors occur simultaneously in an image. The steganographer would require some guarantee that a certain high proportion of the images he/she embeds into will provide error-free secret data to the recipient which cannot be guaranteed with channel-wise error correcting alone.

Depending on the application, occasional errors in retrieved data may be acceptable. However, this work is trying to cater for the more restricted case that error rate should be kept to a

minimum. Therefore we postpone deducing the channel-wise data handling schemes in order to investigate a second layer of error coding on an image-global basis across all channels. In this dissertation, when the term *global* is used to refer to error coding, image-global (across all channels) error coding is implied. Should any errors not be corrected by the channel-wise error correcting it will be caught be the global error correcting scheme. The global error coding will compromise embedding capacity further as a trade-off for providing improved protection against errors and for guaranteeing a low image error rate.

This section describes the implementation of a second layer of BCH code for error correction as well as image-global error detection should the application require strict monitoring of errors in retrieved secret data.

3.6.3.1 Image-Global Error Correction

Firstly, there is a relationship between the channel-wise and image-global BCH codes. If less error correcting is performed on a channel-wise level then more errors in the channels will occur and the global error correcting system will need to be more powerful and vice-versa. Both levels of BCH coding introduce overhead bits, and it is not obvious whether using more overhead per channel or more overhead globally gives better embedding capacity and this is one of the questions addressed Section 3.7.

The additional functionality required in the simulator to accommodate image-global error correction is shown in Figure 3-34. $X_{Total} = X_2 + X_3 + \cdots$ is the total number of bits that can be embedded in all the channels. The X_{Total} bits are divided into m_{Total} blocks of n_{Total}. Any $(X_{Total} - (m_{Total} * n_{Total})$ residual bits are padded with dummy random bits.

Within each block of n_{Total} bits k_{Total} bits are filled with the secret message bits and have FEC code overhead appended to them.

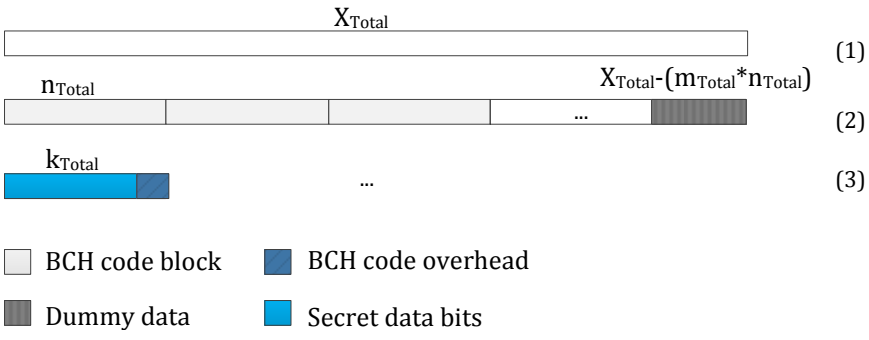

Figure 3-34. Global BCH encoding

These X_{Total} bits that include the message bits, overhead bits and dummy bits are then used to populate the channels as shown in Figure 3-31.

The embedding capacity will now be further affected by the blocking operation during the global BCH encoding and Equation 3-18 can be rewritten to include this. If we call the embedding capacity from Equation 3-18 the local embedding capacity, the number of global coding block is given in Equation 3-19 and the new expression for embedding capacity is given in Equation 3-20.

$$No.\,global\,blocks = floor\left(\frac{Emb.Cap.Local}{n_{global}}\right) \quad \textbf{3-19}$$

$$Emb.Cap. = floor\left(\frac{Emb.Cap.Local}{n_{global}}\right).k_{global} \quad \textbf{3-20}$$

By substituting Equation 3-18 in Equation 3-20, the full expression for embedding capacity is as in Equation 3-21.

$$Emb.Cap. = floor\left(\frac{\sum_{channel} floor\left(\frac{N_{ch}.\gamma_{ch}}{n_{ch}}\right).k_{ch}}{n_{global}}\right).k_{global} \quad \textbf{3-21}$$

In effect, by using the channel characteristics, net embedding capacity plots and coding characteristics we are attempting to optimise Equation 3-21 using code characteristics and graphical methods.

Related to each $(tol., \bar{n}_{ch}, \bar{k}_{ch}, \bar{\Delta}_{ch})$ is a global error-correcting code (n_{global}, k_{global}). The parameters for global error correction depend on the likelihood that errors occur simultaneously in different channels thus contributing to the overall image error rate. The effect of a bit error in a channel on the overall error rate depends on the size of the image.

Assumed sizes of cover images are important because the effect of an individual channel error on the global error rate depends on how many bits were embedded in total across all channels. The size of likely cover images can be deduced by looking at two very popular media-sharing sites, *Flickr* and *Facebook*. Flickr is popular for users to share images but is also widely used to host images for social media and blogs (Statsr.net, 2011). In August 2011, the site was reported to host more than 6 billion images with the number growing (Statsr.net, 2011).

Facebook has already been introduced in Chapter 1. Since the beginning of 2011, Facebook has ranked as the most used social networking service worldwide (Facebook, 2011). Given these statistics, the size of images used on these websites provides a good indication for general trends in digital image sharing.

On Facebook, a standard image may be up to 960x960 (Facebook, 2011), while on Flickr a small image is categorised as 180x240 and a medium image 375x500 (Statsr.net, 2011). The trend is that the size and quality of the images hosted by these websites is gradually increasing. Therefore, in this dissertation, the categories of image sizes are taken as:

- Small – around 180x240, these images provide roughly 300 E-blocks using MULTI
- Medium - around 375x600, these images provide roughly 1500 E-blocks using MULTI
- Large – any image 50% or more greater in number of pixels than medium-sized images

Given the infinite variability in image content, it is impossible to analytically determine dependencies between channels but an estimate can be made using a random set of 200 images not including those used to deduce the channel characteristics. By monitoring the global error in each of these images, (n_{global}, k_{global}) can be deduced for each possibility of $(tol., \bar{n}_{ch}, \bar{k}_{ch}, \bar{\Delta}_{ch})$ according to the maximum observed error.

The acceptable image error rate depends on the nature of the data being transmitted and the patience of the steganographer! For example, some distortion in a video recording will not have the same effect as a shifted decimal place on a bank balance. If the steganographer wishes to check that an image is in error before transmission, he/she can JPEG compress and decompress the stego-image as if it were going through the channel and retrieve the data. Comparing it to the intended secret message would reveal an error and if erroneous the process of embedding and checking could continue until the secret message is found to be transmitted perfectly. However, a steganographer may not like to do this or may become frustrated if many images are in error.

We now deal with setting an image-global error rate (which from now on will be referred to as a global error rate) at a particular level and by using tests deduce global error coding parameters required to meet this.

In this dissertation, an arbitrary though reasonable requirement that less than 1% of observed images have error is insisted upon. Although previously it was said that related to each $(tol., \bar{n}_{ch}, \bar{k}_{ch}, \bar{\Delta}_{ch})$ is a global error-correcting code (n_{global}, k_{global}), for the purposes of

deducing global error correcting requirements, the value of $\bar{n}_{ch}$ (and thus $\bar{k}_{ch}, \bar{\Delta}_{ch}$) does not actually matter since we are not concerned with embedding capacity. Therefore, only the error rate tolerance level $tol.$ is required since this sets the likelihood of a certain amount of error occurring in different channels at the same time.

A value of n_{ch} was randomly chosen as 63 for all channels and (n_{global}, k_{global}) were deduced for various error rate tolerance lines. For small- and medium-sized images, the required global error correcting code along with the corresponding tolerance level is presented in Table 3-2.

Since low image error rate is required, only 95%, 98% and 100% tolerance limits for error are considered. In the case of 100% tolerance, a light global code is used to cater for any outliers missed during channel characterisation.

Table 3-2. Global error correcting parameters for small and medium images at different tolerance levels

Image Size	Tol. X%	(k_{global}, n_{global})	k_{global} / n_{global}	t_{global} / n_{global}
Small	95%	(7,15)	47%	13%
	98%	(16,31)	52%	10%
	100%	(26,31)	84%	3%
Medium	95%	(207,255)	82%	2%
	98%	(231,255)	91%	1%
	100%	(247,255)	97%	0.4%

Table 3-2 shows how larger images require global block codes with larger n. This is because any individual error in a channel gives a much smaller global error rate than for small images. As stated previously, for small error rates larger codes are better suited. This is not to say that smaller block length codes will not work for larger images, but they will not be optimal. While the global error correcting parameters for small images may be applied to larger images, the reverse is not true. Since this work aims to produce a solution that can be applied to any likely size of cover image, it suffices to analyse requirements for small and medium images which are more limiting and which can then be used effectively (though not optimally) in larger images.

Although a second layer of error correction reduces error further, depending on the application it may still be useful to detect the 1% if images that are in error, making the recipient aware of it. Before consolidating global and channel-wise error correction, the final element of global error detection is discussed next.

3.6.3.2 Image-Global Error Detection

Since it is impossible to always guarantee no errors in retrieved data even with two layers of error correction, it seems useful to implement some sort of global error detection code so that the 1% of images that are in error does not go unnoticed by the receiver. In an application

where perfect data recovery is important, on the rare occasion that an error is detected the receiver can request the sender to retransmit the secret message using a different cover image. Again, there is no natural mechanism for feedback but requests for retransmission over some sort of a feedback channel 1% of the time are not substantially suspicious. This section describes implementation of global error detection for this purpose.

The simplest form of error detection is the use of the parity bit. The bit is designated to represent whether there are an odd or even number of 1's in a given bit stream. If the values of the parity bit and data stream are not in agreement, an error has occurred. The parity bit is a special case of what are known as *cycle redundancy check* (CRC) codes (Kuo, Lee, & Tian, 2006). A CRC code is based on polynomial arithmetic. It is calculated by treating the input data message as a polynomial, e.g. the message 11001001 would be treated as $x^7 + x^6 + x^3 + 1$. This polynomial is then divided by a fixed polynomial agreed upon by the sender and receiver. The resultant remainder is appended to the input data and the receiver can then detect errors.

The fixed polynomial is called a generator polynomial $g(x)$ related to the CRC code. There are many possible generator polynomials that can be chosen and selecting the correct one is an important part of successfully implementing error detection. The polynomial depends on the amount of data to be protected, the required error protection and performance.

Some common characteristics of performance include:

(a) If $g(x)$ contains two or more terms then all single-bit errors are detected.

(b) If x+1 is a factor (i.e. if $g(x)$ has an even number of non-zero coefficients) of $g(x)$ then all odd number of erroneous bits are detected.

(c) A CRC checksum of order r can detect burst errors of length less than or equal to r.

Table 3-3 shows the generator polynomials according to some common standards (Hackersdelight.org, 2009).

Table 3-3. Generator polynomials of some common standards in CRC codes

Code	Generator Polynomial g(x)
CRC-8	$x^8 + x^7 + x^6 + x^4 + x^2 + 1$
CRC-12	$x^{12} + x^{11} + x^3 + x^2 + x + 1$
CRC-16	$x^{16} + x^{15} + x^2 + 1$

To cater for small errors, a light CRC-8 code is implemented decreasing payload by only 8 bits.

The CRC code is implemented using in-built functions and the corresponding generator polynomial (MathWorks, 2011).

3.7 Selecting Error Coding Parameters for YASS2/MULTI2

Now that channel-wise and global error correcting and global error detection have been discussed, all of the elements of error coding have been covered and we now return to determining the the final data handling schemes.

Up until now the specifics regarding local error correcting have been discussed and, using net embedding capacity plots for each block size n_{ch} of BCH codes, the data handling procedures that give best embedding capacity for a channel have been derived. In the process we have discovered that a second layer of global image error correction across channels in an image is required to keep the image error rate sufficiently low and the global error correcting parameters have been deduced for different error rate tolerance lines from the channel characteristics. In the case that an image does provide erroneous data at the receiver, a light CRC error detection code is implemented should the application require strict monitoring of errors.

All together the local and global data embedding and error correcting parameters can be described as $(tol., \bar{n}_{ch}, \bar{k}_{ch}, \bar{\Delta}_{ch}, n_{global}, k_{global})$. So far the dissertation has addressed how to determine best embedding capacity points for each channel for n_{ch} and $tol.$. Associated with each $(tol., \bar{n}_{ch}, \bar{k}_{ch}, \bar{\Delta}_{ch})$ is a global (n_{global}, k_{global}) which was determined in Table 3-2 using tests for each error rate tolerance level.

Now that these possibilities have been deduced, we are required to determine which possibility gives best embedding capacity generally across stego-images.

First, in order to determine which error rate tolerance line to use, a random set of 200 images was selected from the database. Each scenario of global error correction in Table 3-2 was implemented in turn for both image sizes with $\bar{n}_{ch}$ set to be uniform across channels and for the situations that $n_{ch} = 31$, 63, 127, 255. For each $\bar{n}_{ch}$, using the 98% error rate tolerance case resulted in the best embedding capacity for 60-70% of the images for all sizes and so was chosen.

Now that the 98% error rate tolerance limit has been chosen to give the best trade-off between local and global error correction, n_{ch} needs to be chosen. In the 98% case, the statistics gathered for small and medium images is shown in Table 3-4 and Table 3-5 when using one n_{ch} for all channels.

It can be seen that n_{ch} =31 gives the best embedding capacity properties for both small and medium images as highlighted in blue in Table 3-4 and Table 3-5. This proves that the advantages in using small n_{ch} outweigh any benefit seen in Figure 3-33.

For small images, in the best case scenario of n_{ch} =31 MULTI embeds on average 3.3 bit per E-block but up to 10 bits per E-block (taking 300 E-blocks per image).

Table 3-4. Characteristics of embedding capacity for small images using a tolerance limit of 98% for several n_{ch}

n_{ch}	$Average$	Min	Max
31	970	144	2808
63	653	121	2192
127	520	52	1605
255	301	20	1155

For medium images, MULTI generates roughly 1500 E-blocks and in the best case scenario of n_{ch} =31, on average 3.6 bits are carried per E-block with up to 11 bits per E-block.

Table 3-5. Characteristics of embedding capacity for medium images using a tolerance limit of 98% for several n_{ch}

n_{ch}	$Average$	Min	Max
31	5410	1155	16863
63	5274	924	17325
127	4863	693	17325
255	4043	231	16632

Even in the best case scenario, the embedding capacity when regarded as the number of bits embedded per E-block appears low. This represents the consequence of including error coding and selection criteria. The embedding capacity is still higher than what can be achieved using YASS and MULTI previously which is explained in Chapter 4.

It is not obvious that a uniform n_{ch} (as used so far) works best and there are many combinations of coding block size for different channels that could be investigated. Given that $n_{ch} = 31$ and $n_{ch} = 63$ have worked the best thus far, a combination of these block lengths in $\bar{n}_{ch}$ is worth investigating. Since lower frequency channels on average have more data embedding capacity, 63 is used for lower frequency coefficients to different extents. The following two $\bar{n}_{ch}$ matrices are are proposed:

$\bar{\Delta}_{ch}(1)$:

x	63	63	31	31	31	31	x	x	x	x	x
63	63	31	31	31	31	x	x	x	x	x	x
63	31	31	31	31	x	x	x	x	x	x	x
31	31	31	31	x	x	x	x	x	x	x	x
31	31	31	x	x	x	x	x	x	x	x	x
31	31	31	x	x	x	x	x	x	x	x	x
31	x	x	x	x	x	x	x	x	x	x	x
31	x	x	x	x	x	x	x	x	x	x	x
31	x	x	x	x	x	x	x	x	x	x	x
x	x	x	x	x	x	x	x	x	x	x	x
x	x	x	x	x	x	x	x	x	x	x	x
x	x	x	x	x	x	x	x	x	x	x	x

Figure 3-35. $\bar{\Delta}_{ch}$ with mixed n_{ch}=64 and 31

$\bar{\Delta}_{ch}(2)$:

x	63	63	63	63	63	31	x	x	x	x	x
63	63	63	63	63	31	x	x	x	x	x	x
63	63	63	63	31	x	x	x	x	x	x	x
63	63	63	31	x	x	x	x	x	x	x	x
63	63	31	x	x	x	x	x	x	x	x	x
63	31	31	x	x	x	x	x	x	x	x	x
31	x	x	x	x	x	x	x	x	x	x	x
31	x	x	x	x	x	x	x	x	x	x	x
31	x	x	x	x	x	x	x	x	x	x	x
x	x	x	x	x	x	x	x	x	x	x	x
x	x	x	x	x	x	x	x	x	x	x	x
x	x	x	x	x	x	x	x	x	x	x	x

Figure 3-36. $\bar{\Delta}_{ch}$ with mixed n_{ch}=64 and 31

The results in embedding capacity for small and medium images at an error rate tolerance level of 98% are shown in Table 3-6 and Table 3-7.

Table 3-6. Characteristics of embedding capacity for small images using a tolerance limit of 98% for two n_{ch}

n_{ch}	$Average$	Min	Max
$\bar{\Delta}_{ch}(1)$	643	112	1824
$\bar{\Delta}_{ch}(2)$	551	80	1808

Table 3-7. Characteristics of embedding capacity for medium images using a tolerance limit of 98% for two n_{ch}

n_{ch}	$Average$	Min	Max
$\bar{\Delta}_{ch}(1)$	5355	1155	16863
$\bar{\Delta}_{ch}(2)$	5276	924	17325

The case of $n_{ch} = 31$ is still observed to result in the best embedding capacity. It should be noted that for the tests thus far image error rate was observed and noted to be less than 1% for all cases.

With the case of 98% error rate tolerance and $n_{ch} = 31$ chosen for all channels, the final conditions of data embedding and correction for cases of medium to small images can be stated as:

$(n_{global}, k_{global}) = (255,231)$ for medium/large images and $(16,31)$ for small images.

$\bar{\Delta}_{ch}$:

x	15	17	22	29	39	37	x	x	x	x	x
16	17	19	23	35	35	x	x	x	x	x	x
17	19	23	32	26	x	x	x	x	x	x	x
18	24	26	40	x	x	x	x	x	x	x	x
24	32	37	x	x	x	x	x	x	x	x	x
27	34	33	x	x	x	x	x	x	x	x	x
35	x	x	x	x	x	x	x	x	x	x	x
34	x	x	x	x	x	x	x	x	x	x	x
40	x	x	x	x	x	x	x	x	x	x	x
x	x	x	x	x	x	x	x	x	x	x	x
x	x	x	x	x	x	x	x	x	x	x	x
x	x	x	x	x	x	x	x	x	x	x	x

Figure 3-37. Final proposed $\bar{\Delta}_{ch}$

$\bar{k}_{ch}$:

x	26	26	26	26	26	11	x	x	x	x	x
26	26	26	21	26	11	x	x	x	x	x	x
26	26	26	21	6	x	x	x	x	x	x	x
26	26	21	26	x	x	x	x	x	x	x	x
26	26	26	x	x	x	x	x	x	x	x	x
21	6	6	x	x	x	x	x	x	x	x	x
11	x	x	x	x	x	x	x	x	x	x	x
6	x	x	x	x	x	x	x	x	x	x	x
6	x	x	x	x	x	x	x	x	x	x	x
x	x	x	x	x	x	x	x	x	x	x	x
x	x	x	x	x	x	x	x	x	x	x	x
x	x	x	x	x	x	x	x	x	x	x	x

Figure 3-38. Final proposed $\bar{k}_{ch}$

In the case where E-blocks are less than 12x12, the top left segment of the matrices of the required size are used. For YASS, the matrices used would be the 8x8 matrix in the top left of the matrices presented.

Two additional terms will now be introduced to discriminate between YASS and MULTI implemented with the data handling systems given in the literature thus far, and the cell-based systems implemented using the data handling systems just derived. YASS2 and MULTI2 will be used to indicate that the new channel model and data handling parameters are used in conjunction with the blocking structure of the stated cell-based stego-system.

3.8 Summary

This chapter presents the concept of grouping E-block DCT coefficients of the same frequency together to form a channel for which more targeted error correcting and data embedding can be performed. This is to accommodate the effects of lossy JPEG compression that any image is likely to be subjected to at some stage of transmission or storage. For a given channel, there are effects that compromise embedding capacity for both small and large delta values, and so there is a value of delta for which these effects combine optimally to provide maximum embedding capacity. In order to plot net embedding capacity versus delta for each channel, the channel characteristics need to be determined. Since they cannot be deduced theoretically for YASS and MULTI, the error rate and embedding rate characteristics of the channels are

deduced over a sufficiently varying image database until they converge. The resultant channel characteristic plots are scatter plots from which tolerance lines can be derived that link error and embedding rate values at a particular delta below which a certain percentage of rate measurements have occurred.

Specifically, BCH codes are appropriate for this application and allow moderate error correction with relatively low overhead. By consolidating the properties of BCH codes with the channel characteristics of 30 usable channels, data embedding and error correcting parameters were found that maximise embedding capacity. Corresponding to a particular set of channel embedding and correcting schemes is an image-global error correcting scheme that aims to correct any residual errors and finally, the implementation of a CRC error detection code to catch any errors that may creep through. The global error correction was set so that 1% of images may show error. It was finally shown that from a reasonable set of possibilities, using an error rate tolerance line of 98% with BCH code block size n_{ch} being 31 for all channels should give good embedding capacity across all stego-image sizes. The derived data handling systems used in conjunction with block structure of existing cell-based systems are indicated by 2, as in for example YASS2.

Chapter 4. Analysis of the Scheme

Cell-based systems are relevant given their good security properties and the fact that they cater for the likely eventuality that a stego-image will undergo JPEG compression at some stage in its transmission and storage. In Chapter 3, the idea was presented of improving data embedding and error correcting schemes in cell-based systems using a channel model that connects E-block DCT coefficients of the same frequency together so that one image contains up to 144 channels depending on the cell-based system used. Following on from this, channel characteristics were determined which, combined with error coding requirements and general limits on stego-image size, lead to the proposal of channel-wise and image-global data handling parameters that give good embedding capacity properties.

This chapter tests these parameters further by placing them back into context and testing YASS2 and MULTI2 for security. The self-imposed boundary on image error rate of 1% is also further verified and some final comments regarding embedding capacity improvements are made.

4.1 Steganalysis

The data embedding and error coding parameters have been determined without specific mention of testing security against blind steganalysers. This is because it was assumed that the random nature of embedding would ensure security even if delta values were altered. In this section, the performance of YASS2 and MULTI2 are tested against a prominent steganalyser to analyse this assumption and to check that good security properties have been maintained.

4.1.1 Detection Rate

With regard to resistance of a stego-system against steganalysis, the result that determines security of a particular system is *detection rate* P_d, which represents the likelihood of a steganalyser correctly identifying a stego-image. More mathematically, it can be represented as shown in Equation 4-1.

$$P_d = 1 - P_{error} \quad \textbf{4-1}$$

where P_{error} is the likelihood of the steganalyser making a mistake in classifying a given image as innocent or corrupt. A steganalyser is in error if it falsely categorises an innocent cover-image as corrupt, or a corrupt stego-image as innocent. Let I_i be the event that an innocent image is analysed and I_c be the event that a corrupt stego-image is analysed. Let Y_i be the event that the steganalyser detects an innocent image and Y_c be the event that the

steganalyser detects a data carrying stego-image. Then P_{error} can be written as in Equation 4-2.

$$P_{error} = P(I_i)P(Y_c|I_i) + P(I_c)P(Y_i|I_c) \quad \textbf{4-2}$$

Define $P(Y_c|I_i)$ and $P(Y_i|I_c)$ as false negative and false positive rates P_{FP} and P_{FN} respectively, then Equation 4-2 may be written as Equation 4-3.

$$P_{error} = P(I_i)P_{FP} + P(I_c)P_{FN} \quad \textbf{4-3}$$

Assuming that the same number of innocent and corrupt images are presented to the steganalyser, $P(I_i) = P(I_c) = 1/2$. Therefore, Equation 4-1 can be rewritten as Equation 4-4.

$$P_d = 1 - {}^1\!/_2\, P_{FP} - {}^1\!/_2\, P_{FN} \quad \textbf{4-4}$$

Let's assume the most primitive of steganalysers where it classifies all images as always either innocent or corrupt. Given an equal likelihood of either type of image $P_{FP} = P_{FN} = 1/2$ and $P_d = 1/2$.

Therefore, we consider a stego-system secure if a blind steganalyser has a detection rate of 0.5 implying it is taking a guess with each classification, with a detection rate of under 0.6 considered to be adequately secure (Dawoud, 2010).

4.1.2 Resistance against PF-274

Among blind steganalysers that exist in the literature, (Pevny & Fridrich, 2006) and (Pevny & Fridrich, 2007) are considered the most effective and are used to test security in the cell-based system literature. In this thesis, the scheme will be referred to as *PF-274*.

The functionality of a blind steganalyser has been referred to throughout this dissertation. Blind steganalysers do not assume any particular stego-system, but aim to determine features of an image that tend to distinguish corrupt stego-images from innocent cover images and which they can use in conjunction with a large number of images to train a classifier. In particular, finding the correct features that vary with embedding but not with natural variation between image content is the most challenging element of implementation. The feature set is usually large and is derived from many statistical characteristics of an image.

(Pevny & Fridrich, 2006) describe that traditionally classifiers have used two types of features: DCT features and Markov features. DCT features are a set of parameters derived from the distribution of DCT coefficients in both the RGB and YCbCr colour spaces, statistics regarding change in DCT coefficients in different directions and the inter-block dependencies between DCT coefficients. The Markov feature set produces a model of the absolute difference of neighbouring DCT coefficients. As the name implies, it produces a Markov model which is effectively a statistical process where each future state is only conditionally dependent on the directly-preceding state (Weisstein, 2011). The specifics of the mathematics are beyond the scope of this dissertation and may be found in the quoted papers, but the gist of (Pevny & Fridrich, 2006) is the idea that Markov features capture *intra-block* dependency among DCT coefficients of similar spatial frequencies within the same 8x8 block whereas DCT features model *inter-block* dependencies. In this way the two features used together complement each other and, as the paper shows, they enhance performance when used together with the disadvantage that more images need to be used for training given a larger training feature set.

Contact was made with the authors of (Pevny & Fridrich, 2006) and (Pevny & Fridrich, 2007), and code was received that extracted 274 features from images. However, there was no code to train a classifier with these features. Therefore, modules were written in Matlab that took images from the image database (Schaefer & Stich, 2004) and which, in conjunction with the received code, was used to extract the 274-element vector from each image and to insert it into a matrix with as many columns as images. The features were then used to train an analyser using 2000 images – 1000 innocent and 1000 corrupt images, giving two [274 1000] matrices (with each row corresponding to a particular extracted feature). The corrupt images were generated using the cell-based systems with embedding at full capacity. The images were medium-size images, 375x500.

Using these matrices, the Neural Network Toolbox (MathWorks, 2011) was used to train the neural network with a mixture of the innocent and corrupt features. Neural networks operate in 3 steps:

1. By *training* themselves through recognising and grouping patterns or trends in a given feature set.
2. The resultant neural network then undergoes *validation* where the generalisation of the network is measured and where training is stopped to prevent the neural network from becoming too fitted to the training images.

3. Finally the neural network undergoes *testing* where the network determined using training and validation is implemented to categorise another set of images.

The ratio of the input images used was 70% for training, 15% for validation and 15% for testing i.e. 1400 images for training, 300 for validation and 300 for testing. These are the default parameters recommended in general by the Matlab toolbox.

Statistics regarding security of YASS (Solanki, Sarkar, & Manjunath, 2007) and MULTI (Dawoud, 2010) are taken from the respective papers and given in Table 4-1 and Table 4-2.

Table 4-1 shows the case where PF-274 is most effective in detecting YASS when the hiding quality factor Q_h=50. B represents the width of the B-block. Recall that $Q_a$represents the advertised quality factor used during the JPEG compression process after data embedding.

The values in the tables were confirmed using the steganalysis module written in code, confirming it to be a legitimate implementation of the system.

Table 4-1. Performance of YASS against PF-274

Q_h	Q_a	Steganalytic Method	Detection rate: B=9	Detection rate: B=14
50	75	PF-274	0.72	0.60
75	75	PF-274	0.56	0.53

Table 4-2. Performance of MULTI against PF-274

Q_a	Steganalytic Method	Detection rate: B=9-14
75	PF-274	0.54

Where YASS has a worst case performance, MULTI has achieved much better security.

The corresponding average detection rate for YASS2 and MULTI2 are shown in Table 4-3 and Table 4-4.

Table 4-3. Performance of YASS2 against PF-274

Q_a	Steganalytic Method	Detection rate: B=9	Detection rate: B=14
75	PF-274	0.73	0.61

Table 4-4. Performance of MULTI2 against PF-274

Q_a	Steganalytic Method	Detection rate: B=9-14
75	PF-274	0.55

Table 4-3 and Table 4-4 show that the security levels of the schemes have been maintained even when using the new parameters for data embedding.

The slight elevation in detection rate of 0.01 is probably due to the fact that the derived delta values for QIM are slightly higher than the ones used previously. A side-by-side comparison of the delta values used in YASS with Q_h=50 and YASS2 are shown in Figure 4-1.

x	11	10	16	24	40	x	x
12	12	14	19	26	x	x	x
14	13	16	24	x	x	x	x
14	17	22	x	x	x	x	x
18	22	x	x	x	x	x	x
x	x	x	x	x	x	x	x
x	x	x	x	x	x	x	x
x	x	x	x	x	x	x	x

(a)

x	15	17	22	29	39	37	x
16	17	19	23	35	35	x	x
17	19	23	32	26	x	x	x
18	24	26	40	x	x	x	x
24	32	37	x	x	x	x	x
27	34	33	x	x	x	x	x
35	x	x	x	x	x	x	x
34	x	x	x	x	x	x	x

(b)

Figure 4-1. Delta values used in YASS with Q_h=50 (a) and from Chapter 3 (b)

Specifically, the increase in the low frequency delta values would contribute to increases in detectability, as described in Chapter 2. However these results show that the random nature of embedding sufficiently overcomes this.

4.2 Image Error Rate

The image error rate relates to the extent to which an application allows for errors and how they affect the way in which the retrieved message is understood by the recipient. For example, the requirements on error for voice data over those representing a bank balance are significantly different.

For the purposes of this dissertation, the more restrictive case is assumed and the data embedding and error coding systems were selected so that image error rate is kept to a minimum of 1%. By this, it is meant that less than 1% of images transmitted using cell-based systems with the new data handling systems will provide erroneous message data to the recipient when retrieved. So that image errors are noticed in this case and so that the sender does not need to keep testing a stego-image for errors before transmission, a light CRC error detecting code was implemented that, while introducing almost negligible reduction in embedding capacity, could prove crucial to the success of transmission.

In this section, the deduced data embedding and error coding parameters are implemented over 400 images taken from the image database (Schaefer & Stich, 2004). The images are also made to vary in size with about a third of medium size, a third small and a third large. The

purpose of these experiments was to verify that image error rate was below the 1% target set and that CRC error detection code does detect all errors.

The steps for determining image error rate were:

1. The 400 images were embedded into using all available capacity in all of the channels using the MULTI blocking systems and $(tol., \bar{n}_{ch}, \bar{k}_{ch}, \bar{\Delta}_{ch}, n_{global}, k_{global})$ determined from Chapter 3. All of the error correcting and detecting mechanisms were in place.
2. The input messages to the images were stored separately.
3. The images underwent JPEG compression and decompression using an advertised quality factor Q_a of 75.
4. The data was then retrieved from the image using the data de-embedding and error correcting systems. CRC error detection was also performed on the images, which showed which images were *detected* to be in error.
5. The retrieved messages from the images were compared to the original input messages to identify which images were *actually* in error.

The detected and actual errors were then compared. The CRC code detected all errors and out of 400 images only 3 were found to be in error, with 0.2% of bits in error average across the 3 images. Two of the images in error were medium-sized and one was large-sized. This confirms that an image error rate of 1% has been maintained and that the CRC code has operated correctly in detecting cases of error.

4.3 Embedding Capacity

In Chapter 3, the process of identifying data embedding and error coding systems could be divided into two parts. The first was the determination of different possibilities of $(tol., \bar{n}_{ch}, \bar{k}_{ch}, \bar{\Delta}_{ch}, n_{global}, k_{global})$ that met security, error rate and embedding capacity requirements which stemmed from the new definition of a channel. The second part involved selecting a case from the possibilities such that the requirements would be met across all image sizes and contents. Since the derivation of the parameters themselves demonstrated that good properties can be produced, these tests will not be repeated here. Rather, this section concentrates on comparing relative performance between YASS2/MULTI2 and YASS/MULTI and on stating embedding capacity as a proportion of image size.

4.3.1.1 Comparison to YASS and MULTI

It should be highlighted again that the focus of existing cell-based systems literature has not been to address particulars regarding appropriateness of data embedding and error coding

parameters. Therefore, a direct comparison between embedding capacities achieved using YASS or MULTI data embedding parameters and those using YASS2 or MULTI2 would not be particularly fair or relevant as the original papers were not attempting to maximise capacity. However, making a comparison can serve 2 purposes:

- The comparison is required to confirm that in fact some improvement was made over the original system, and that versus original rough propositions on data handling, a steganographer using YASS2 or MULTI2 would indeed be able to transmit more data per image than previously.
- One of the goals of this research was to determine the extent to which channels more volatile than the first 19 could be used in combination with error coding to produce a substantial increase in embedding capacity. By comparing the embedding capacities achieved, an overview of the extent to which the use of these channels benefits embedding capacity can be found.

The comparisons were made by taking two identical images, and by determining the amount of space for data in YASS using only the first 19 coefficients, with selection criteria using the delta values given the JPEG quantisation matrix dictated by a hiding factor Q_h and using a RA code with a factor of 10. Using a code rate of $1/10$ is a very optimistic estimate because (Solanki, Sarkar, & Manjunath, 2007) recorded using a repeat rate of between 10 and 40, meaning the best case scenario has been taken here.

YASS2 was then implemented and the embedding capacity was measured. It is not informative to perform the comparison for MULTI too because YASS and MULTI only really differ in E-block sizes and since the usable channels (apart from one) are contained in the first top left 8x8 cell in each E-block there is no real benefit in performing the comparison for MULTI again. For each image, the ratio of the two embedding capacity values were taken, with the embedding capacity using YASS2 as the numerator. For these tests, 100 small and medium –sized images were used.

Since (Solanki, Sarkar, & Manjunath, 2007) performed tests using Q_h =50 and 75, a comparison to YASS is made at both of the hiding factors and a histogram of gain in embedding capacity is shown in Figure 4-2.

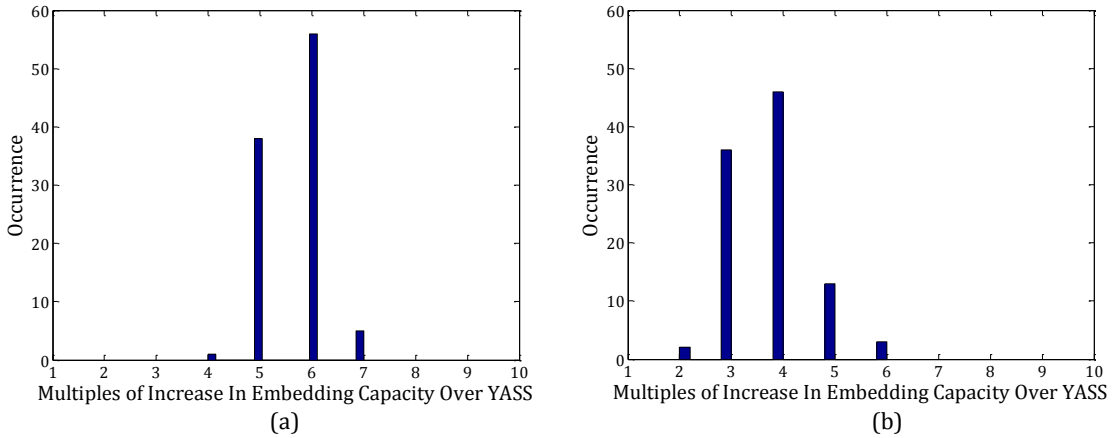

Figure 4-2. Histogram of the number of times increase in embedding capacity over a YASS system with Q_a=75 and Q_h=50 (a) and Q_h=75 (b)

In the case of $Q_h = 75$, the improvement in embedding capacity is lower compared to $Q_h = 50$ because the delta values associated with a higher hiding factor are smaller and so more candidate DCT coefficients meet the selection criterion improving embedding capacity and providing a great advantage. The smaller delta values imply that a more powerful RA code would need to be used but the optimistic case of repetition of 10 is assumed as a worse case. A side-by-side comparison of the delta values used in YASS with Q_h=75 and those in YASS2 are shown in Figure 4-3.

x	6	5	8	12	20	x	x
6	6	7	10	13	x	x	x
7	7	8	12	x	x	x	x
7	9	11	x	x	x	x	x
9	11	x	x	x	x	x	x
x	x	x	x	x	x	x	x
x	x	x	x	x	x	x	x
x	x	x	x	x	x	x	x

(a)

x	15	17	22	29	39	37	x
16	17	19	23	35	35	x	x
17	19	23	32	26	x	x	x
18	24	26	40	x	x	x	x
24	32	37	x	x	x	x	x
27	34	33	x	x	x	x	x
35	x	x	x	x	x	x	x
34	x	x	x	x	x	x	x

(b)

Figure 4-3. Delta values used in YASS with Q_h=75 (a) and in YASS2 (b)

The extent to which more vulnerable channels are used in combination with more careful data embedding and error correcting schemes to increase embedding capacity is clear when the images for which the best and worst improvements are made are examined. An image that gave only twice the improvement in embedding capacity with some enlarged segments is shown in Figure 4-4. There is little texture in the skin and sky areas, so regardless of the scheme it has limited capacity to carry data.

Figure 4-4. Example image where least improvement in embedding capacity is made

An image where 7 times the embedding capacity can be achieved with the new scheme is shown in Figure 4-5. Compared to Figure 4-4, this image is dominated by high texture and so higher frequency channels would be usable. Assuming that the channel characterisation process has a good mix of relatively textured and un-textured images for training, the potential in higher frequency channels was captured and is used.

Figure 4-5. Example image where most improvement in embedding capacity is made

Recall that the data embedding and error coding parameters were designed to cater for the more limited cases of medium and small images. In particular, better global error correcting parameters could be chosen for larger images but a global solution rather than an optimal one was preferred.

However, to show that data embedding and error correcting schemes are also effective on large images, a set of 100 images twice the size of medium ones were used to test the increase in embedding capacity over YASS the same way to what was done previously. The increases in embedding capacity versus an equivalent YASS system are shown in Figure 4-6.

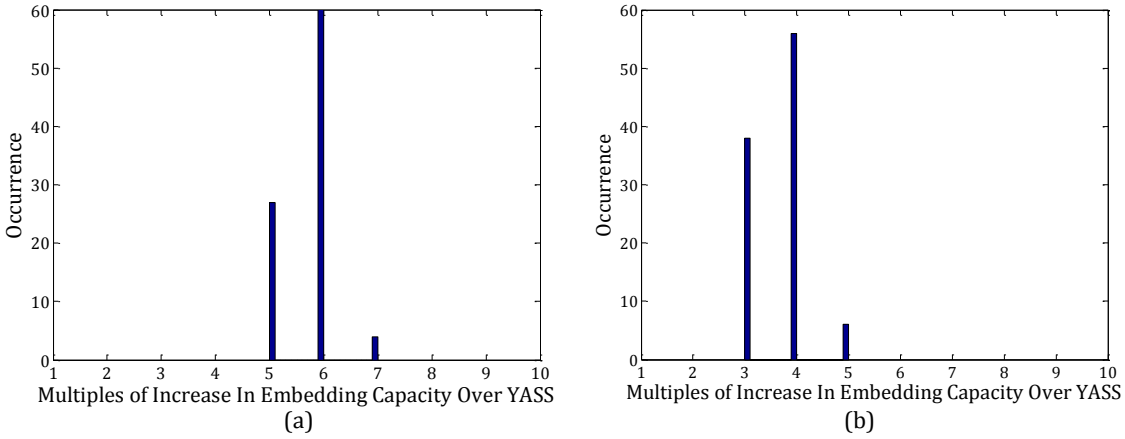

Figure 4-6. Histogram of the number of times increase in embedding capacity over a YASS system for large images with Q_a=75 and Q_h=50 (a) and Q_h=75 (b)

From these histograms, there is an indication that overall for large images, there is less gain in embedding capacity using YASS2 with the recommended parameters than there is for small and medium size images. This is in line with the expectation that the derived parameters could be improved for larger images. The result does still show significant improvement, however.

4.3.2 Capacity as a Proportion of Image Size

The number of bits that can be embedded into small- and medium-sized images for MULTI2 was shown in Chapter 3 as part of the process of determining the improved data handling parameters. In this section, this is done again using the 400 images from above. The number of data bits that could be embedding into the images using MULTI2 and YASS2 were recorded.

Since LSB embedding is such a commonly-referenced stego-system which embeds one bit per pixel, it seems intuitive to state the embedding capacity as the number of information bits that can be embedded versus the number of pixels in the image. Equivalently, the embedding capacity is stated as the proportion of the embedding capacity achieved using LSB embedding that can be achieved using YASS2 and MULTI2. Table 4-5 shows these results.

Table 4-5. Embedding Capacity for MULTI2 and YASS2 as a percentage of number of image pixels

Cell-Based System	Percentage Embedding Capacity		
	Min	Average	Max
MULTI2	1.7%	4.4%	9.8%
YASS2 with B = 9	2%	6.4%	15%
YASS2 with B = 14	0.8%	2.6%	6.6%

Since data carrying DCT coefficients (all apart from one) lie in the top 8x8 of each E-block (according to the deduced data handling system in Chapter 3) the main factor influencing embedding capacity is B-block size which determines how spread out the E-blocks in the stego-image are. As expected, YASS2 with the small B-block has the highest embedding capacity followed by MULTI2 which has a variety of B-block sizes and lastly YASS2 with the largest B-block has the smallest embedding capacity because E-blocks are the most spread out.

Generally, embedding capacity is low for cell-based systems as a consequence of the highly randomised embedding processes and is the sacrifice made for good security properties. As we have seen, the better the embedding capacity properties, the worse the performance of the cell-based systems against blind steganalysers. It is perhaps worth noting that a 4.4% embedding ratio for a 375*500 medium image allows approximately 1000 bytes of embedded data; about the content of this and the previous paragraph.

4.4 Summary

This chapter has placed the data embedding and error coding parameters deduced in Chapter 3 back into context and tested the resilience of YASS2 and MULTI2 against steganalysis. In particular, PF-274 is a very strong blind steganalyser that uses merged DCT and Markov features together. The features from 2000 images were used to train, validate and test the steganalyser against YASS2 and MULTI2. It was shown that the security levels have been maintained. The image error rate is found to be less than 1% over a new random set of 400 images made to vary over likely ranges of image size and randomly in content. The embedding capacity was addressed in the process of determining parameters in Chapter 3, but in this chapter the relative increase in embedding capacity over YASS is presented to show the extent to which the new data handling parameters take advantage of images with texture whereas the previous schemes would have not. Relatively, the increase in embedding capacity is also shown to exist for large images even though global error correcting parameters would not be optimal in this case. As a proportion of the number of pixels in an image, MULTI2 embeds up to 9.8% information bits, YASS2 with B=9 up to 15% and YASS2 with B=14 up to 6.6%. The low embedding capacity relative to other simpler stego-systems such as LSB embedding is a sacrifice made for good security properties.

Chapter 5. Conclusion

Cell-based systems have been shown to have good security properties at the cost of relatively low embedding capacity. As part of the remedy for this, the data embedding and error coding parameters for cell-based systems have been derived more analytically than in previous literature, with the result that embedding capacity has indeed been improved.

Now that the main results of this research have been presented, this chapter gives an overview of the flow of the dissertation and the most relevant points in each chapter. It is intended to give the reader a terminating global view of the breadth and depth of work explored in this dissertation. The extent to which the original research problem statement has been addressed is also explained.

The chapter terminates with ideas for future research. The suggestions are concerned with improving the results found here and addressing some assumed limitations on the stego-systems.

5.1 Summary of Dissertation

5.1.1 Chapter 1

Chapter 1 starts by presenting an overview of the amount of media that is shared over the Internet using facilities such as social media websites, blogs and emails. The sheer scale of the online media-sharing culture and the ease with which content can be shared by almost anyone has made security of transactions pertinent. In particular, steganography is introduced as a mechanism for ensuring security and the prisoner's problem is used to explain the main elements of a stego-system. Steganography is defined as the science of hiding information in innocent objects with the objective of avoiding suspicion from anyone viewing these objects. The definition of steganography is further clarified by contrasting it with its sister concepts of cryptography and watermarking.

Although relatively new in the digital domain, steganography can be traced back to the Golden Age in Greece where it was used in conjunction with wax tablets to transmit secret information. Since then, it was widely used in the 1900s during the wars. Some of the popular examples of this are invisible inks and microdots. Until the 1900s, steganography was used mainly by spies and involved clever tricks with little theoretical basis but given the transition of communication to the digital domain it has experienced a renaissance to become a highly technical and mathematical field. Since electronic communication is susceptible to eavesdropping, security and privacy are more important than ever. Also given that digital

steganography may be used by criminals or terrorists or to carry malicious data such as viruses, research into steganography is important also to be able to counteract this.

Steganography's nemesis is steganalysis, which is the operation performed by the warden in the passive situation where transactions are not tampered with. Within steganalysis, blind and targeted approaches are possible. They differ according to the amount of information known about the observed stego-system transactions *a-priori* and the extent to which the analyser caters for a number of systems.

Steganography that uses digital images as covers (digital image steganography) is especially relevant because digital images are the most popular form of media online. Digital images can be represented in either compressed or uncompressed forms. Given the bandwidth limitations on Internet connections, the compressed versions are more practical. In particular, JPEG compression is the most popular form of compression online and therefore digital image stego-systems should be designed to cater for this. A vital consideration is that JPEG compression is lossy meaning the image data is corrupted during the compression process. If data is embedded into an image before it undergoes compression then the compression process tends to disguise embedding artefacts but error coding needs to be implemented to correct for data corruption.

Within digital image steganography, cell-based systems cater for JPEG compression and have very good security properties due to the random nature of embedding and the fact that embedding is performed before compression. However, because the entire cover image is not used to carry data and because error coding is required, cell-based systems have a particularly low embedding capacity. Data embedding and error coding schemes in cell-based systems have not been determined analytically in the literature previously and it is believed that these schemes could be chosen more methodically with the consequence of improving embedding capacity. This is presented as the primary research goal of this dissertation.

An overview of the research methodology is then given in steps – from first investigating the field around cell-based systems and the context within which they were created, to defining a new approach to determining data embedding and error coding schemes, to finally deducing the schemes and testing them in the context of cell-based systems. The chapter ends with a brief overview of the chapter contents.

5.1.2 Chapter 2

Chapter 2 focuses on digital image steganography specifically and starts by explaining the most pertinent characteristics assumed for the stego-systems in this dissertation. In particular, a public key, passive warden stego-system by cover modification is assumed because these characteristics are the most popular in current literature. Following this, a formal flow chart of the stego-system model is given along with relevant terminology.

The measures of success of stego-systems are defined- imperceptibility, capacity and robustness. The three characteristics tend to counteract each other so no system can be found that has all three excellent qualities. Out of them, imperceptibility is the most important. The concept of visual imperceptibility is discussed, and the failings of the mean square error measurement are shown. Given that media objects transmitted over the Internet are likely to be displayed and seen, it would be foolish for any stego-system to introduce clear visual artefacts. As a result, the battle between steganography and steganalysis has moved to the more subtle statistical level. Embedding artefacts are determined by detecting statistical discrepancies rather than visual ones. Given this transition from naïve to complex systems, the term detectability is introduced to refer to the resistance of a system to statistical analysis whereas imperceptibility is re-defined to be limited to the extent to which a stego-system does not introduce visual embedding artefacts. Statistical properties regarding security are then presented, including Cahin's definition of security and the concept of a Ɛ-secure system.

The taxonomy of digital image steganography is then explained starting with naïve spatial domain techniques. At this point in the report, the spatial representation of images is explained and in particular intensity images are of interest. The concept of colour spaces and is also described.

Within naïve digital steganography, two primary fields exist. The first is LSB embedding where the LSB of the binary representation of the intensity of the pixels in an image are changed to the secret message bits. While this does not cause any visual artefacts, analysis of the statistical distribution of the LSB plane of the stego-image shows clear traces of tampering. If bits other than the LSB are used for data hiding then visual defects may appear, known as the bleeding effect. The second form of naïve steganography uses quantisation and dithering in palette images but this usually results in visual artefacts and due to its limited applications is not a popular research topic.

With regard to complex spatial domain stego-systems, the goal is generally to camouflage data within an image so that natural statistical distributions are maintained. One example is to

attempt to mimic natural noise inserted into an image during image acquisition with a digital camera. Another example is to aim to preserve some specific statistical property such as the shape of an image histogram used usually by steganalysers. In particular, LSB embedding has become popular as an adaptive scheme where data is hidden in select regions with more texture and where more statistical redundancy exists. The topic of adaptive schemes is discussed to some detail.

Although spatial domain techniques are still being investigated, the chapter describes how they are not very useful because they do not cater for the likely possibility of an image being JPEG compressed. The transform representation (DCT) and JPEG compression are then described. The physical significance of the DCT and the properties of low and high frequency components are given. In particular, it is shown that low frequency components are the most significant part of an image visually and that high frequency components represent the detail in an image. JPEG compression operates on the premise that the human visual system is insensitive to detail in an image and thus works to remove high frequency DCT coefficients. The lossy part of JPEG compression occurs with rounding after division by the corresponding element from the quantisation matrix. Transform domain digital image stego-systems lend themselves to accommodating lossy JPEG compression because JPEG involves generation and manipulation of transform coefficients of an image. JPEG stego-systems such as Jsteg, F5 and Outguess are then described.

The JPEG stego-systems explained up to this point embed data into images after the lossy stage of compression and thus have not implemented error coding. The dissertation explains that cell-based system has emerged as a transform-based system that embeds into the DCT coefficients of an image before lossy JPEG compression. Instead of trying to camouflage statistical artefacts of embedding, it attempts to disable a blind steganalyser's ability to estimate original cover image statistics by randomising data embedding. In particular, the areas of the image used for data carrying are varied randomly.

The steps of YASS, the first cell-based system to appear in the literature, are then presented. The concepts of blocking, RA coding and QIM are explained. YASS is also explained to embed into the first 19 DCT coefficients of an E-block. In particular, the description of the delta values using QIM in the literature is deferred to Chapter 4. Selection criteria and the rejection of the DC coefficients from embedding are elaborated upon as requirements to prevent clear statistical embedding artefacts. Extending on the ideas of YASS, the MULTI scheme was presented which introduces two orders of increase in complexity of steganalysis over the

original YASS scheme by allowing variation of B-block and E-block sizes in an image. While the cell-based systems have rigorously addressed security, the parameters of error coding, QIM and the use of only the first 19 AC DCT coefficients in an E-block have not been analytically determined.

Seeing the effect of JPEG compression on various coefficients, it becomes clear that correcting for error across image blocks is not necessarily optimal since the data handling procedure would be required to cater for a very wide range of error characteristics whereas a more targeted approach would perform better. This idea plants the seed for the channel model presented in the next chapter.

5.1.3 Chapter 3

Chapter 3 starts by explaining the main shortcomings of the traditional model of a channel as a string of all of the DCT coefficients in all E-blocks sequentially. In particular, the range of errors likely to be incurred will vary dramatically between low and high frequency DCT coefficients so the data handling schemes would not be focused and efficient – they would either greatly overcompensate in some places or undercompensate in others. A new channel model is presented where an image is defined to contain many channels in parallel and where a channel constitutes a string of all DCT coefficients from all E-blocks at a particular position (frequency) in the E-Block. The idea behind this is that JPEG compression introduces a particular grade of error to DCT coefficients of a particular frequency and so using the new channel model, more targeted data handling procedures can be derived which are anticipated to have a positive effect on embedding capacity.

The exact effects of JPEG compression on coefficient movement are then investigated. In the case of JPEG-GRID the E-blocks and grid blocks used during JPEG compression are exactly aligned and limits on the change in coefficient value due to JPEG compression can be predicated precisely using the JPEG quantisation matrix. In the case of MULTI and YASS, this cannot be done so precisely because E-blocks and JPEG compression grid blocks do not align, although using a random sample of images the trend of increasing movement for higher frequency channels is shown to still hold true.

Given the newly acquired knowledge regarding DCT coefficient movement, an explanation is now given as to how data embedding parameters have been determined in cell-based systems thus far. In the case of JPEG-GRID, the JPEG compression process can be rendered lossless by using delta values corresponding to the JPEG quantisation matrix implemented during compression and so JPEG quantisation matrices are used to provide delta values in YASS and

MULTI literature as a rough extension. Generally speaking, the delta matrix has a correct look since delta values would be expected to be larger for higher frequency channels but in the case of YASS or MULTI there is no obvious reason why this collection of delta values would be optimal.

The concept of how delta relates to embedding capacity is then investigated. In particular, at low delta, effects of higher error rate impact negatively on capacity whereas at high delta, selection criteria impact negatively on embedding capacity. This leads to the idea that there should be a moderate delta at which these factors combine optimally to produce maximum embedding capacity. The target of the research is then defined to be the determination of the plot of net embedding capacity versus delta for each channel from which data handling parameters can be derived.

In order to plot embedding capacity versus delta, channel characteristics need to first be determined. The most crucial of the characteristics are embedding rate (which represents the proportion reduction in embedding capacity due to selection criteria) and error rate (which represents the amount of error in the data carrying DCT coefficients that survive selection criteria).

Since the characteristics regarding movement of YASS and MULTI cannot be determined decisively as in the case of JPEG-GRID, the assumption is made that if measurements of channel characteristics are made over a large enough number of images, eventually the characteristics will converge and provide a good global representation. Deriving characteristics in the most general case of MULTI will make characteristics applicable to all cell-based systems since they all commonly involve simply generating random positions for DCT coefficients for data carrying.

The main modules of the simulator are then expressed, and the assumption of Q_a=75 is justified as the most commonly advertised JPEG quality factor in the literature. Using batches of 100 coefficients, the channel characteristics are then determined as scatter plots of the measurements.

To get an overview of the shape and trends in the scatter plots in order to detect convergence, tolerance lines linking points below which a certain percentage of measurements exist are drawn. These lines are analysed for movement over an ever-increasing number of images until they stop moving.

Given the channel characteristics, if the effects of error coding are consolidated with them, then the plot of embedding capacity versus delta can be generated and the point of maximum embedding capacity can be read which provides the data embedding and error coding parameters for optimal embedding capacity.

The exact nature of the error coding is then explored. In particular, if embedding is done in a scattered fashion then random error correcting is appropriate. Additionally, the application lends itself to block coding and BCH codes, which are particularly effective and flexible. Coding should also be light since correcting for large amounts of error requires a high number of overhead bits which doesn't provide much benefit in terms of embedding capacity. The simulator is edited appropriately to provide for channel-wise BCH coding scheme.

As a first step, channels with high error correcting requirements are rejected and from those that remain plots of embedding capacity versus delta can be produced. It was found that 30 channels are usable per 12x12 E-block contradicting the assumption in previous literature that only the first 19 channels are usable.

Since the error rate is required to be kept as low as possible, determination of the final channel characteristics is delayed to consider further reducing image error rate. To cater for any residual errors in the channels, this work designs for a global BCH code to keep image error rate below the decided limit of 1%. In order to detect image errors, a light CRC code is implemented. The global BCH code parameters are then matched for each possibility of error rate tolerance level and the corresponding case of data handling parameters are generated. As a result, there are now many possibilities of $(tol., \bar{n}_{ch}, \bar{k}_{ch}, \bar{\Delta}_{ch}, n_{global}, k_{global})$.

The choice between these parameters is made based on measurements of which combinations of elements produced the best embedding capacity in small and medium images. This estimate of likely size of cover images is made by analysing the popular image-sharing websites Flickr and Facebook. Finally it was found that using an error tolerance of 98% with n_{ch} being 31 for all channels gives the best embedding capacity and since it was derived for small- and medium-sized images it would also apply for large images. A cell-based system that uses the derived data handling systems is defined to be represented by a 2, as in YASS2 or MULTI2.

5.1.4 Chapter 4

Chapter 4 places the data handling parameters derived in Chapter 3 into context and measures resistance of YASS2 and MULTI2 against steganalysis and image error rate requirements.

An explanation of detection rate and the operation of a powerful blind steganalysis scheme, PF-274, is given. Out of all blind steganalysers, PF-274 has been found to be the most effective in detecting YASS and combines DCT and Markov measurements as features used to train a neural network. The results show that security requirements continue to be met. There is an elevation in detection rate in 1% for YASS and MULTI with the new data handling parameters but this is probably due to slightly elevated delta values for low frequency channels.

Image error rate is then tested by embedding data into 400 images of varying size and checking the number of images in error manually and using the CRC code. The image error rate was found to be 0.75% meeting the original requirements of 1%. In addition, the CRC code correctly identified the erroneous image.

Since cell-based parameters originally didn't attempt to address data handling systems rigorously, directly comparing the new parameters with the old ones does not make a powerful point but it does show that a steganographer can achieve better embedding capacity using the new data handling systems than previously. Using an optimistic RA coding rate of 10, the two systems are compared in the case of YASS for small and medium –sized images and significant improvement is shown. The images for which the worst (2x) and best (7x) improvement is made are analysed and it is found that the best improvement is made where an image is highly textured and the worse for where the image is lightly textured. This shows that there is benefit in using more vulnerable channels than just the first 19 as used by YASS originally. The same experiment is repeated for large images and while improvements are not as large due to the global error correcting parameters not being optimal, there is still significant benefit.

As a proportion of the number of pixels in an image, MULTI2 embeds up to 9.8% information bits, YASS2 with B=9 up to 15% and YASS2 with B=14 up to 6.6%. The low embedding capacity relative to other simpler stego-systems such as LSB embedding is a sacrifice made for good security properties.

5.2 Concluding Comments

The original goal for this research was to investigate an approach to determining data embedding and error correcting schemes more analytically than has been done before in the literature with the aim of increasing embedding capacity in cell-based systems while maintaining good security properties. This dissertation has presented such an approach and deduced data handling schemes such that a low image error rate and good embedding

capacity can be achieved over all expected image contents and sizes. It can be concluded then that the original goals were met in their entirety.

5.3 Future Work

Any future work will address limitations in the results of this research to provide further improvement in embedding capacity and security. Some suggestions are:

1. Generate a technique that selects the parameters for data embedding and local and global error correcting adaptively based on a given cover-image so that these processes are optimised. This would also require the adaptive parameters to be somehow communicated to the intended recipient which could be performed by embedding them in a standard way in more reliable areas of an image.
2. Address the scenario where not of all of the space in a cover image is used for data carrying, i.e. where embedding capacity is less than 100%. This work would address the best way to distribute data around the image to ensure security, and would provide provision for some sort of aggression level for embedding.
3. QIM could be used to embed symbols rather than individual bits to increase embedding capacity. The details of how to do this would still need to be addressed.
4. By taking the approach presented here, comparing the effectiveness and suitability of various error correcting schemes (versus only using BCH codes) could be analysed.
5. Instead of accepting the elevated delta values for low frequency channels as in Chapter 4, the extent to which lowering them to sub-optimal points for security purposes could be explored.

References

JPEG. (2007). Retrieved November 2011, 19, from JPEG Homepage: http://www.jpeg.org/jpeg/index.html

The President Elect's Favorite Movies and Books. (2008, November 24). Retrieved April 6, 2011, from Dublin Library: http://dublinlibrary.wordpress.com/2008/11/

cat + blanket - created by cocor . (2010). Retrieved April 6, 2011, from pixleyes.com: http://www.pxleyes.com/photography-picture/4d6392d1ecb42/cat---blanket.html

ReadWrite Cloud. (2010, August 10). Retrieved April 2, 2011, from How Facebook Scales with Open Source: http://www.readwriteweb.com/cloud/2010/08/how-facebook-scales-with-open.php

Rst. (2010). Retrieved April 5, 2011, from Earth System Science, Mission to Planet Earth, and the Earth Observing System: http://rst.gsfc.nasa.gov/Sect16/Sect16_1.html

Answers.com. (2011). Retrieved April 2, 2011, from How many pictures are uploaded onto facebook every second?: http://wiki.answers.com/Q/How_many_pictures_are_uploaded_onto_facebook_every_second

JPEG. (2011, November 22). Retrieved April 6, 2011, from Wikipedia: http://en.wikipedia.org/wiki/JPEG

Anderson, R. (1996). *Information Hiding: First International Workshop.* Berlin: Springer-Verlag.

Beaullieu, S., Crissey, J., & Smith, I. (2000). Retrieved April 5, 2011, from BPCS Steganography: http://www.ianrichard.com/bpcs/abstract.pdf

Braga, M. (2010, July 28). *Tested*. Retrieved November 2011, 19, from JPEG and You: How the Most Popular Photo Format Works: http://www.tested.com/news/jpeg-and-you-how-the-most-popular-photo-format-works/614/

Brassil, J., Low, S., Maxemchuk, N., & O'Gorman, L. (1995). Hiding information in document images. *Proceedings of the Conference on Information Sciences and Systems, CISS* (pp. 482-489). Baltimore: John Hopkins University.

Brewster, D. (1857). *Microscope, volume XIV. Encyclopedia Britannica or the Dictionary of Arts, Sciences, and General Literature - Application of photography to the microscope.* Edinburgh.

Cahin, C. (2004). An information-theoretic model for steganography. *Information and Computation, Vol. 192(1)*, 41-56.

Chandramouli, R., & Subbalakshmi, K. (2003). Active steganalysis of spread spectrum image steganography. *Proceedings of the 2003 International Symposium on Circuits and Systems, 2003. ISCAS'03, volume 3*, (pp. III-830 - III-833). Hoboken.

Cheddad, A., Condell, J., Curran, K., & McKevitt, P. (2010). Digital image steganography: Survey and analysis of current methods. *Signal Processing*, 727-752.

Chen, B., & Wornell, G. (2011, May 4). Quantization Index Modulation: A Class of Provably Good Methods for Digital Watermarking and Information Embedding. *IEEE Transactions on Information Theory*, pp. 1423-1443.

Cole, E., & Krutz, R. (2003). The Growth of Steganography. In E. Cole, & R. Krutz, *Hiding in Plain Sight. Steganography and the Art of Covert Communication* (pp. 53-54). Indianapolis: Wiley Publishing, Inc.

Dabeer, O., Sullivan, K., Madhow, U., Chandrasekaran, S., & Manjunath, B. (2004). Detection of hiding in the least significant bit. *IEEE Transactions on Signal Processing, Supplement on Secure*, 3046–3058.

Dawoud, P. (2010). An Improved Randomisation of a Multi-Blocking JPEG Based Steganographic System. M.Sc. Thesis.

Debattista, K. (2010, January 11). *TalkTechToMe*. Retrieved November 24, 2011, from The Threats of Steganogrphy: http://www.gfi.com/blog/threats-steganography/

Facebook. (2011, November 18). *Facebook*. Retrieved November 18, 2011, from Statistics: https://www.facebook.com/press/info.php?statistics

Fan, K., & Wediong, K. (2004). A Secure Steganography Scheme Based on (N,t) Threshold. *18th International Conference on Advanced Information Networking and Applications* (p. 536). Fukouka: AINA.

Franz, E., & Schneidewind, A. (2005). Pre-processing for adding noise steganography. *Information Hiding, 7th International Workshop* (pp. 189-203). Barcelona: Springer-Verlag.

(2010). In J. Fridrich, *Steganography in Digital Media: Principles, Algorithms, and Applications* (pp. 83-85). New York: Cambridge University Press.

Fridrich, J. (2010). Introduction. In J. Fridrich, *Steganography in Digital Media - Principles, Algorithms, and Application* (pp. 6-7). New York: Cambridge University Press.

Fridrich, J. (2010). Steganographic Channel. In J. Fridrich, *Steganography in Digital Media: Principles, Algorithms and Applications* (pp. 50-56). New York: Cambridge University Press.

Fridrich, J., & Du, R. (1999). Secure Steganographic Methods for Palette Images. *Information Hiding: Third International Workshop* (pp. 47-60). Dresden: Springer-Verlag.

Fridrich, J., & Goljan, M. (2002). Practical Steganalysis - State of the Art. *Security and Watermarking of Multimedia Contents, vol. 4675*, 1-13.

Fridrich, J., & Goljan, M. (2003). Digital Image Steganography Using Stochastic Modulation. *Proceedings SPIE, Electronic Imaging, Security and Watermakring of Multimedia Contents V* (pp. 191-202). Santa Clara: Springer-Verlag.

Fridrich, J., & Kodovsky, J. (2008). Influence of Embedding Strategies on Security of Steganographic Methods in the JPEG Domain. *SPIE, Electronic Imaging, Security, Forensics, Steganography, and Watermarking of Multimedia Contents X, volume 6819* (pp. 200-213). San Jose, CA: SPIE.

Fridrich, J., Goljan, M., & Hogea, D. (2003). Steganalysis of JPEG Images: Breaking the F5 Algorithm. *Petitcolas, F.A.P. (Ed.): Inf. Hiding: 5th Intl. Workshop. LNCS, 2578* (pp. 310-323). Berlin: Springer-Verlag.

Fridrich, J., Goljan, M., Lisoňek, P., & Soukal, D. (2004). Writing on wet paper. *ACM Workshop on Multimedia and security*. Magdeburg, Germany.

Fu, D., Shi, Y., Zou, D., & Xuan, G. (2006). JPEG Steganalysis Using Empirical Transition Matrix in Block DCT Domain. *IEEE 8th Workshop on Multimedia Signal Processing*, (pp. 310-313). Victoria.

Gonzalez, R., & Woods, R. (2002). Image Types. In R. Gonzalez, & R. Woods, *Digital Image Processing Using Matlab* (pp. 24-14). New Jersey: Prentice Hall, Inc.

Gonzalez, R., & Woods, R. (2002). JPEG. In R. Gonzalez, & W. RE, *Digital Image Processing Using Matlab* (pp. 318-321). New Jersey: Prentice Hall, Inc.

Gordhamer, S. (2009, October 16). *Mashable*. Retrieved November 18, 2011, from 5 Ways Social Media is Changing Our Daily Lives: http://mashable.com/2009/10/16/social-media-changing-lives/

Guo, J.-M., & Le, T.-N. (2010). Secret Communication Using JPEG Double Compression. *IEEE Signal Processing Letters, Vol. 17, No. 10*, 879-882.

Hackersdelight.org. (2009, 7 28). *Hackersdelight.* Retrieved November 20, 2011, from CRC: http://www.hackersdelight.org/crc.pdf

Hass, C. (2008). *Impulse Adventure.* Retrieved 11 1, 2011, from JPEG Compression, Quality and File Size: http://www.impulseadventure.com/photo/jpeg-compression.html

Hedieh, S., & Jamzad, M. (2008). Cover Selection Steganography Method Based on Similarity of Image Blocks . *IEEE 8th International Conference on Computer and Information Technology Workshops, 2008. CIT Workshops 2008*, (pp. 379-384). Jeju.

Hedieh, S., & Jamzad, M. (2010). BSS: Boosted steganography scheme with cover image preprocessing. *Expert Systems with Applications*, 7703–7710.

Herodotus. (1992). The Histories. In Herodotus, *The Histories* (pp. Chapter 5 - Terpischore). New York: J.M. Dent & Sons, Ltd.

Hetzl, S., & Mutzel, P. (2005). A graph theoretic approach to steganography. *9th IFIP TC-6 TC-11 International vol. 3677*, (pp. 119–128). Salzburg.

Hetzl, S., & Mutzel, P. (2005). A graph-theoretic approach to steganography. In *Lecture Notes in Computer Science* (pp. 119-125). Bath: Springer.

Hsiao, J.-Y., & Chang, C.-T. (2011). An adaptive steganographic method based on the measurement of just noticeable distortion profile. *Image and Vision Computing*, 155-166.

Huang, F., Huang, J., & Qing Shi, Y. (2010). An Experimental Study on the Security Performance of YASS. *IEEE Transactions on Information Forensics and Security, Vol. 5, No. 3*, 374-491.

Huang, F., Huang, J., & Shi, Y. Q. (2010). An Experimental Study on the Security Performance of YASS. *IEEE Transactions on Information Forensics and Security, Vol. 5, No. 3*, 374-491.

Johnson, N., & Sallee, P. (2008). Detection of hidden information, covert channels and informations flows. In J. Voeller (Ed.), *Wiley Handbook of Science Technology for Homeland Security* (pp. 20-22). New York: Wiley & Sons, Inc.

Kahn, D. (1996). The Rise of the West. In D. Kahn, *The Code Breakers - The Comprehensive History of Secret Communication from Ancient Times to the Internet* (pp. 106-125). New York: Scribner.

Kawaguchi, E., & Eason, E. (1998). Principle and Applications of BPCS-Steganography. *Proceedings SPIE*, (pp. 464-473). Beijing.

Kerckhoffs, A. (1883). La Cryptographie Militaire. *Journal des Sciences Militaires, Vol. IX*, 5-83.

Kermani, Z., & Jamzad, M. (2005). A robust steganography algorithm based on texture similarity using gabor filter. *Proceeding of IEEE international symposium signal processing and information technology*, (pp. 578–582). Athens.

Kharrazi, M., Sencar, H., & Memon, N. (2006). Cover Selection for Steganographic Embedding. *Proceedings of the International Conference on Image Processing*, (pp. 117-120). Atlanta.

Kumar, K., Raja, K., Chhotaray, R., & Pattnaik, S. (2010). Coherent steganography using Segmentation and DCT. *2010 IEEE International Conference on Computational Intelligence and Computing Research (ICCIC)*, (pp. 1 - 6). Coimbatore.

Kuo, S.-M., Lee, B., & Tian, W. (2006). Cyclic Redundant Code. In S.-M. Kuo, B. Lee, & W. Tian, *Real-Time Digital Signal Processing: Implementations and Applications* (p. 563). West Sussex: John Wiley & Sons.

Li, B., Huang, J., & Shi, Y. Q. (2009). Steganalysis of YASS. *IEEE Transactions on Information Forensics and Security, Vol. 4, No. 3*, 369-382.

Lin, E., & Delp, E. (1999). A review of data hiding in digital images. *Proceedings of the Image Processing, Image Quality, Image Capture Systems Conference, PICS'99*, (pp. 274-278). Savannah.

Lin, K. T. (2011). Hybrid encoding method by assembling the magic-matrix scrambling method and the binary encoding method in image hiding. *Optics Communications*, 1778–1784.

Lin, S., & Costello, D. (1983). Types of Codes. In A. Simpson (Ed.), *Error Control Coding: Fundamentals and Applications* (pp. 3-5). Englewood Cliffs: Prentice-Hall, Inc.

Luo, W., Huang, F., & Huang, J. (2010). Edge Adaptive Image Steganography Based on LSB Matching Revisited. *IEEE Transactions on Information Forensics and Security, Vol. 5, No. 2*, 201-214.

MathWorks. (2011). *MathWorkd*. Retrieved November 29, 2011, from Neural Network Toolbox: http://www.mathworks.com/products/neural-network/index.html

MathWorks. (2011). *R2011b Documentation - Communications System Toolbox*. Retrieved November 29, 2011, from bchenc: http://www.mathworks.com/help/toolbox/comm/ref/bchenc.html

MathWorks. (2011). *R2011b Documentation - Communications System Toolbox*. Retrieved November 29, 2011, from bchdec: http://www.mathworks.com/help/toolbox/comm/ref/bchdec.html

MathWorks. (2011). *R2011b Documentation - Communications System Toolbox*. Retrieved November 29, 2011, from comm.CRCGenerator class: http://www.mathworks.com/help/toolbox/comm/ref/comm.crcgeneratorclass.html

McCullagh, D. (2001, February 7). *Wired*. Retrieved November 29, 2011, from Bin Laden: Steganography Master?: http://www.wired.com/politics/law/news/2001/02/41658?currentPage=all

Mielkainen, J. (2006, May). LSB matching revisited. *IEEE Signal Processing Letters, Vol. 13, No. 5*, pp. 285-287.

Naughton, J. (2010, August 15). *The Guardian*. Retrieved November 18, 2011, from The internet: is it changing the way we think?: http://www.guardian.co.uk/technology/2010/aug/15/internet-brain-neuroscience-debate

Negrat, K., Smko, R., & Almarimi, A. (2010). Variable length encoding in multiple frequency domain steganography. *2010 2nd International Conference on Software Technology and Engineering (ICSTE)*, (pp. 305-309). Kuala Lumpur.

Pevny, T., & Fridrich, J. (2006). Multi-Class Blind Steganalysis for JPEG Images. *Proceedings of SPIE* (pp. 1-13). San Jose: SPIE.

Pevny, T., & Fridrich, J. (2007). Merging Markov and DCT Features for Multi-Class JPEG Steganography. *Proceeding of SPIE*, (pp. 3-4). San Jose.

Pfitzmann, B., & Anderson, R. (1996). Information hiding terminology. *Information Hiding: First International Workshop* (pp. 347-350). Cambridge: Springer-Verlag.

Proakis, J., & Salehi, M. (2002). Coefficients of the Generator Polynomials of BCH Codes. In J. Proakis, & M. Salehi, *Communication Systems Engineering Second Edition* (pp. 621-622). Upper Saddle River: Prentice-Hall, Inc.

Provos, N. (2000). Defending against statistical steganalysis. *10th USENIX Security Symposium, Washington DC, USA of the IEEE 22nd Annual EMBS International Conference*, (pp. 280-283). Chicago.

Rockwell, K. (2007, June 1). *KenRockwell.com*. Retrieved November 2011, 19, from How We See: http://www.kenrockwell.com/tech/how-we-see.htm

Rosenberg, M. (2011, May 11). *About.com Geography*. Retrieved November 18, 2011, from Most Populous Countries Today: http://geography.about.com/cs/worldpopulation/a/mostpopulous.htm

Sajedi, H., & Jamzad, M. (2008). Cover Selection Steganography Method Based on Similarity of Image Blocks. *IEEE 8th International Conference on Computer and Information Technology Workshops*, (pp. 379-384). Sydney.

Sajedi, H., & Jamzad, M. (2010). *HYSA: HYbrid Steganographic Approach using multiple steganography methods.* Retrieved March 24, 2011, from Wiley Online Library: wileyonlinelibrary.com

Sallee, P. (2003, September). Retrieved June 1, 2011, from Matlab JPEG Toolbox: http://www.philsallee.com/jpegtbx/index.html

Sallee, P. (2004). Model-based steganography. In T. Kalker, I. Cox, & Y. Ro, *LNCS, vol. 2939* (pp. 154–167). Heidelberg: Springer.

Sarkar, A., Nataraj, L., Manjunath, B., & Madhow, U. (2008). Estimation of Optimum Coding Redundancy and Frequency Domain Analysis of Attacks for YASS - A Randomised Block Hiding Scheme. *15th IEEE International Conference on Image Processing, ICIP 2008.* (pp. 1292 - 1295). San Diego, CA: IEEE.

Sarkar, A., Solanki, K., & Manjunath, B. (2008). Further study on YASS: steganography based on randomized embedding to resist blind steganalysis. *Proc. Electronic Imaging, Security, Forensics, Steganography, and Watermarking of Multimedia Contents X.* San Jose: SPIE.

Schaefer, G., & Stich, M. (2004). UCID - An Uncompressed Colour Image Database. *Storage and Retrieval Methods and Applications for Multimedia* (pp. 472-480). San Jose: SPIE.

Shi, Y., Chen, C., & Chen, W. (2006). A Markov Process Based Approach to Effective Attacking JPEG Steganography. *8th Information Hiding Workshop.* Old Town Alexandria.

Simmons, G. (1984). The prisoner's problem and subliminal channel. *Advances in Cryptology, Proceedings of CRYPTO* (pp. 51-67). CRYPTO.

Smith, J., & Comiskey, B. (1996, Moay). Modulation and Information Hiding in Images. *Springer-Verlag Lecture Notes in Computer Science*, pp. 207-226.

Solanki, K., Jacobsen, N., Madhow, U., Manjunath, B., & Chandrasekaran, S. (2004, December). Robust Image-Adaptive Data Hiding Using Erasure and Error Correction. *IEEE Transactions on Image Processing, Vol. 13, No. 12*, pp. 1627-1639.

Solanki, K., Sarkar, A., & Manjunath, B. (2007, June). YASS: yet another steganographic scheme that resists blind from 9th International Workshop on Information Hiding. *Information Hiding: 9th International Workship*, (pp. 16-31). Saint Malo.

Solanki, K., Sullivan, K., Madhow, U., Manjunath, B., & Chandrasekaran, S. (2005). Statistical restoration for robust and secure. *Proc. ICIP*, (pp. II 1118–1121). Genova.

Solanki, K., Sullivan, K., Madhow, U., Manjunath, B., & Chandrasekaran, S. (2006). Probably secure steganography: Achieving zero K-L divergence using statistical restoration. *Proc. ICIP*, (pp. 125–128). Atlanta.

Stanescu, D., Stangaciu, V., & Stratulat, M. (2010). Steganography on new generation of mobile phones with image and video processing abilities. *2010 International Joint Conference on Computational Cybernetics and Technical Informatics (ICCC-CONTI)*, (pp. 343-347). Timisoara.

Statsr.net. (2011, 6 10). *Statsr.net*. Retrieved November 20, 2011, from Flickr Stats: http://statsr.net/flickr-stats/

Su, P.-C., & Kuo, C.-C. J. (2003). Steganography in JPEG2000 Compressed Images. *IEEE Transactions on Consumer Electronics, Vol. 49, No. 4*, 824-832.

Sullivan, K., Madhow, U., Chandrasekaran, S., & Manjunath, B. (2006, February). Steganalysis for Markov Cover Data with Applications to Images. *IEEE Transactions on Information Forensics and Security*, pp. 275-287.

Sun, Q., Qiu, Y., Ma, W., Yan, W., & Dai, H. (2010). Image Steganography Based on Sub-Band Coefficient Adjustment in BDCT Domain . *2010 International Conference on Multimedia Technology (ICMT)*, (pp. 1-4). Ningbo.

Tseng, Y.-C., Chen, Y.-Y., & Pan, H.-K. (2002). A Secure Data Hiding Scheme for Binary Images. *IEEE Transactions on Communications, Vol. 50, No. 8*, 1227-1231.

Upham, D. (1993). Retrieved March 5, 2011, from JPEG–Jsteg: http://zooid.org/~paul/crypto/jsteg/

Vaudenay, S. (2002, July 15). *LASEC - Security and Cryptography Laboratory*. Retrieved 12 15, 2011, from Introduction to Decorrelation Theory: http://lasecwww.epfl.ch/memo/dec_manual.shtml

Velasco, C., Nakano, M., Perez, H., Martinez, R., & Yamaguchi, K. (2009). Adaptive JPEG steganography using convolutional codes and synchronization bits in DCT domain. *52nd IEEE International Midwest Symposium on Circuits and Systems, 2009. MWSCAS '09*, (pp. 842-847). Cancun.

Weisstein, E. (2011). *MathWorld-A Wolfram Web Resource*. Retrieved November 29, 2011, from Markov Process: http://mathworld.wolfram.com/MarkovProcess.html

Westfeld, A. (2001). High capacity despite better steganalysis (F5-a steganographic algorithm). *Information Hiding. LNCS, vol. 2137*, pp. 289–302.

Westfeld, A., & Pfitzmann, A. (1999). Attacks on Steganographic Systems. *Information Hiding, 3rd International Workshop* (pp. 61-75). Dresden: Springer-Verlag.

Wilkins, E. (1954). *A History of Italian Literature.* London: Oxford University Press.

Xiaoyi, Y., & Babaguchi, N. (2008). Breaking the YASS algorithm via pixel and DCT coefficients analysis. *19th International Conference on Pattern Recognition, 2008. ICPR 2008*, (pp. 1-4). Florida.

Yang, C.-H., Weng, C.-Y., Tso, H.-K., & Wang, S.-J. (2011). A data hiding scheme using the varieties of pixel-value differencing in multimedia images. *The Journal of Systems and Software*, 669-678.

Yeung, M., & Yeo, B. (1998, February 11). Fragile Watermarking of Three Dimensional Objects. *IEEE Computer Society*, pp. 442-446.

Yu, L., Zhao, Y., Ni, R., & Shi, Y. (2010). A high-performance YASS-like scheme using randomized big-blocks . *2010 IEEE International Conference on Multimedia and Expo (ICME)*, (pp. 474-479). Singapore.